MASTER OF SCIENCE BY RESEARCH

Aerodynamic designing and position optimization of roof box

George, Bryant

Award date:
2014

Awarding institution:
Coventry University

AERODYNAMIC DESIGNING AND POSITION OPTIMIZATION OF ROOF BOX

By

BRYANT GEORGE

MScR in Mechanical and Automotive Engineering

SEPTEMBER 2014

AERODYNAMIC DESIGNING AND POSITION OPTIMIZATION OF ROOF BOX

By

BRYANT GEORGE

SEPTEMBER 2014

A thesis submitted in partial fulfilment of the University's requirements for the Degree of Master of Research

DECLARATION

The work described in this report is the result of my own research. All segments of the content and outcomes that has been acquired from different meetings are completely referred. I understand that cheating and plagiarism constitutes a breach of University regulations and will be dealt with accordingly.

Signed [Bryant George]

ABSTRACT

This project examines the influence of aerodynamic factors of newly designed roof box at various positions over different car geometries. A baseline design of roof box was created and tested using MIRA reference cars in three different configurations at various positions to understand the behavior of the flow. A scaled design of roof box was also considered to understand the trends at various positions. Further investigation was conducted by varying the shape of the box. There was a lack of information in the literature on this subject. The existing data was insufficient to predict the optimum position of a roof box on a vehicle to reduce aerodynamic drag force.

This project includes the analysis of a baseline design of roof box and its design variation which was inspired from Thule Motion 800 using CATIA V5 R20. It also includes the analysis at various positions in three perpendicular directions over MIRA vehicles. The key factor analyzed throughout the project was drag coefficient. In parallel, moment coefficients and flow behavior around the car and box were also evaluated.

The numerical investigation of flow around MIRA cars and roof box were carried out using Computational Fluid Dynamics toolbox - Star-CCM+ V8.04. Due to the large number of experiments required to understand the influence of the position variation of roof box, Design of Experiments (DOE) using Taguchi method and general full factorial method in MINITAB were employed. Using Taguchi method, two-thirds of the simulations can be reduced.

Out of the three geometric shape vehicles tested, the roof box has the highest influence on fastback car and least effect on squareback car. The average variation of drag due to roof box on squareback and fastback cars were 3% and 30% respectively. It was observed that there was a difference of 20% drag between the lowest and highest drag obtained with fastback car and that of squareback car was 5%. Nearly 6kW excess engine power was required to pull the fastback car along with fully loaded roof box. Due to the variation in design of roof box, 6% drag reduction was obtained on fastback car. Even if the individual drag due to roof box was higher, the overall drag remains less due to the interaction of flow between car and roof box. The results from various positions of roof box were compared using both methods in MINITAB. The result shows that Taguchi method was suitable to reduce the number of simulations in external aerodynamics.

ACKNOWLEDGEMENT

This dissertation could not have been finished without the help and support from many professors, research staff, graduate students, and my family. It is my great pleasure to acknowledge people who have given me guidance, help and encouragement.

Firstly, I thank the Almighty for giving me a chance to do this project and helping me throughout this research. I would like to thank my professor, my Director of Studies, Mr. Remus-Mihai Cirstea for providing me a wonderful opportunity to be a part of the project. Without his supervision and support, this work will be incomplete. Once again I take this opportunity to thank him for his guidance, encouragement and inspiration. I would like to thank Adrian P. Gaylard for inspiring me throughout this project.

I would like to express my gratitude to my parents and my brother, Blessent George for helping and supporting me in all stages. Last but not least, I would like to thank all my friends for supporting me throughout my research.

CONTENTS

LIST OF FIGURES

LIST OF TABLES

LIST OF EQUATIONS

NOMENCLATURE

GPa	- Giga Pascal
kg	- Kilogram
m	- Metre
mm	- Millimetre
MPa	- Mega Pascal
mpg	- Miles per gallon
mph	- Miles per litre
V_{eff}	- Average local free stream velocity near the car body
X, Y, Z	- Axis of Cartesian co-ordinate system
$C_{1\varepsilon}$, $C_{2\varepsilon}$, C_{μ}	- Constants in k- ε model
$C_{2,}$ A_0, A_s	- Constants in realizable k- ε model
Y_m	- Contribution of fluctuating dilation in compressible turbulence to the overall dissipation rate
ρ	- Density of air
y	- Distance to nearest wall
C_D	- Drag force Coefficient
$\frac{\rho v^2}{2}$	- Dynamic pressure
.igs	- File format of IGES
F_X, F_Y, F_Z	- Forces acting on the control volume
V_∞	- Free stream velocity
C_f	- Friction coefficient (0.00217)
u*	- Friction velocity

A	- Frontal area of the car
h/w	- height to width ratio
ϑ	- Kinematic viscosity
μ	- Laminar viscosity of the flow
U, V, W	- Local instantaneous velocities in x, y, z directions
P	- Local static pressure
Y^+	- Non-dimensional wall distance
C_P	- Pressure Coefficient
P_k, P_b	- Production of turbulent kinetic energy due to mean velocity gradients and buoyancy
Re_x	- Reynold's number
S	- Tangential surface area of car
δ	- Turbulent boundary layer thickness
ε	- Turbulent dissipation rate
k	- Turbulent kinetic energy
σ_k, σ_ε	- Turbulent Prandtl numbers for k and ε
C_μ	- Turbulent viscosity coefficient
μ_t	- Turbulent viscosity of the flow
S_k, S_ε	- User defined source terms in k- ε model

ABBREVATIONS

3-D	- Three Dimensional
CAD	- Computer Aided Design
CATIA	- Computer Aided Three dimensional Interactive Application
CFD	- Computational Fluid Dynamics
DNS	- Direct numerical Simulation
DOE	- Design of Experiment
EVM	- Eddy Viscosity Model
GUI	- Graphical User Interphase
GBP	- Great Britain Pound
HPC	- High Performance Computer
IGES	- Initial Graphics Exchange Specification
LCVTP	- Low Carbon Vehicle Technology Project
LES	- Large Eddy simulation
MIRA	- Motor Industry Research Association
RANS	- Reynolds Averaged Navier Stokes
RKE	- Realizable k-ε
SST	- Shear Stress Transport
UD scheme	- Upwind Differencing scheme
UV	- Ultra violet

1. Introduction

Aerodynamics has a significant influence on the performance of automobiles. The developments in this area over the past three to four decades are remarkable. Aerodynamicists are trying to reduce drag force acting on the vehicle's body. This will help the vehicles to perform better. Attachments like mirrors, aerials, roof rails, roof box etc. on the car will increase the air resistance by 5-35% (Chowdhury et al. 2012), which affects the performance of the vehicle. There was an increase in fuel consumption and a corresponding increase in emission. In order to improve the efficiency of a vehicle, the drag force acting on a vehicle along its attachments should be reduced to a minimum.

There are many areas in vehicle aerodynamics which need to be improved. In this research, the author is trying to concentrate on roof box - an attachment over the car. There are many roof boxes designed without much research on it. Companies like Halfords, Karrite etc. are least interest in optimizing the shape of roof box. Due to the lack of optimization, there will be an increase in fuel consumption. Koenigsegg Agera R's roof box is the only designed roof box according to the shape of the car (Thule 2014). There are no data published on the position variation of roof box over the car. This project is mainly concentrating on position variation, designing and modifying a roof box aerodynamically.

1.1. Roof Box

Roof box is one of the exterior attachments which are supported over roof rails. Various types of roof boxes are designed by different companies according to customer preferences. As in Figure 1, the main types of boxes are short wide, long wide, medium wide and narrow types of boxes. According to the size, the box can be used to carry objects like baggage, camping and sports equipments (The Roof Box Company 2014).

Figure 1: Types of roof boxes (The Roof Box Company 2014)

The safety of the passengers should be considered as a major factor. Placing excess luggage in the rear side of an estate model car without any safety nets will lead to dangerous situation. To eliminate this hazardous situation, a roof box is essential. The position of the roof box should be arranged such that it will not contact the deck lid of the car in its open position. Even if the vehicle consumes 5-10% excess fuel, the journey will be safer and more comfortable.

The lower side of the box was designed such a way that it can be mounted on the roof of the car. The first and foremost factor which leads to the selection of roof box is its external appearance. Style, shape and colour are the leading factors which control the external appearance. Quality of roof box is another factor to be considered which includes durability and reliability. It should be strong enough to withstand aerodynamic drag and shaking while travelling.

The roof boxes are totally scratch resistant and should not lose their quality for a long time. The box should be stable, even if the speed exceeds motorway limits. The overall height of the vehicle, manufacturability, easiness in mounting and removing, safety, directional stability and wind noise are some factors to be considered. Short wide roof boxes are designed mainly for carrying luggage and camping items. Long wide box can carry almost every type of baggage. Different specifications of roof boxes are shown in Table 1.

Table 1: Various size of roof box (The Roof Box Company 2014)

Narrow roof boxes are specially made to carry mountain skis, snow boards or surfing boards since they have enough length to carry those equipments (The Roof Box Company 2014). Thule, Karrite, Hapro, Kamei, Atera, Inno etc. are the leading companies in producing roof boxes. Each organisation has their own design and they produce variety of boxes in above mentioned specification.

There are various materials used in manufacturing roof boxes. The material selection varies according to the factors mentioned below.

- Weight of roof box (directly proportional to the thickness),
- Mechanical properties like strength, toughness, hardness, rigidity etc.,
- Other properties like service temperature, durability, chemical resistance and manufacturability.
- High surface quality (high gloss) after manufacturing. The surface should be water repellent in nature.
- Other factors involved are overall cost, safety, aesthetics and reliability (Happian-Smith 2001).

Carbon fibre shows excellent characteristics in manufacturing roof box. But, the final product is too expensive. ABS is another material which is less expensive and it has moderate performance when compared to carbon fibre. Most of the manufacturers and customers prefer this material.

1.2. Aims

This project will make use of designing software (CATIA) for generating and modifying roof box. Further testing and analysis can be completed using CFD toolbox (Star-CCM+). This investigation includes the study of variation of drag due to roof box over MIRA cars like fastback, notchback and squareback cars. Other than aerodynamic drag, pressure coefficient, total pressure coefficient, variation of flow direction due to roof box in specified area around the car, variation in pitch, roll and yaw moments from car models alone, vortices and wake structures due to car and box are also analyzed. This software generates a virtual wind tunnel environment and it reduces huge experimental costs.

In order to position the roof box over the car, trial and error method is considered. The Design of Experiment in MINITAB will reduce the count of simulations. Two different DOE methods (general full factorial design and taguchi design) were adopted to validate MINITAB using the CFD results.

1.3. Project Objectives

The following objectives should be achieved for the successful fulfilment of this project.

- Model a 3D roof box for CFD analysis.
- Conduct CFD analysis of roof box over various MIRA reference cars using Star-CCM+.
- Investigate how the position variation and design of roof box over the car influences the aerodynamic performance and how this performance affect the overall power consumption.
- Modify the existing design to achieve minimum drag.
- Use Design of Experiments in MINITAB to optimize the number of simulations effectively.
- Investigate the influence of roof box by analyzing the pressure variation around the car and box.

1.4. Project Limitations

Before starting the investigation, there were some limiting factors that affect the project. They are mentioned below.

- Lack of information about the design and position variation of roof box to compare the data.
- Inability to use the wind tunnel to validate CFD results.
- Limitation in available computational power.

1.5. Overview of the Report

The overall structure of this research report is as follows. Second chapter is a review of literature of an initial research of roof box, basic principles of aerodynamics, CFD and DOE in MINITAB. In the third chapter, methods adopted were clearly explained. The results were tabulated and plots of several CFD simulations at different positions, trends of scaled box and redesigned box were included in chapter four. Further results were tabulated in Appendix II. In the fifth chapter, the results of the simulations were compared and analyzed. The results from MINITAB were analyzed in chapter six. Excess fuel consumption due to roof box was also discussed in this chapter. The whole results were concluded and future works were added in chapters seven and eight.

2. Literature Review

2.1. Introduction

The literature review will discuss numerous topics namely, materials and cost, aerodynamic performance, functionality and safety of roof box, key aerodynamic terms used in this project, CFD and MINITAB. CFD is one of the methods for analyzing aerodynamic performance of a vehicle. It plays an important role along with wind tunnel and road tests in the field of engineering design. In order to improve the design and to minimize the overall expense and effort, engineers depend on numerical methods. A number of factors need to be considered while selecting a turbulence model. However, the selection of an exact model can lead to an improved accuracy in predicting better results. Till now, there is no model which can predict exact results for all circumstances. The aim is to produce a coherent overview of research into roof box design and position variation since the information related to this topic is scattered in various studies.

2.2. Vehicle Aerodynamics

The air flow around the exterior attachments will affect the performance of the vehicle. Hucho (1998) clearly described about aerodynamics of various MIRA vehicles in detail and discussed the drag, downforce and velocity vector fields at the rear end of those cars. The highlighted sections in Figure 2 are the area of interest in this research.

Th

Figure 2: Aerodynamic effects on vehicle operations and vehicle performance (Scheunert, DaimlerChysler and Sindelfingen 2004)

This project was mainly concerned with exterior air flow around the vehicle with a roof box. Aerodynamic factors are the main factors that affect vehicle performance. Other factors are fuel consumption and emission; directional stability, cooling and comfort (Scheunert, DaimlerChysler and Sindelfingen 2004).

2.3. Initial Research

2.3.1. Materials and Cost

Standard materials used for manufacturing roof boxes are Acrylonitrile butadiene styrene(ABS), Polystyrene(PS), High impact polystyrene(HIPS), Polyvinyl chloride (PVC), Polyethylene terephthalate(PET), Glycol-modified polyethylene terephthalate (PETG), High density polyethylene(HDPE), Polyethylene(PE), Poly methyl methacrylate(PMMA), polycarbonate(PC) (Marur 2013). More details about the materials are explained in chapter 3 and appendix II. A recent study (Thule 2014) shows that roof box by Thule made of 100% carbon fibre mounted on Koenigsegg Agera R can withstand up to a speed of 300 kmph. These high gloss materials are light weight and can sustain UV rays. Thus, maximum additional weight provided by the add-on is about 10-30 kg. Therefore every material listed above meets the environmental protective requirements.

The cost of the box varies with styling, capacity, quality and colour of the box. Overall cost of the box is in the range from £150-£1000 (The Roof Box Company 2014). Carbon fibre and other reinforced polymer or plastic costs more than the other standard materials (University of Cambridge 2013).

2.3.2. Aerodynamic Performance of Vehicle Due to Roof Box

The performance of a vehicle can be analysed by measuring forces and moments acting on it. When an object is attached on the car, frontal area increases and drag on the car changes. This will affect fuel consumption, emission and stability of the car (Scheunert, DaimlerChysler and Sindelfingen 2004). About 80% of drag is contributed by pressure difference and the remaining is due to skin friction (Browand 2005).

According to (Chowdhury et al. 2012), drag of various add-ons attached on the roof of the vehicle (0^0 pitch and yaw angle) increases from 5-35% as frontal area changes from 0.8-5%. The weight added by the attachments is less than 10 kg. For a mid-range car, the average fuel consumption is 35-45mpg. There is a reduction of 1mpg when drag increases by 0.04 without changing the vehicle mass. When mass of the vehicle increased by 100kg and drag coefficient by 0.04, the mileage of the vehicle decreases

by 2mpg (Scheunert, DaimlerChysler and Sindelfingen 2004). When carrying a Thule Atlantis 780 model roof box over a 1.8L Passat estate, the fuel economy reduces by 2-3mpg and nearly 6mpg when there are strong crosswinds. The roof box has a capacity of 480 litres. The additional mass of roof box with the baggage was nearly 100kg and it has a frontal area of $0.3m^2$ (Stargazer 2007).

One of the customer commented that there was a reduction of 2mpg from the average value when the car mostly travels at a speed of 70mph with a roof box (AdrianHi 2011). Flow around the vehicle was disturbed due to roof box. To achieve good fuel economy, the box should be designed aerodynamically. Attaching a wrong roof box will increase the fuel consumption and overall cost of travel.

2.3.3. Functionality, Safety and Comfort

The roof box provides extra space by increasing the size of the vehicle. As the frontal area increases, drag on the car increases, fuel consumption and emission from the car increases. For example, if the exterior attachment does not fix to roof rails properly, it will swing on the cross rails. This will increase driving instability and it may lead to accidents. Exterior add-ons are critical in terms of aerodynamic forces exerted on it (Piatek and Schmitt 1998). Crash test for safety, test with water to study the leak and wind channel tests to study the stability should be considered to check the quality of roof box.

2.4. Aerodynamic Terms and Definitions

2.4.1. Boundary Layer

The boundary layer is a thin layer of fluid from the surface of an object wherein the viscosity effects are important (McDonald, Kreith and Berger 1999). Figure 3 shows boundary layer and velocity gradient over a flat plate.

Figure 3: Boundary Layer and Velocity gradient over a flat plate (McDonald, Kreith and Berger 1999)

The air particles adjacent to the surface are contacted on to it. Hence velocity of the particles is zero / relative to the object. This will retard the flow of adjacent layer to a certain limit. This creates two different areas in the flow. The inner area is dominated by viscosity and the outer area has less effect of viscosity. The effect of boundary layer is calculated by the help of its thickness. According to flat plate theory, the flow beyond critical Reynolds number is considered to be turbulent. This will depend on the length of the plate (x), free stream flow velocity (V_∞) and atmospheric conditions. Boundary layer thickness is related to length of the plate and Reynolds number. They are represented in Equation 1.

$$Re_x = \frac{V_\infty * x}{\vartheta} = 5 * 10^5 \qquad \delta = \frac{0.16 * x}{Re_x^{1/7}}$$

Equation 1: Critical Reynolds number (Hucho 1998) and Turbulent boundary layer thickness (White 2011)

The turbulent boundary layer grows as $x^{6/7}$ far more rapidly than the laminar boundary layer increase $x^{1/2}$ (White 2011).

2.4.2. Force acting on a car

As the vehicle travels through the road, different forces act due to air interaction. The main two forces acting on the car which the vehicle needs to overcome are the drag and lift forces.

The drag force is the force acting against the relative motion of the vehicle related to the surrounding air flow. More than 80% of the total drag force is obtained from pressure difference and the remaining is due to skin friction. Lift is the component of the force acting on the vehicle that is perpendicular to the flow direction (Browand 2005). Aerodynamic performance is determined according to drag coefficient and it is represented in Equation 2.

$$C_D = \frac{2F}{\rho A V_\infty^2}$$

Equation 2: Drag force coefficient (Hucho 1998)

When the shear stress acting on the surface and surface area of the vehicle increases, the friction drag increases. This is due to molecular friction of air particles. Pressure drag is obtained when there is pressure variation in the flow. Various forces and moments are represented in Figure 4.

Figure 4: Aerodynamic forces and moments acting on a body (SAE International 1994)

2.4.3. Wakes and Vortices

When the air flows through boundary layer, some energy is required to overcome the frictional force. This energy cannot be recovered and the flow is disturbed. There will be some adverse pressure and velocity variations due to the energy loss. The flow is separated and it cannot follow the path of the vehicle's body and this is due to pressure variation in the flow. Wake is an immediate area of disturbed flow behind the vehicle (low pressure and low velocity region). Due to low pressure, the car is sucked back and drag increases. Vortex is a type of wake and the movement of the generated vortex is perpendicular to the direction of flow and its axis is parallel to line of separation (Hucho 1998). Sometimes the vortex generates from A-posts, tail or near the wind shield of the vehicle and it will travel for a long distance. Wake behind notchback and squareback car is shown in Figure 5 and structure of a vortex is shown in Figure 6.

Figure 5: Wake behind notchback (left) and squareback car with rounded upper hatch (right) (Hucho 1998)

Figure 6: Vortex core line (red) (WeinKauf 2012)

Some vortices will be generated due to the external attachments on the car. “The kinetic energy of the vortex field is rapidly dissipated by turbulent mixing and irreversibility converted into frictional heat” (Hucho 1998). Hence a pressure loss is obtained in the rear side of the object. The work equivalent to this energy is generated by the engine to overcome the pressure drag.

2.4.4. How is turbulence generated?

There will be unsteady swirling flows which provide higher momentum transfer rates from laminar boundary layer in turbulent boundary layer (Andersson 2012). Turbulent boundary layer is divided into two regions: the inner region (δ<20% of total thickness) and the outer region (δ>20% of total thickness) as in Figure 7 (Versteeg and Malalasekara 2007). In viscous sub-layer, flow is almost laminar and molecular viscosity comes into action. Viscous flow tends to reach maximum and Reynolds stress reaches zero (due to viscous damping and kinematic blocking) as the distance from the wall tends to zero. As the distance from the wall increases, both turbulent and viscous stresses are significant (Andersson 2012). Fully turbulent sub-layer is the area where viscous effects have less influence when compared to turbulent effects.

Figure 7: Sub-Layers in inner region (Andersson 2012)

There is an intermediate layer named as buffer layer. These effects are identified using a non-dimensional wall distance called Y^+. The values are shown in Table 2.

Table 2: Y^+ for different sub-layers (Versteeg and Malalasekara 2007)

The above mentioned are the key terms for this research. The next section will present one of the method for analysing these terms.

2.5. Computational Fluid Dynamics (CFD)

2.5.1. Various Turbulence Models

Computational studies were carried out in last two decades on several shapes using various turbulent models. Lopes and Carvalheira (2003) did their research on streamlined car using k-ε model and SST model. Three different turbulence models namely, URANS simulation, steady RKE model and small-scale unsteadiness simulation on mean flow were carried out to analyse the aerodynamics of pickup truck (Holloway et al. (2009). A range of models such as linear, non-linear EVMs and RST models were used in the simulation of the flow around a bluff body (Perzon, Janson and Hoglin 1999).

"Though DNS and LES are theoretical and more physically realistic, the computer requirements to use these methods for wall-bounded flows with realistic Reynolds numbers is still out of reach for years to come in the design environs" (Holloway et.al. 2009). Due to insufficient performance of the computer during that time, engineers were forced to obtain the solution using above mentioned physical models. So there were errors in computational results (Perzon, Janson and Hoglin 1999). The standard models are classified according to the number of extra transport equations and they are shown in Table 3.

Table 3: Classification of turbulence models (Versteeg and Malalasekara 2007)

2.5.1.1. The k-ε model

The k-ε model is one of the RANS based two equation linear EVM. It is widely used in industrial applications (Perzon, Janson and Hoglin 1999). However, it cannot perform well when there is an unfavourable pressure gradient. This model is more preferable because of less computational cost than other two equation turbulence models. Different turbulence models and discretization schemes used by Perzon et al. (1999) are presented below in Table 4.

Table 4: Aerodynamic drag generated by different schemes and turbulent models (Perzon, Janson and Hoglin 1999)

Drag predicted using 1st order UD is much higher than other types of discretization schemes. Numerical schemes like QUICK and MARS mentioned in above table also over predicts the drag, but in a lesser manner. RNG k-ε model predicts the lowest variation in drag when compared to other turbulence models. The dissipation rate in new model is based on mean square vorticity fluctuation at large turbulent Reynolds number (Krastev and Bella 2011). A better prediction can be done with RKE than standard model with unfavourable pressure gradients. Holloway et.al commented that RKE model was unable to solve transient problem on pickup truck since this model cannot predicts a good results when compared to other models. Table 5 below shows drag, lift and pressure coefficients using different turbulent models on a streamlined car body.

Table 5: Drag, lift and pressure coefficient created by different schemes and turbulence models on a streamlined car body (Lopes and Carvalheira 2003)

Lopes and Carvalheira (2003) employed k-ε model to analyse streamlined car body. Using k-ε model, they removed incompatibility of wall function method by implementing scalable wall functions. The analysis was completed with an assumption that the

surface of the body coincides with laminar sub-layer. The authors argued that C_D predicted by 2nd order UD was 25% less than the actual drag. UD scheme was rejected by them due to over-prediction of the results. C_P obtained along the symmetric plane using both the discretization schemes and turbulence models shows similar results from nose to tail of the car body.

2.5.1.2. Other Turbulence Models

SST model (two equation RANS based turbulence model) was created by combining standard k-ε model and k-ω model. This model was used by Lopes and Carvalheira (2003) to analyse streamlined car body. There was not much difference in results between SST and k-ε model in 2nd order differencing scheme. Figure 8 below shows the drag coefficient generated using different turbulence models.

Figure 8: Computed total C_D for 25^0 back light angle of Ahmed model (Krastev and Bella 2011)

Spalart-Allmaras model is based on RANS turbulence equations. For recent years, this one equation linear EVM acquired some fame in external aerodynamics due to low computational cost and easiness to execute the problem into LES or unsteady RANS models. The drag becomes constant after a particular period of time. However, this model results in less accurate value when compared to other turbulence models. This model cannot be used to analyse air flow under the vehicle because it over-predicts C_P by 40% (Krastev and Bella 2011).

RST model contains seven extra transport equations for solving a turbulent flow. RST model is not validated like k-ε model and this model performs bit poorer than k-ε model.

More computational time is required to solve any problem using this model when compared to all other models (Versteeg and Malalasekara 2007).

2.5.2. Why k-ε turbulence model?

There are a number of reasons for selecting k-ε model rather than other models for the purpose of this project. They are as follows.

- Realizable k-ε model predicts exactly on Ahmed body[1] with slant angle of 25^0 and shows a stunning performance in industrial sector (Krastev and Bella 2011).
- Most widely validated turbulence model (Versteeg and Malalasekara 2007).
- Less computational time when compared to RST model (Holloway et al. 2009).

2.5.3. Reynolds-Averaged Navier-Stokes (RANS) Equations

This is a hypothetical model turbulence model and it has steady, viscous and equation of motion of fluid flow. The Navier-Stokes equations are shown in Figure 9.

Figure 9: Navier-Stokes equations (Wilcox 2006)

The RANS equation contains terms like mean velocity, pressure and mean of unsteady velocity component products. RANS equations are derived from Navier-stokes equations and they are represented in Figure 10.

[1] Ahmed body – A reference car model described by Ahmed in his experimental work.

Figure 10: RANS equations (University of Texas)

2.5.4. The k-ε and Realizable k-ε model

The k-ε model is one of the most common turbulent models used for industrial applications. Other than RANS equations; 2 more equations for turbulent kinetic energy and dissipation rate are also modelled. In total there will be 7 unknowns and 7 equations. There are some modifications in ε-transport equation by keeping k-transport equation unchanged when compared to base model for realizable model (CD Adapco 2012). The equations for turbulent kinetic energy, dissipation and viscosity are shown in Figure 11 and transport equation for RKE model are shown in Figure 12.

Figure 11: Transport Equations of k-ε model and Modelled turbulent viscosity (CFD online 1994)

Figure 12: Turbulent dissipation rate transport equation in realizable k-ε model (Fluent Ansys 2006)

C_μ is a function of mean strain of rotation rates and angular velocity of the system's rotation turbulence fields (Fluent Ansys 2006). The predicted results of the modified model had a better improvement from its base model. The drag coefficient was very close when compared to experimental value (Krastev and Bella 2011). The term 'realizable' means that this model meets some constraints in Reynolds stress model. It is also consistent with the physics of turbulent flows and predicts good results where strong recirculation, rotation, strong streamline curvature and area of separation or adverse pressure gradient in boundary layer (CD Adapco 2012).

2.5.5. Y+ Wall Treatment

Wall treatment is used to determine the turbulent production due to k and ε in the cells on and near to the surface. The surface exposed to flow is considered as 'no slip' condition because viscous effects are dominated (Andersson 2012). The k-ε equations are not valid in near wall region because of dominated viscous effects. To avoid this condition, some modifications should be considered in this area. There are two options for doing this process. One is to avoid the viscous area and another is to solve the region using some mathematical equations. Various wall treatments are discussed below.

- *Low Y^+ wall treatment (Y^+<1)* - In this approach, viscous sub-layer is properly resolved and it is consistent with low Reynolds number (CD Adapco 2012).
- *High Y^+ wall treatment (30<Y^+<100)* - In this approach, viscous sub-layer is not solved. This approach will derive wall shear stress, turbulent dissipation and turbulent production from equilibrium turbulent boundary layer theory (CD Adapco 2012). As viscous sub-layer is not

solving in this approach, overall cell count reduces. Hence computational time reduces.

- *All Y^+ wall treatment (1*>Y^+>30) - As it is a hybrid method, it can take the behaviour of both high and low Y^+ wall treatment according to the size of the mesh (CD Adapco 2012).
- *Two-Layer All Y^+ Wall treatment* - This approach is similar to that of *all Y^+ wall treatment* and suggested as a solution to various problems. A wall boundary condition for turbulent dissipation is included with two layer formulation (CD Adapco 2012).

2.5.6. Justification for two layer method

The exact idea of two layer approach is that the entire computation is divided into two layers. The turbulent viscosity and dissipation of the layer near to the wall is considered as the function of wall distance (CD Adapco 2012). The Reynolds number in turbulent sub-layer is calculated using Equation 3.

$$Re_y = y\frac{\sqrt{k}}{\vartheta}$$

Equation 3: Relation between wall distance and Reynolds number (Andersson 2012)

where y represents the near wall distance, k is turbulent kinetic energy and ϑ is kinematic viscosity. There will be a viscous sub-layer formation in a turbulent flow. This layer creates some challenges to solve as it is very near to the surface of the vehicle. By using two layer method, the challenges can be overcome. The Reynolds number for completely turbulent sub-layer region is greater than 200 and when below 200 it is considered to be viscous affected region (Andersson 2012).

2.5.7. Effect of Blockage

There are unrestricted spaces in all directions for the air to flow in road vehicles. The flow tends to bend and stay parallel to the surface. There is a restricted boundary for an object in a wind tunnel. So the air will squeeze inside the test section and it is explained in Figure 13. When the surface of the object is very near to the wall of the wind tunnel, there is not much room for the air to flow. Hence, experimental values will be higher than actual ones. Normally a 10% blockage ratio is acceptable in educational sector due to less computational resources. Blockage ratio is defined in Equation 4. In automotive companies like Jaguar Land Rover, the blockage ratio for each experiment is taken as 0.01%. Other than the solid blockage, overall result will be affected due to

wake blockage and horizontal buoyancy (Hucho 1998). The wake blockage is due to velocity defect in airstream behind the body and horizontal buoyancy is caused by non-uniformity of velocity across the airflow inside the tunnel. In order to increase the accuracy of the results obtained from simulations, blockage effect should be minimum.

$$Blockage\ Ratio\ (\%) = \frac{Frontal\ Area\ of\ the\ object}{Frontal\ area\ of\ test\ section} * 100$$

Equation 4: Blockage Ratio

This item has been removed due to 3rd Party Copyright. The unabridged version of the thesis can be viewed in the Lanchester Library Coventry University.

Figure 13: Free flow and Wall constrained flow around an object (Hucho 1998)

2.6. Estimated Skin Friction Drag

An estimated skin friction drag can be calculated using flat plate theory. The results are obtained with some approximation. The equation for calculating the friction drag is mentioned below.

This item has been removed due to 3rd Party Copyright. The unabridged version of the thesis can be viewed in the Lanchester Library Coventry University.

Equation 5: Friction drag coefficient (Hucho 1998)

2.7. MINITAB - Numerical Analysis Software

It is a powerful software program with a broad range of basic and superior capabilities for numerical analysis (Ryan, Joiner and Cryer 2005). Initially, it was a command based system. The updates from Release 9 onwards provide a full Windows interface. The GUI is simple to understand and easy to use. The output provided by MINITAB is accurate, reliable and faster than computing statistics (Rowell and Duffey 2004). Alongside this project, MINITAB is undergoing a validating process where the arguments from other areas are found to be true in this field as well.

2.7.1. Design of Experiments (DOE)

In industries, DOE is mainly used to investigate different product variables that influence the quality of product. Paul Mathews defined DOE as a methodology for learning any response that differs as a function of one or more independent variables (2005). DOE in MINITAB is more efficient and more sophisticated in recognising the

occurrence of more than one variable at a time rather than one variable at a time (OVAT) approach. The acceptance of this method in MINITAB is due to the remarkable efficiency in results. There are four options for validating this software. Out of that, factorial design and Taguchi design are applicable for this project.

2.7.1.1. General Full Factorial Design

In full factorial design, results of all combination of experimental results are used (according to number of factors and levels). Each experiment is considered as a 'run' in this software and a group of runs leads to a 'design'. As the number of levels and factors increases, number of runs increases. Design with more than two levels reduces screening of runs. Equation 6 shows the number of runs in general full factorial design is given below.

$$\text{Number of runs} = Levels^{factors}$$

Equation 6: Number of runs in full factorial design

In this design, one can change the number of factors and number of levels in each factor. If there are 3 levels and 3 factors on each level, the analyst requires 27 runs. In this design, 2-15 factors and 2-100 levels can be provided. The number of runs can go up to 1,00,000 (Ryan, Joiner and Cryer 2005).

2.7.1.2. Taguchi Designs

Taguchi design is a designed experiment that allows an analyst to select a product which can perform more effectively in a working atmosphere (Minitab 2014). This method uses a unique set of runs so called orthogonal arrays. The main aim of selecting orthogonal arrays is to shorten the number of runs which provide most information of all factors that affect the performance of the product. In this design, no factor is weighted more or less. Due to this reason each factor can be analysed independently (Minitab 2005). A part of full factorial design is considered for orthogonal array.

3. Methodology

3.1. COMPUTER AIDED DESIGN

A roof box was designed to analyse the behaviour of flow structures. Various forces and moments acting on the box were calculated using CFD simulations. The position and structure of the roof box will affect the drag generated on the car. A base model was designed in CATIA V5 R20 with initial research results about various dimensions of roof box. It was decided to design a roof box which falls under medium wide category. CATIA is 3-D modelling software in which surface designing is simpler than any other software. Generative shape design work bench was used to model the roof box.

3.2. Comparing with Original Roof Box

A roof box was designed by keeping *Thule Motion 800* as a base model since the size of the box falls under medium wide category. The external and internal dimensions are shown in Table 6.

Table 6: Comparison of specifications of two models (The Roof Box Company 2014)

The CAD model is not the exact replica of base model. By looking on two models, CAD model is very simple with fewer curvatures. The cornering on every area is less when compared to base model. These are not added to the CAD model because the more complex the geometry, the more computational time is required for analysis. The CAD model and base model are shown in Figure 14.

Figure 14: CAD Model and Thule motion 800 (The Roof Box Company 2014)

3.3. Class of Car Geometries

Three different MIRA reference vehicle models namely, fastback, notchback and squareback cars were used in this project. This company provides high quality engineering services to global automotive and transport sector. The actual models were represented in Figure 15 with roof box kept in the datum position and Table 7 shows various dimensions of cars.

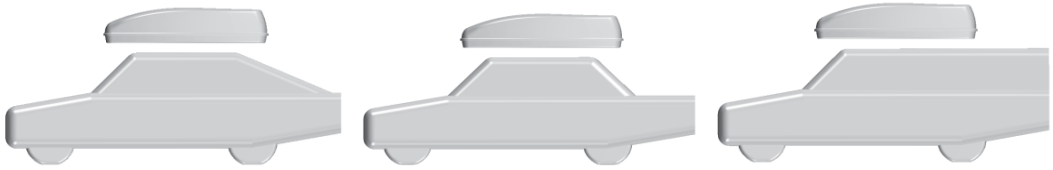

Figure 15: Roof box in datum position over MIRA cars

Specifications	Fastback	Notchback	Squareback
Length	4160mm		
Width	1625mm		
Height	1228mm		
Back light angle	23.42°	21° (effective angle)	0°
Roof length	1382mm	1428mm	2643.5mm
Roof width	1206mm		

Table 7: Specifications of MIRA reference cars

The roof box was placed exactly at the centre of the roof of fastback and notchback car when viewing from top. This position was considered as datum position for all simulations. Initially, it was decided to keep the roof box 125 mm away from the roof of the car. This gap was provided for roof rack and it was manually measured and then decided to keep an average height. When mounting the roof box over fastback and notchback car model, it will overhang 650 mm from the point of cross roof rail attachments to either side.

A small box was attached underneath of the tyre of the model and it is denoted as ‘b1’ in Figure 16. The main reason to attach this box was not to squeeze the air underneath the tyre. This will increase the accuracy of lift calculation.

Figure 16: Small box underneath of the tyre

3.4. Wind Tunnel Size

The inlet dimensions of the wind tunnel can be calculated using frontal area of the object and the blockage ratio. The total length of the wind tunnel was taken as eight times the length of the object. For calculating the size, the blockage ratio was taken as 5% and h/w ratio as 0.7 (Hucho 1998). In some simulations, the car and roof box are symmetrical along a plane normal to Y axis. In order to save computational cost and time, half wind tunnel was considered and extrapolates the results. The wind tunnel dimensions are shown in Table 8. A 3-D view of wind tunnel and its cross sectional area is shown in Figure 17.

Type of simulation	Frontal area (m^2)	Length (m)	Width (m)	Height (m)
Car alone	1.858	34.0	7.28	5.10
Box alone	0.343	16.4	3.13	2.19
Car and box	2.201	34.0	7.93	5.55

Table 8: Wind tunnel dimensions

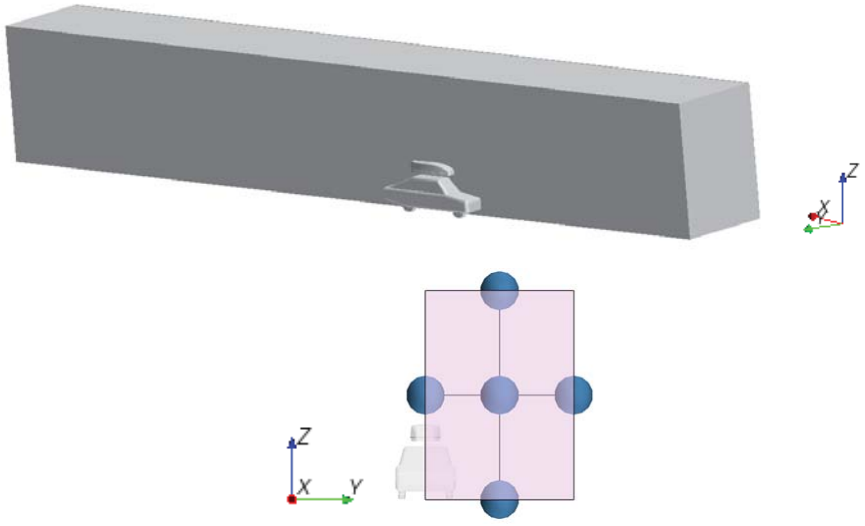

Figure 17: Wind tunnel with C.S. area with car and roof box

3.5. Reynolds Number, Boundary Layer Thickness and Mach number

Reynolds number varies with characteristic length of the object. The car and box have different Reynolds number and boundary layer thickness. Mach number will be same since there was no variation in air flow velocity. All values are represented in Table 9.

Parameters	Car	Box
Reynolds number	7.966×10^{6}	3.925×10^{6}
Boundary layer thickness	68.75mm	37.48mm
Mach number	0.0867	0.0867

Table 9: Reynolds number, Mach number and boundary layer thickness

For calculations, the default values in the software for density and dynamic viscosity are 1.18415kg/m^3 and 1.85508Pa-s respectively. The free stream flow velocity was taken as 30 m/s.

3.6. Modifications on Roof Box

3.6.1. Scaled Roof Box

The roof box was scaled using following factors to analyse the trends with that of full scaled model. The factors are shown in Table 10.

Scale direction	Scale factor
X (along the length of the box)	0.75
Y (along the width of the box)	0.85
Z (along the height of the box)	0.8

Table 10: Scale factors on Roof box

As the overall size decreases, the inner volume also decreases. The approximate volume of scaled box was 270 litres. The frontal area of original roof box was 0.3431m^2. Now it was reduced to 0.233 m^2 (32% less). This in turn affects the wind tunnel size. The size of wind tunnel was reduced to maintain a constant blockage ratio throughout the research. Modified size of wind tunnel is shown in Table 11.

	Length (m)	Width (m)	Height (m)
Roof box	1.538	0.714	0.36
Wind tunnel with car and box	34	7.73	5.41
Wind tunnel with box alone	12.3	2.58	1.81

Table 11: Size of scaled roof box and corresponding wind tunnel

New Reynolds number for roof box was 2.9 $\times 10^6$. Corresponding boundary layer thickness was 29.35mm. There was no change in Mach number because of constant velocity.

3.6.2. Design Variations

As a part of project objectives, design modifications on roof box were generated. The optimization of the shape of roof box was done manually to achieve better results. The modifications were carried out by maintaining the internal volume and exterior frontal area as constant. To follow this procedure, the length of the box was increased by 50mm. Another modification was adding a taper at the rear side bottom portion of the roof box. By implementing taper on roof box, the drag decreases to a certain amount. They are represented in Figure 18 and 19.

Figure 18: Comparing the shapes of modified box with original roof box

Figure 19: Taper on roof box

Taper angles of 0^0 to 3^0 were applied on modified box. The length of the taper was 650mm. This distance was decided because the overhanging length of the box to the rear side after clamping was 700mm. So, less than 700mm for taper length was allowable.

3.7. Mounting Positions of Roof Box

To find an exact position of roof box where C_D becomes the lowest, various locations over the car were tried. It was executed on three cars in three different directions. All the dimensions are measured from datum position. The directions of movement of roof

box were mentioned in Table 12 and various positions in X, Y and Z of roof box were represented in Table 13. Combination of X, Y and Z was the position of the box from datum. Positions of modified box are mentioned in Table 14.

Negative Direction	Movement
X	Towards the rear of the car (Viewing from side)
Y	To left side of the car (viewing from front)
Z	Towards the roof of the car (Viewing from side)

Table 12: Movement description of roof box in various directions

Car type	Position (mm)		
	X	Y	Z
Fastback and Notchback car	-200, -100, 0, 100, 200	-150, -75, 0	-50, -25, 0, 25, 50
Squareback car	-700,-600, -500, -400, -300, -200, -100, 0, 100, 200	-150, -75, 0	-50, -25, 0, 25, 50

Table 13: Various positions of Roof Box

Car type	Position		
	X (mm)	Y (mm)	Z (mm)
Fastback and Notchback car	-200, -100, 0, 100, 200	0	-50
Squareback car	-700, -400, -200, -100, 0, 200	0	-50

Table 14: Positions of modified roof box

3.8. Star CCM+ 8.04.007

Star CCM+ is an engineering simulation software developed by CD-Adapco. This software will reduce engineering cost and time associated with bringing products to the market. This software will help us to simulate the model in a virtual wind tunnel for external aerodynamic study. By clicking various radio buttons, one can set an environment similar to a real wind tunnel or an on-road condition. Since CATIA file itself cannot be accepted by the software, it was converted to '.igs' format. Through this neutral data format, a digital exchange of information will happen among the CAD systems without losing any data.

3.9. Types of Meshing Techniques

The process of fragmenting a complex structure into simpler elements is defined as meshing. Three different meshing types were used in all simulations; polyhedral mesher, prism layer mesher and surface remesher.

3.9.1. Surface Remesher

While importing the geometry into Star-CCM+, it was initially meshed into triangles and the size of each triangle varies. In order to increase the quality of existing surface and to improve the surface for volumetric meshing model, surface remesher was used (CD Adapco 2012). In Figure 20, the box in the left hand side has larger triangles (before applying remesher) and in the right hand side has smaller triangles (after applying remesher). Other than default options, aligned meshes and retain geometric features are added into it. This will improve meshing at cornering and fillets. There will be an improved accuracy in results.

Figure 20: Surface of roof box before and after surface remesher

3.9.2. Polyhedral Mesher

Polyhedral meshing is one of the meshing methods currently using in industries. It provides automatic meshing benefits like other types of meshing methods, but it has some advantage over those methods (Peric and Ferguson). Polyhedral meshing model generates polyhedral cells. Each cell can be linked to 10-14 cells. Another model that has been used widely was tetrahedral meshing.

For tetrahedral cells, the neighbouring cells will be only 4. At edges and corners, they will reduce to only 2. Polyhedral cells can stretch much more than tetrahedrons. Due to this reason, polyhedral meshing provides better results. After creating tetrahedral mesh, some special treatments like cell wise local mesh refinement, sliding grid interface, periodic boundaries are required for refining. These refinements are not necessary for polyhedral meshes. Polyhedral mesh can effectively handle recirculating flow. With a fewer number of cells, polyhedral cells can achieve the accuracy of tetrahedral meshes (Peric and Ferguson). A comparison of pressure drop due to tetrahedral and polyhedral with respect to cell count is shown in Figure 21.

Figure 21: Comparison of pressure drop due to tetrahedra and polyhedra with respect to cell count (Peric and Ferguson)

In order to attain a pressure drop of 5Pa, 40,000 tetrahedral cells were required. Using one-fourth of polyhedral cells, same results can be generated.

3.9.3. Prism Layer Mesher

In order to obtain orthogonal prismatic cells near to the surface of the object, prism layer meshing was preferred. This is mainly used along with a core volume mesh. Prism layer can be described using its thickness, number of layers, size distribution of layers (stretching mode) and stretching function (CD Adapco 2012). Prism layer and polyhedral meshes on roof box are shown in Figure 22.

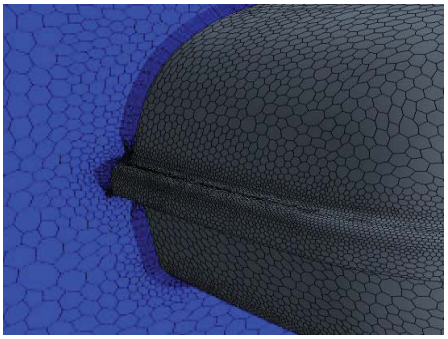

Figure 22: Prism layer and polyhedral meshing

Polyhedral cells are created from the end cells of prism layer. “Numerical diffusion (or dissipation) is a discretization error that smears the discontinuities of large gradients in a finite volume advection scheme” (CD Adapco 2012). This can be minimised by keeping the flow aligned with the mesh. In order to solve the flow near to the wall, prism layers were used. Prism layer has a serious role in resolving turbulent boundary layers. To solve turbulent shear layer properly, 60-70 prism layers are required. Fewer layers (8-12) were necessary to attain good results. This will reduce the cell count.

Hence, less storage memory and computational time are required. Stretching factor and geometric progression were taken as stretching parameters for size distribution of prism layers. Stretching factor is the ratio of thickness of two successive layers and its minimum value is 1.

3.10. Setting the Regions

Without creating a region, one cannot assign the functions of wind tunnel or the associated parts in the simulation. Before setting up the region, it is important to split the entire object into various boundaries. In general, the virtual wind tunnel splits into inlet, outlet and wall. Wind tunnel splits into two halves along Y axis in some of the simulations due to symmetry. After setting the region, each boundary is assigned with a function. They are shown in Table 15.

Type of Boundary	Function
Car, Roof box and box underneath the tyre	Wall
Inlet	Velocity inlet
Outlet	Pressure outlet
Wall	Wall
Symmetry	Symmetry plane

Table 15: Various boundaries and its functionality

3.11. Customizing Surface mesh sizes

The base size of the mesh was 200mm and surface size for each boundary was taken as percentage of base size. Prism layer property was disabled other than car and box. A slip condition was provided to the walls. Table 16 below shows different parameters used in generating the mesh.

Boundary	No: of prism layers	Prism layer stretching	Prism layer thickness (mm)	Minimum surface size (%)	Target surface size (%)
Car	8	1.05	10	1	12
Box	10	1	12	1	5
Box under tyre	8	1.05	10	0.25	2

Table 16: Customized mesh sizes

3.12. Volumetric Controls

Volumetric control over the object was created for refining or coarsening the mesh in that particular volume (CD Adapco 2012). The accuracy of the results increases as mesh density increases. For every simulation 3 volumetric controls were set to refine the mesh near the box and the car. As shown in Figure 23, one volumetric control was over the car and another one over the box. The third volumetric control was flush to the roof box. Both polyhedral and prism layer mesher was activated in those volumetric controls. The relative size of different volumetric controls is shown in Table 17.

Volumetric control	Relative size (% of base size)
Over the car	10
Over the box	10
Snap to the box	5

Table 17: Volumetric control and its relative size

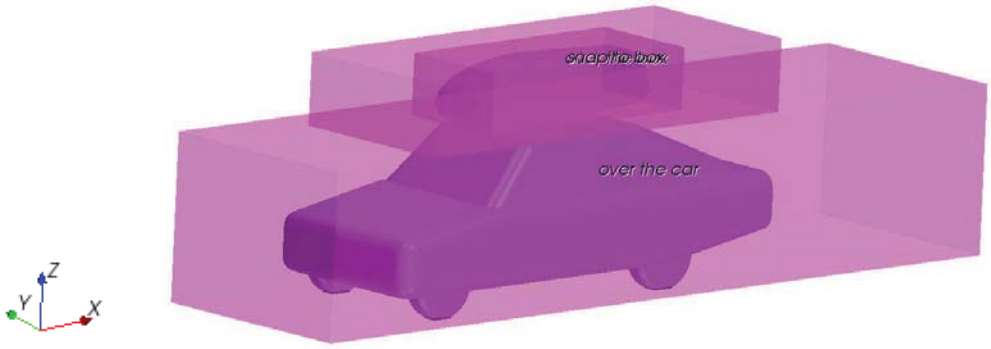

Figure 23: Volumetric controls

3.13. Physics Conditions

In order to set up the physics, one needs to analyse the space, time, motion of the object, material of flow, type of flow, equation of state, viscous regime and turbulence models. There are many types of models which an analyst can select depending up on the type of problem. The physics conditions used are as follows:

There are many reasons in choosing these models. A 3-D mesh was generated for the flow structure analysis. The flow was considered as *steady.* This will eliminate small eddies and reduce the overall computational time. Because the fluid flow around the object is air, option *gas* is chosen. Segregated flow model solves the flow equations (one velocity and one pressure equation) separately. The cell count was over 4 million, and segregated flow model take less time than coupled flow model. For coupled flow,

the flow equations are solved as a combined manner. It will take more time to resolve the equations. The Mach number of the flow was 0.087. The flow was considered as incompressible since the Mach was less than 0.3. So the *density was constant.* The Reynolds number of the flow was much higher than critical Reynolds number. Hence the flow was turbulent. In this research, Reynolds-Averaged Navier-Stokes equation was automatically selected along with turbulent flow model. The k-ε model, RKE model and two layers all Y^+ wall treatment models were selected. The selected models are shown below in Table 18.

Enabled Models	Justification for selecting the model
Three dimensional model	Three dimensional flow structure was analysed
Steady	Flow was considered to be steady
Segregated flow	Less computational time for more cell count
Constant density	Flow was incompressible
Turbulent	Reynolds number was above critical Reynolds number
RANS equation	Refer section 2.5 for more details
k-ε model turbulence	
RKE with two layer	
Two layer All Y^+ wall treatment model	

Table 18: Physics models and reason for selecting the model

3.14. Initial Conditions

Only a few initial conditions need to be provided while using k-ε model. The reference pressure for the entire flow is taken as one atmosphere (101325 Pa).

- The free stream flow velocity was taken as 30 m/s.
- The outlet pressure was considered to be zero Pascal.
- To specify turbulence, three options were available. Out of three, turbulent intensity ($0.01<I<0.1$) and viscosity ratio ($10<\mu_t/\mu<100$) were chosen and the values were used in all simulations were 0.01 and 10 respectively (CD Adapco 2012). The values for k and ε were calculated using the above two values to avoid divergence during initial iterations. It's hard to identify those two values to describe turbulence. Due to this reason, the lowest values of those parameters were chosen. For external flows, it is not possible to determine a good characteristic length (second available option) (Saxena A. 2014).

3.15. Reports and Plots

Report of various functions provides a lot of information in deciding next step. There are many reports developed after running the simulation. In this research, the various parameters are plotted against iterations. Table 19 below shows various parameters analysed through this research.

Forces	Force coefficients	Others
Drag force Lift force	Drag force coefficient Lift force coefficient Pitching moment coefficient Rolling moment coefficient Yawing moment coefficient	Mass flow averaged pressure Frontal area

Table 19: Reports

3.15.1. 3-Dimensional Wireframe Graphs (3-D Surface graph)

This type of graph shows the variation of one factor against other two factors. A sample plot shows the variation of C_D against X and Y direction as can be seen in Figure 24.

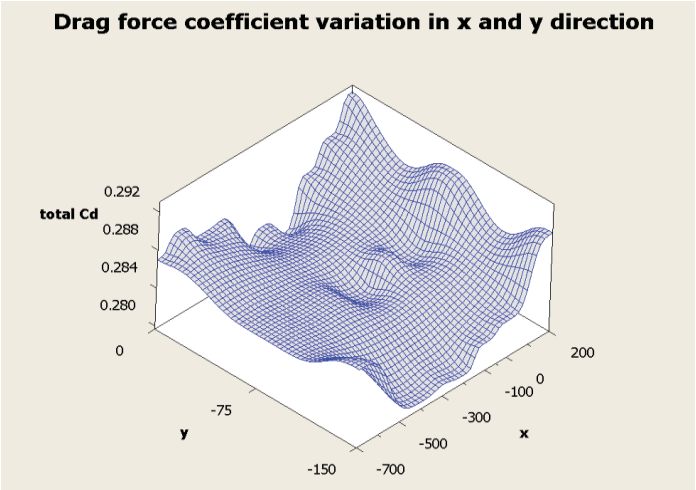

Figure 24: Sample 3-D Surface plot

The drag decreases as Y value varies from 0mm to -150mm. As X value varies from 200mm to -100mm, drag decreases gradually and then increases.

3.15.2. Main Effects of Drag Vs Factors

Figure 25 shows the variation drag force coefficient when X, Y and Z co-ordinates vary for when roof box was kept on squareback car.

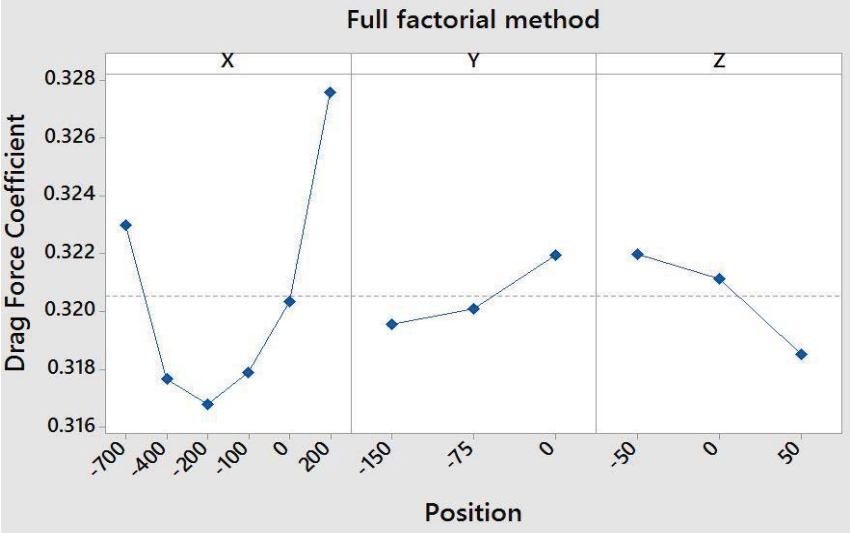

Figure 25: Graph showing various effects

3.15.3. Vector and Scalar plots

Velocity parameter was taken as vector plot in Star-CCM+. Through vector plot, it is easy to find out the localised separation regions and wake regions. Figure 26 shows a vector plot (rear end wake structure of fastback car). A colour bar was also attached to the picture to identify the parameter in that particular area. Scalar plot was generated for various parameters such as pressure, total pressure and its coefficients and wall Y^+. Figure 27 shows the variation of wall Y^+ over the car and box.

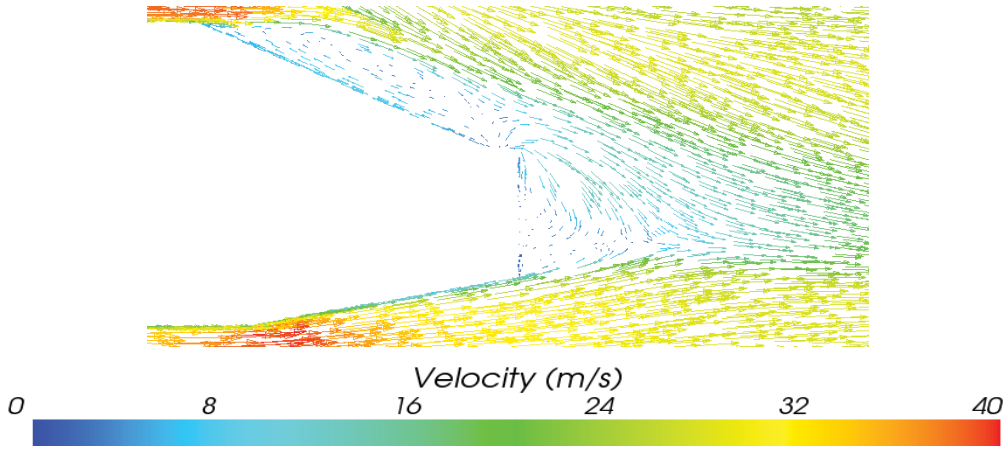

Figure 26: Sample vector plot

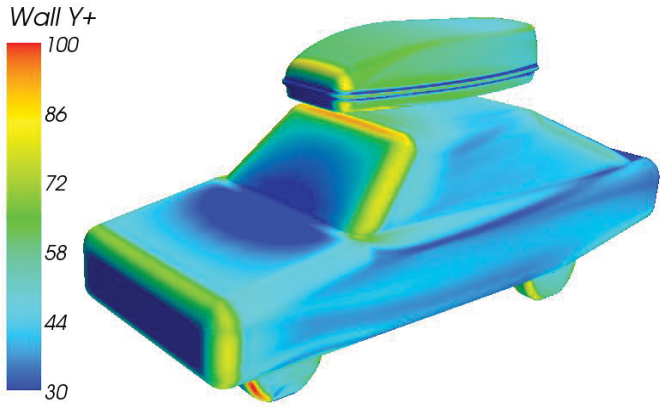

Figure 27: Sample scalar plot

3.15.4. Streamline plots

There are two types of plots namely, streamline and constrained streamline plot. By plotting streamlines, one can study the flow structure in a particular area. The streamline plots in Figure 28 helps to learn more about the exterior flow around the solid body like wake area and vortex generation. Constrained streamlines represents the flow structure on the car and roof box.

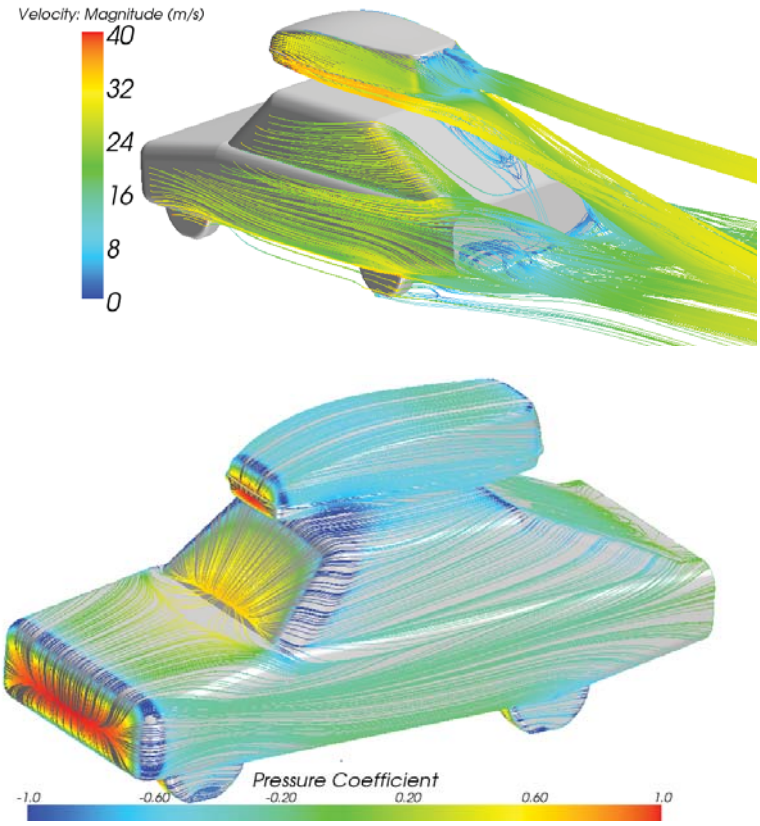

Figure 28: Constrained streamline flow on car and roof box

3.15.5. X-Y Plots

These types of plots are used for analysing different parameters on an object in a particular plane. From Figure 29, one can recognize the low pressure and high pressure regions easily.

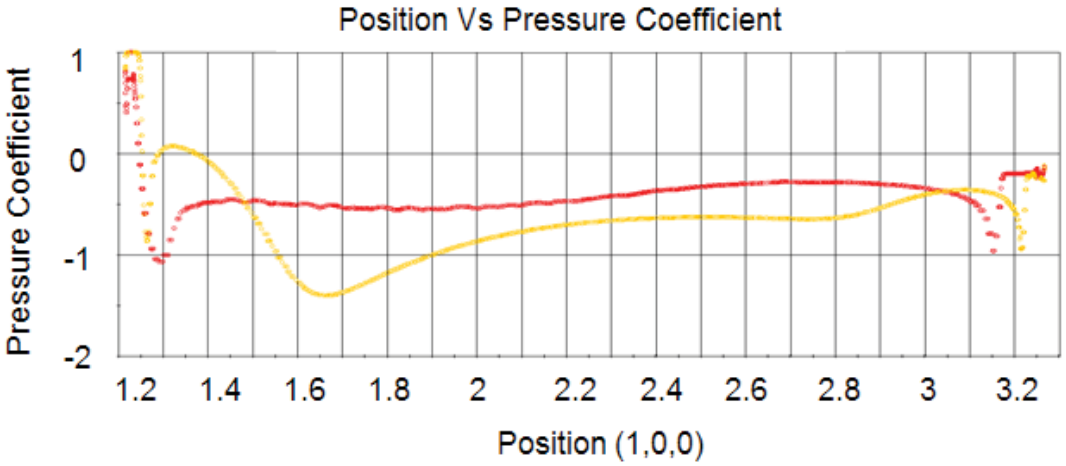

Figure 29: Sample X-Y Plot

3.16. Mesh Sensitivity Study

This study was conducted by varying the base size of the mesh. Table 20 represents the base size used in mesh sensitivity study and the corresponding number of cells obtained in each base size.

Base size (mm)	Number of cells (millions)
500	0.70
400	1.09
300	1.60
200	4.86
180	6.39

Table 20: Number of cells at different base size

As the base size decreases the number of cells increases. Total drag force coefficient of fastback car and roof box at datum position was considered for mesh sensitivity study. Figure 30 below shows the variation of drag coefficient against the base size of the mesh.

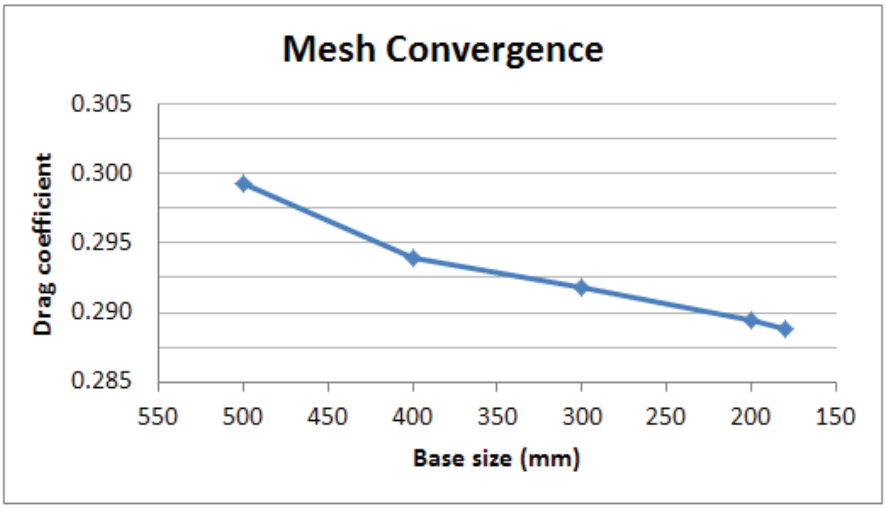

Figure 30: Mesh Convergence

As the number of cells increases the drag coefficient reduces. There was no much variation (less than 1 count) in drag coefficient when the base size varies from 200mm to 180mm. Hence the base size was chosen as 200mm. As the number of cells increases, the computational time increases. The cell count was restricted below 5 million for half wind tunnel simulations since more than 100 simulations need to be conducted. Figure 31 shows the residuals at different base size.

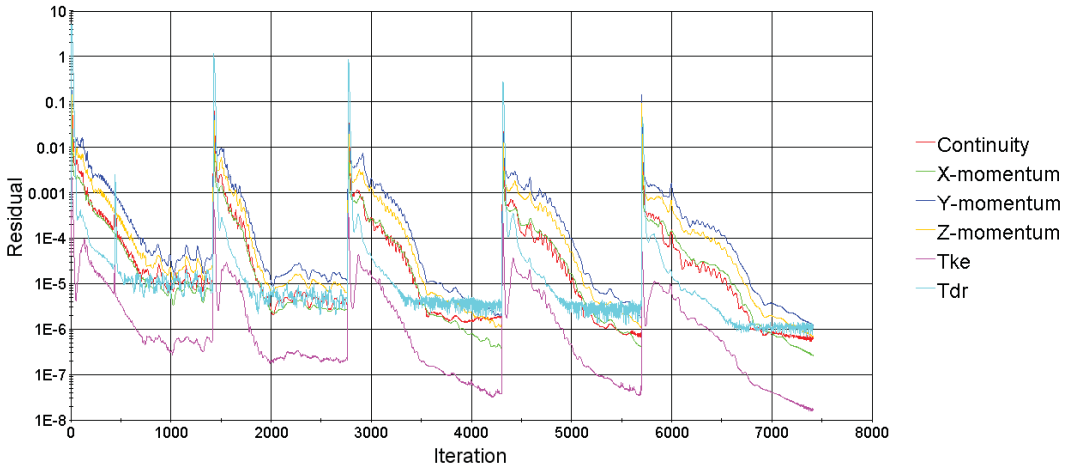

Figure 31: Residuals

Each peak in the above figure represents the residuals at different base size ranging from 500mm to 180mm as mentioned in Table 20. All the residuals were below 10^{-4} and they were fluctuating after some iteration.

3.17. Material selection

In the early stage of manufacturing of roof box, thermoplastics were used (Happian-Smith 2001). Meantime, the manufacturers started adding filler material for more strength and weight reduction. Recently, Thule developed a roof box for Koenigsegg Agera R with 100% carbon fibre (Thule 2014). The cost is high because carbon fibre sheets are very expensive. The common materials and their properties along with an approximate cost are shown in Appendix II.

"The principal attraction of composite materials is that they are lighter, stiffer and stronger than most other structural materials" (Happian-Smith 2001). Even for highly complicated shapes, plastics are easy to mould (Norbye 1984). While using the filler material, the overall manufacturing cost increases. Different kinds of materials are designed by adding different composition of filler materials. Sometimes, more than one filler material is used to attain specific property. They are shown in Appendix II. Even though filler materials increase the density of the composite material, it drastically increases overall strength, stiffness and ductility of polymers. When compared to metal, the stiffness to weight ratio is poor and it has an acceptable strength to weight ratio (Happian-Smith 2001). To achieve those properties, fillers are added to form composite material. Not only composition of filler material but also form of the material will decide its properties. Various forms such as unidirectional, biaxial, quasi-isotropic, short and long fibre, particulate and laminated structures are available in the market (University of Cambridge 2013). Carbon fibre is the best filler material to improve the strength of the material. The cost of material increases according to the composition of carbon fibre. One cannot decide the material for roof box straightaway. In order to select a material, various trial and error experiments should be conducted.

3.18. Manufacturing Methods

Several methods are followed in the production of roof box using polymers or composites. Two manufacturing processes mainly used in the production of roof box are mentioned below.

3.18.1. Thermoforming

This is one of the processes used for shaping thermoplastic sheets. The polymers that are recommended through this technique are ABS, PS, PC, PET and short fibre reinforced thermoplastics.

Thermoforming sheets are heated in an oven to a desired temperature. Then the sheets are placed into the mould and stretched into a preferred shape and finally it is cooled to attain the final shape. Roof box requires thick gauge thermoforming technique (t>3mm) (University of Cambridge 2013). If the box is less than a specified thickness, it will rattle in normal motorway speed.

In vacuum forming, the sheet is heated to a required temperature. Then the air between the sheet and the mould is sucked using a vacuum pump. This will allow the sheet to follow the structure of the mould. Thermoforming is clearly explained in Figure 32. Depending on the material some solvents are used on the mould for it not to stick on the surface. In plug-assisted thermoforming, a male or female die is used along with vacuum forming. Using this method, 6mm sheet thickness can be formed (University of Cambridge 2013). With this method, the final products will have excellent physical properties. The manufacturing cost using this method is moderate because the relative tooling cost and relative equipment cost is lower than manufacturing methods. It is useful for both small and large batch production (University of Cambridge 2013).

3.18.2. Injection Moulding

This method is common in the production of equipment in various fields. The material is added to the machine in the form of granules. The machine consists of a screw which injects the material into the mould with high pressure and velocity with the help of a reciprocating screw. A particular amount of polymer will be injected into the mould with a certain velocity and pressure. Every activity in this process is in a controlled manner. Above mentioned procedures are shown in Figure 32. The obtained shape will have a good surface finish (University of Cambridge 2013). The overall manufacturing cost for each product is low even if it has high tooling cost and equipment cost. The variation of the cost depends on the size, complexity and surface finish of the product. So this is more suitable for high batch of runs.

This item has been removed due to 3rd Party Copyright. The unabridged version of the thesis can be viewed in the Lanchester Library Coventry University.

Figure 32: Thermoforming and Injection moulding (University of Cambridge 2013)

3.19. How to Design an Experiment in MINITAB?

The following steps are to be considered while designing an experiment.

- *Identifying the factors* that affect the performance of the product,
- *Decide number of levels* for each factor. The performance may vary linearly, parabolic or even with higher order. If it is linear, the number of levels need to be provided is 2. It should be higher according to the relation between performances of the object and factor (Ryan, Joiner and Cryer 2005).
- *Selection of orthogonal array.* According to the number of factors and levels, one can choose the number of runs.
- Before conducting the experiment, *providing the independent variables to each column.*
- *Provide the results to successive column.*
- *Run the experiment.*
- *Analyse the data from various results and infer from it.*

Figure 33 below shows a L9 (3**3) set of experiments which contain 3 factors and 3 levels in each factor. Inside the brackets, the first term represents the number of levels and the last term denotes the number of factors. In general full factorial design, the number of runs was 27 with the same number of factors and levels.

↓	C1	C2	C3	C4
	x	y	z	Cd
1	1	1	1	0.2682
2	1	2	2	0.2622
3	1	3	3	0.2609
4	2	1	2	0.2608
5	2	2	3	0.2713
6	2	3	1	0.2760
7	3	1	3	0.2569
8	3	2	1	0.2666
9	3	3	2	0.2651

Figure 33: Sample data for L9 (33)**

3.20. Procedures Followed in MINITAB

Results from different simulations were required to validate MINITAB. In the above section, it was specified that the roof box is tested in various positions. Testing all the positions was time consuming. So a selected number of positions were tested and validated using them. Other than validating the software, optimizing the position of roof box was also required. In MINITAB, different positions were considered as factors and number of values in each position was considered as levels in both Taguchi and

factorial design. In fastback and notchback car, there are 3 factors and 3 levels on each factor. In squareback car, more positions were considered in X direction. Selected positions and number of runs are shown in Table 21. Results of number of simulations for validating MINITAB using full factorial and Taguchi method are shown in Table 22.

Car type	Position (mm)		
	X	Y	Z
Fastback, Notchback	-200, 0, 200	-150, -75, 0	-50, 0, 50
Squareback	-700,-400,-200, -100, 0, 200	-150, -75, 0	-50, 0, 50

Table 21: Selected Positions of full scaled roof box

Type of Car	Number of runs	
	Full factorial design	Taguchi design
Fastback / notchback	27	9
Squareback	54	18

Table 22: Number of runs in validation process of MINITAB

3.21. Estimation of Excess Power Consumption

To estimate the excess power consumed due to roof box by considering aerodynamic force and weight of a fully loaded box, following equation is used. This is the equation for engine horsepower using trap speed method (Raymond 2012).

$$Horsepower = weight * \left(\frac{velocity}{234}\right)^3 \quad kW$$

Equation 7: Horsepower calculation (Raymond 2012)

4. Results

4.1. Validation of CFD Results

In this section, the MIRA reference car data were validated using the results obtained from different simulations. In some simulations, the car and the box were symmetry along Y axis. The simulations were performed using a symmetry plane and forces were doubled when tabulated. There was a minor change in the results while following that procedure. A simulation is said to be converged as the residuals of the simulation tend to zero. As it is time consuming the solution is considered to be converged when the residuals drops below 10^{-3} and remain constant in that in the following iterations (Franke et.al. 2007). The wind tunnel test data from LCVTP for MIRA cars were taken as reference. Corrections for wind tunnel blockage were applied on the CFD results. The deviation in drag of car without roof box and MIRA car was calculated using Equation 8 and the values were shown in Table 23.

$$\%\ deviation = \frac{Car\ drag\ coefficient - Reference\ car\ drag\ coefficient}{Reference\ car\ drag\ coefficient} * 100$$

Equation 8: % Deviation in drag from MIRA car

Type of car	Reference car C_D	Car C_D	Deviation (%)
Fastback car	0.230	0.2155	-6.30%
Notchback car	0.277	0.2543	-8.30%
Squareback car	0.329	0.3120	-5.16%

Table 23: Comparison of previous data with CFD results of half wind tunnel

The deviation in drag of half car to that of full car was calculated using Equation 9 and the values were shown in Table 24.

$$\%\ deviation = \frac{Full\ car\ drag\ coefficient - half\ car\ drag\ coefficient}{Reference\ car\ drag\ coefficient} * 100$$

Equation 9: % Deviation in C_D between full car and half car

Type of car	Total C_D		Deviation (%)
	half car	full car	
fastback car	0.2155	0.2167	0.52%
Notchback car	0.2543	0.2451	-3.32%
squareback car	0.3120	0.3033	-2.64%

Table 24: Variation in full car and half car CFD simulations

Total error was calculated by adding the deviations from Table 23 and 24. The % total deviation was shown in Table 25.

Type of car	total error
Fastback car	-5.78%
Notchback car	-11.62%
Squareback car	-7.80%

Table 25: Total error in CFD results of various class of geometries

The CFD results of original half box and full box along with the deviation was organised in Table 25.

Total C_D		Deviation (%)
half car	full car	
0.1563	0.155	-0.8%

Table 26: Variation in full box and half box CFD simulations

The negative value indicates that the CFD under-predicts the C_D value.

4.2. Estimated Skin Friction Drag on Car and Roof Box

An estimated skin friction drag was calculated using Equation 5 in section 2.6. The estimated friction drag for different cars and roof box were shown in Table 27.

Type	Estimated friction drag	% of total drag
Fastback car	0.0313	14.45
Notchback car	0.0312	12.71
Squareback car	0.0328	10.82
Roof box	0.0364	23.47

Table 27: Estimated friction drag

The effect of friction drag in overall C_D of roof box was 24% and remaining 76% was due to pressure difference. For MIRA cars, the friction drag was less than 15% of overall drag.

4.3. Position variation of Roof Box

The initial part of the research involves the positioning of roof box relative to the car. Various locations were investigated. In datum position (0,0,0), the box overhangs nearly 650mm to the front and rear from the clamping point. The data investigated was as follows.

- Drag coefficient on car and box,

- Total and corrected drag coefficient using frontal area of car,
- Deviation and % deviation in C_D from car alone,
- Pitch, roll and yaw moment coefficient.

The lift coefficient was also investigated. The results show that there was a change in lift coefficient due to roof box. When the weight of the roof box and belongings were considered, the change in lift coefficient was negligible. It was impossible to predict rolling and yawing moment coefficient for some cases because the simulations were completed using half wind tunnel. A colour code was applied inside the table to easily understand the position where the highest and lowest drag was occurred. The *blue colour* represents *lowest drag* produced and *red colour* indicates *highest drag* generated due to box. The results were tabulated in Appendix III.

4.3.1. Position variation in X Direction

Figure 34 shows the drag coefficient of various cars in X direction. Thick graph lines in this figure show the C_D of car with box and transparent line shows MIRA reference car drag coefficient. Here Y and Z positions were constant and it was 0mm.

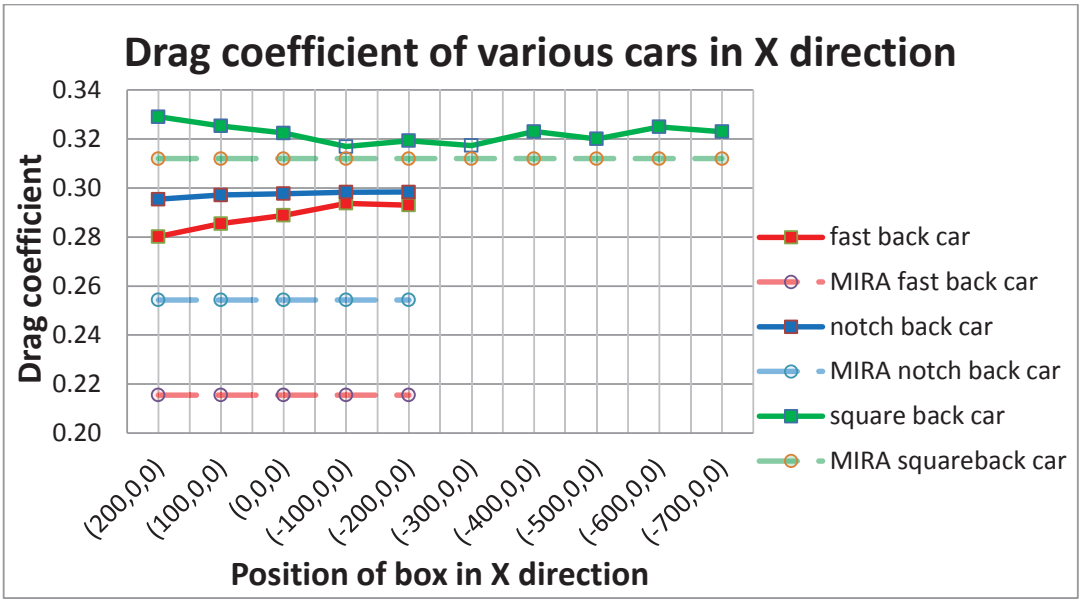

Figure 34: C_D of various cars in X direction

When roof box was positioned at rear of fastback car, overall C_D value increases. When compared to MIRA reference data, there was a variation of 30-36% in C_D value due to roof box. There was a minor change in drag coefficient when the box was

positioned at five different locations on notchback car along flow direction. The corrected drag was in the range of 0.295-0.298.

The total drag coefficient of the squareback car and box was fluctuating and there was no characteristic trend when compared to other cars. When the values was checked individually, the drag on the car increases by 26 counts from extreme front position to (-400,0,0) and then decreases by 18 counts when the box was placed towards extreme rear. The lowest drag generated due to squareback car when the roof box positioned in X direction was placed at (-100,0,0).

The trends in drag coefficient for fastback car was increasing in nature when the roof box positioned from (200,0,0) to (-200,0,0) and vice versa for squareback car. The C_D value was constant for notchback car with roof box.

4.3.2. Position Variation in Y Direction

The results at different Z and X positions were classified according to the distance from the roof of the car. It can be identified using 3 colours. They are shown in Table 28 below.

Drag coefficient	Position	% deviation
Z=0mm	Datum	% deviation- Z=0mm
Z=50mm	Extreme top	% deviation- Z=50mm
Z=-50mm	Extreme bottom	% deviation- Z=-50mm
X=0mm	Datum	% Deviation-X=0mm
X=200mm	Extreme front	% Deviation-X= 200mm
X=-200mm	Extreme rear	% Deviation-X=-200mm

Table 28: Representation of colours in results

Thick line in the above table represents the drag coefficient (values in primary axis) and dashed transparent line shows the % deviation of drag from car without roof box (values in secondary axis).

4.3.2.1. Fastback Car

The graphs in Figure 35 below shows C_D and % deviation when the box was placed at X=0mm, 200mm and -200mm and variation in Z direction at different Y positions on fastback car. The legends in Figure 35 are represented in Table 28.

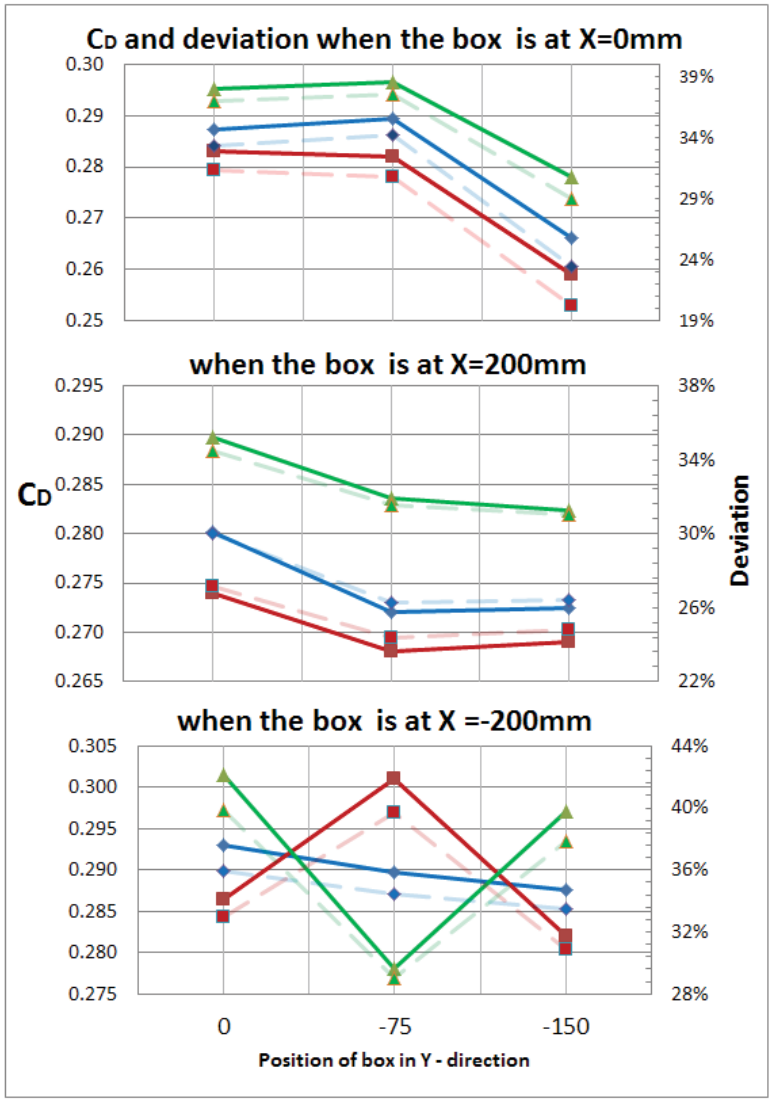

Figure 35: C_D and % deviation when the box was positioned at X=0mm (top), X=200mm (middle), X=-200mm (bottom) and variation in Z direction on fastback car

When the box was positioned to the left side of the car from datum point by 75mm, the drag slightly increases initially and then decreases by 10% as it positioned 75mm further. When the box was placed at (0,-150,50), the C_D value recorded the lowest (0.259). When the box was positioned at extreme front position, the C_D value decreases and then remains constant. When the box was placed at extreme front or

datum position and shifts away from the roof of the car, drag recorded the lowest when compared to other positions. At extreme rear position, Z=50 and -50mm shows opposite trend. At Z=0mm, the drag decreases as the box was positioned away from datum in Y direction.

4.3.2.2. Notchback car

Figure 36 below shows C_D and % deviation when the box was placed at X=0mm, 200mm and 200mm and variation in Z direction at different Y positions on notchback car. The legends in Figure 36 are represented in Table 28.

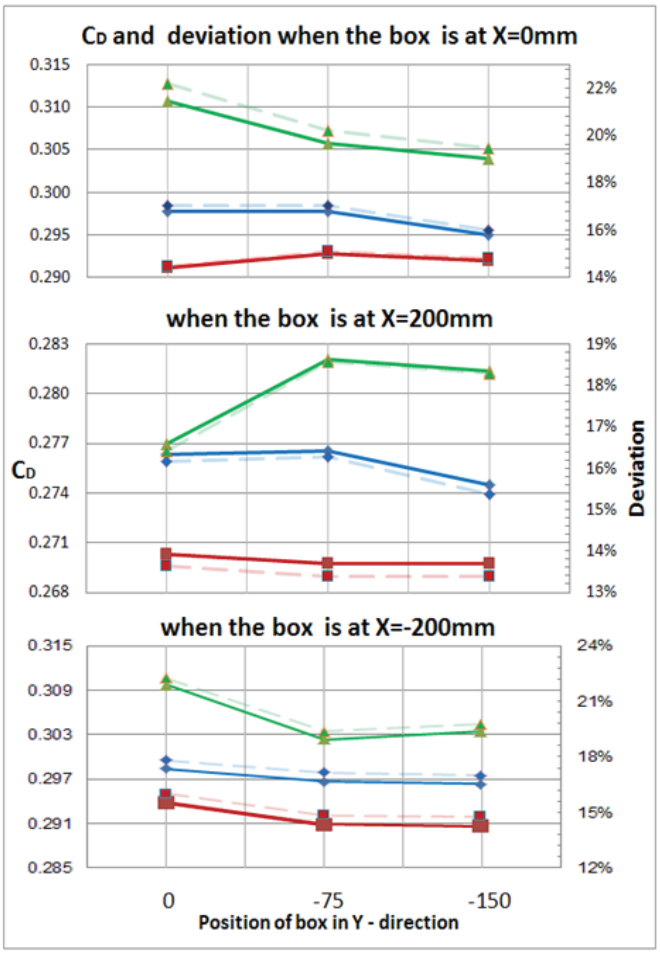

Figure 36: C_D and % deviation when the box was placed at X=0mm (top), X=200mm (middle), X=-200mm (bottom) and variation in Z direction on notchback car

From all set of simulations over notchback car in the graph mentioned above, the position of roof box with highest drag obtained was at extreme bottom position and the lowest drag was placed at extreme top position. When the box was positioned from (200,0,-50) to (200,-75,-50), C_D value increases by 3% and remains constant. When

the box was positioned at (0,Y,-50), drag coefficient decreases. When the box was placed at extreme top from datum position, the drag coefficient remains constant. The C_D value remains constant from 0mm to 75mm towards left in Y direction and then decreases when the box was placed at (0,Y,0) and (200,Y,0).

4.3.2.3. Squareback Car

Figure 37 shows C_D and % deviation at six different X positions (200mm, 0mm, -100mm, -200mm, -400mm, -700mm) and variation in Z direction at different Y positions on squareback car. The legends in Figure 37 are represented in Table 28.

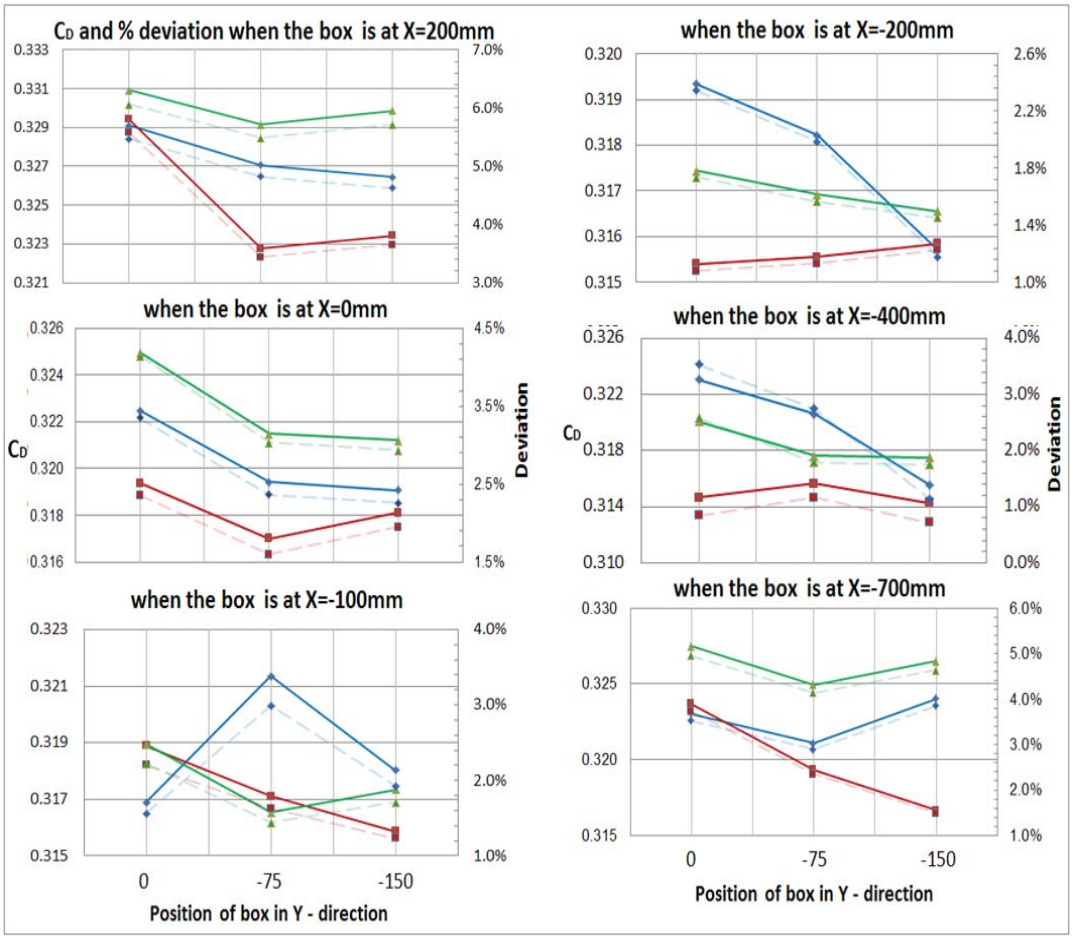

Figure 37: C_D and % deviation when the box was placed at X=200mm (top left), X=0mm (middle left), X=-100mm (bottom left), X=-200mm (top right), X=-400mm (middle right), X=-700mm (bottom right) and variation in Z direction on squareback car

When the box was placed at datum, extreme front position and 50mm away from datum position in Z direction (away from roof of the car), the C_D value decreases initially and then slightly increases when the box was positioned along Y direction from

datum. In the case when the box was placed at (-100,Y,50) and (-700,Y,50), the drag value was always decreasing. The position of roof box in which lowest drag generated was at (-400,-150,50). This was around 0.75% variation from squareback car. When the box was positioned at (-100,Y,0) and (-100,Y,-50), the drag variation from squareback car shows opposite trend.

4.3.3. Position variation in Z Direction

Figure 38 displays C_D and % deviation in various X positions on fastback, notchback and squareback car at 5 different Z positions. Here Y position was constant (0mm). The legends in Figure 38 are represented in Table 28.

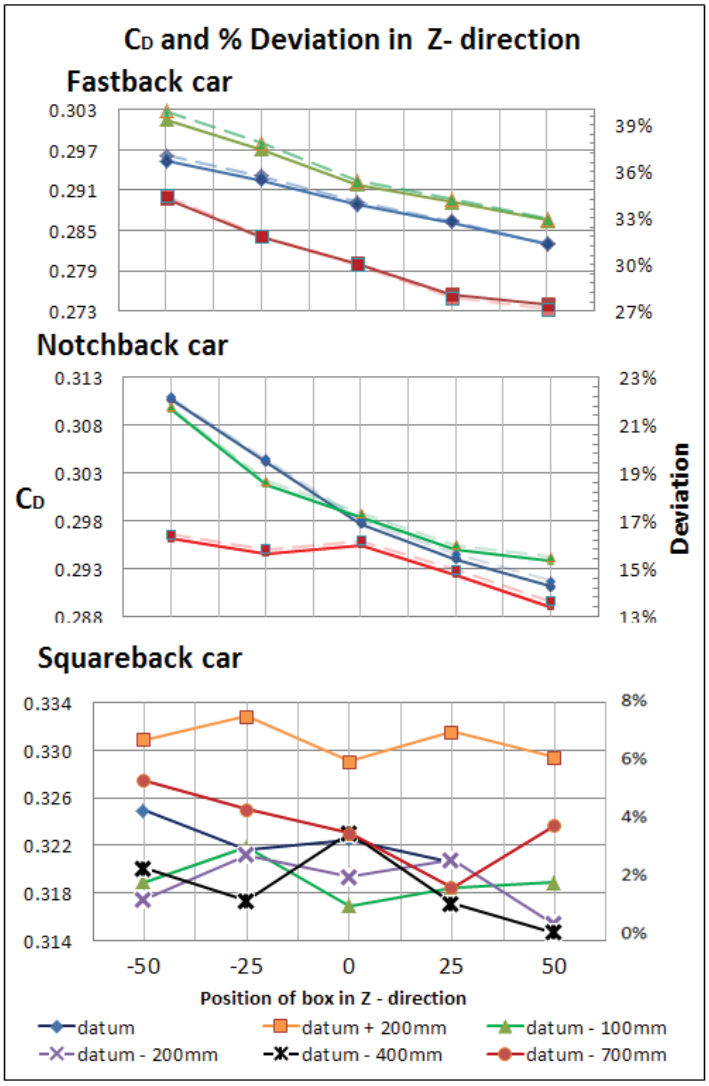

Figure 38: C_D and % deviation in various X positions on fastback (top), notchback (middle) and squareback car (bottom)

For a fastback car, when the box was positioned from (X,0,-50) to (X,0,50), drag coefficient always reduces at 3 different X positions. The position where the maximum deviation from fastback car occurs at (-200,0,-50) and it was nearly 40%.

When the box was positioned from (200,0,-50) to (200,0,0) on a notchback car, the drag remains constant. When the box was positioned from (-50)mm to 50mm in Z direction (with respect to datum position) at datum and extreme rear position, the drag decreases by 7%.

For squareback car, when the box was positioned at extreme front position, the overall drag generated was much higher than any other positions. Highest C_D value was obtained at extreme front position (30 counts). 75% of the result shows that the effect of roof box was less than 4% drag of squareback car. No common trend was occurred in this graph.

4.4. Results of Roof Boxes Implemented in this Research

The drag force and coefficient generated due to the different roof box were shown in Table 29.

Type of box	Total drag force	Total C_D
Original box	30.08	0.1563
Scaled box	18.52	0.1415
Scaled re-designed box	23.94	0.183
Scaled re-designed box with 2^0 taper	20.78	0.1589

Table 29: C_D of various roof boxes

The C_D value for re-designed scaled box was nearly 40 counts higher than that of scaled box. There was less variation in drag coefficient when a taper was included underneath the roof box. The drag was reduced by 25 counts due to 2^0 taper from above mentioned case.

4.4.1. Fastback Car

Figure 39 shows the drag coefficient of various type of boxes at different X positions when Y=0mm and Z=-50mm on a fastback car.

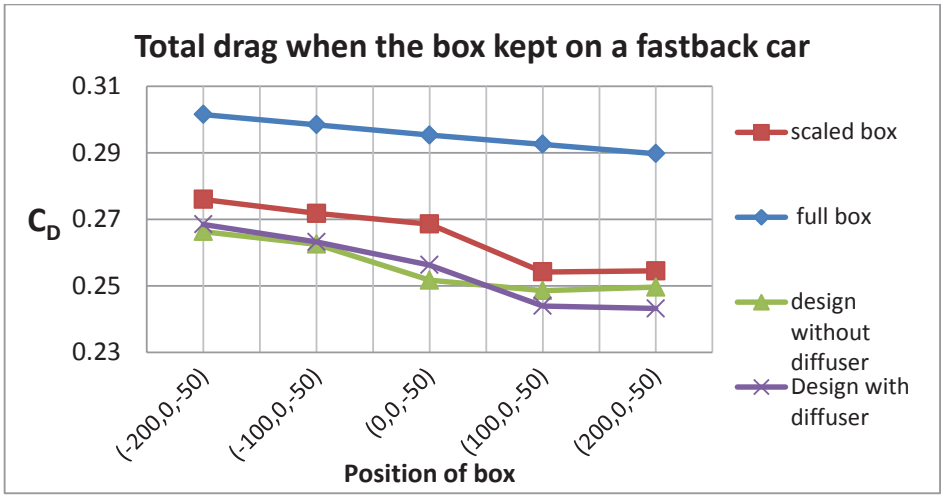

Figure 39: Total C_D when roof box kept on fastback car

When roof box was positioned from rear to front, drag decreases by 10-20 counts. There was some significant variation due to taper when the box was positioned towards the front from datum. As the roof box was positioned towards the rear, there was no much effect due to taper angle. When C_D value was analysed between scaled box and box without taper, there was a decrease of 6 counts of drag initially. The re-designed roof box with 2^0 taper was effective in only two positions, which were (200,0,-50) and (100,0,-50). The drag at these positions was almost same.

4.4.2. Notchback Car

Figure 40 shows the drag coefficient of various type of boxes at different X positions when Y=0mm and Z=-50mm on a notchback car.

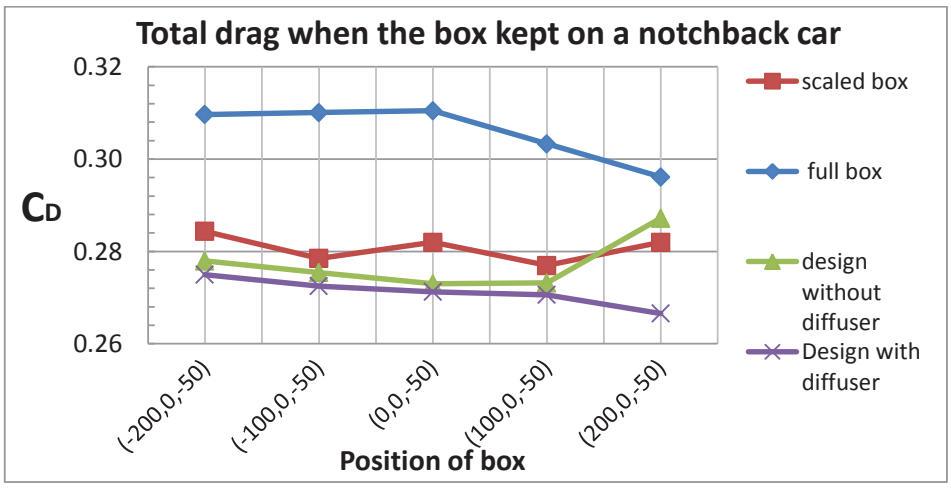

Figure 40: Total C_D when roof box kept on notchback car

The drag due to taper in roof box was less than that of other design over notchback car and all positions were favourable. When full box and scaled box was compared, the drag remains constant till datum from rear and decreases when the box was positioned to the front. The drag coefficient fluctuates in a zig-zag manner when a scaled box was placed on notchback car at (X,0,-50). When roof box without taper was placed on notchback car, the drag decreases gradually as it positioned from rear to front. When the roof box was positioned from (100,0,-50) to (200,0,-50), the C_D value increases by 5% of notchback car. This same trend was expected when a taper was added to roof box. But, it provides a different result. A constant reduction of 2-3 counts of overall drag was generated due to taper. Instead of increasing the drag at the last position, the drag was reduced by 4 counts.

4.4.3. Squareback Car

Figure 41 shows the drag coefficient of various type of boxes at different X positions when Y=0mm and Z=-50mm on a squareback car.

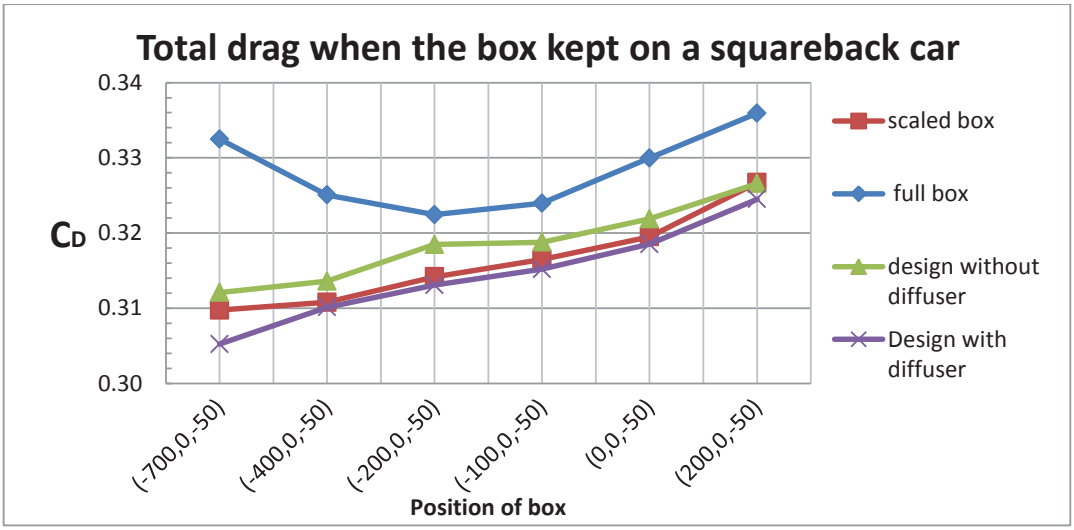

Figure 41: Total C_D when the roof box was on squareback car

Drag generated at (-200,0,-50) was lowest when a full sized roof box was placed on squareback car. The trends were bit different for other designs. When a scaled or newly designed box was placed over the car, the lowest drag was obtained at the extreme rear position from datum. There was only a minor difference in drag coefficient due to taper. The drag deviation due to taper was nearly 3 to 6 counts of drag which was very small when compared to total drag. All the results were tabulated in Appendix III.

4.5. Results of Roof Box with Different Taper Angle

In order to identify which taper angle was better for optimum drag and internal volume, different taper angle were experimented. The positions were selected such that the drag obtained was lowest from section 4.4. For fastback and notchback car, the drag was lowest when the box was placed at extreme front position and extreme rear position for squareback car. For each degree of taper angle, there will be a reduction of 2.5L from total volume. The results are shown in Table 30 and the graphs are represented in Figure 42.

Lowest drag position	(200,0,-50)		(200,0,-50)		(-700,0,-50)	
Angle /Car	Fastback car	% variation	Notchback car	% variation	Squareback car	% variation
0	0.25	0.0%	0.287	0.0%	0.307	0.0%
1	0.244	-2.2%	0.265	-7.7%	0.297	-3.1%
2	0.243	-2.8%	0.267	-7.0%	0.3	-2.3%
3	0.237	-5.1%	0.262	-8.8%	0.296	-3.5%

Table 30: Drag and % variation of 3 MIRA cars with different taper angle on roof box

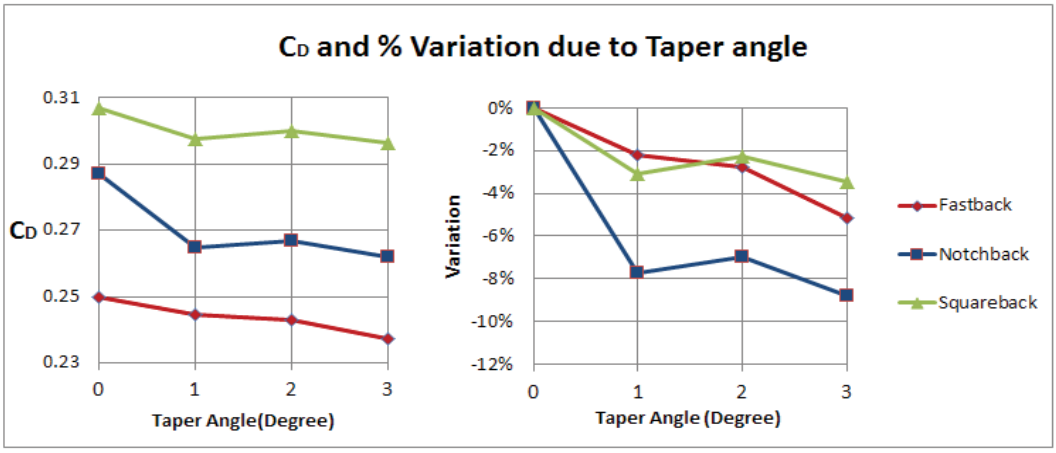

Figure 42: C_D and % variation due to taper angle

When the roof box was placed over fastback car and the taper angle was varied from 0 to 3, the drag decreases constantly by 5%. For notchback car and roof box with a taper angle of 1^0, the overall drag decreased by 8%. As the taper angle increases, the drag value fluctuates and then decreased to 9% of notchback car. For squareback car, C_D value fluctuates as like notchback car, but the values were in the range from 0-4%.

5. Analysis

The only reference for this research was C_D value of MIRA vehicle geometries. These reference values were corrected for blockage. These results were validated using available computational power. Even the results were under-predicted; they were satisfactory with the existing computational power.

More than 100 simulations were considered to find out the exact position where C_D was lowest for different MIRA cars. Also, the lowest and highest drag coefficient position of roof box on three car geometries was examined. The following analysis was classified according to the type of the car. The shape of the roof box was critical in terms of aerodynamics. The front portion of the top part was created such a way that the air can easily travel without deflecting the direction too much from the free stream flow direction. All sharp edges were cornered to avoid localised flow separation and it is shown in Figure 43.

Figure 43: Final design of roof box

An estimated study of skin friction coefficient was calculated to check the contribution of and friction drag. Friction drag was lowest for squareback car in terms of percent format. This was nearly 10% of the total drag coefficient. For notchback car, there was an increase of 2%, but the actual drag was 0.0016 less than squareback car. This was because of lesser surface area of notchback car. Upon considering the fastback car, the friction coefficient was nearly 0.0313. Friction coefficient varies according to the speed of the vehicle (Hucho 1998).

5.1. Fastback Car

5.1.1. X Direction

Figure 44 shows the wake behind the car and box when the box was placed at extreme front and rear positions.

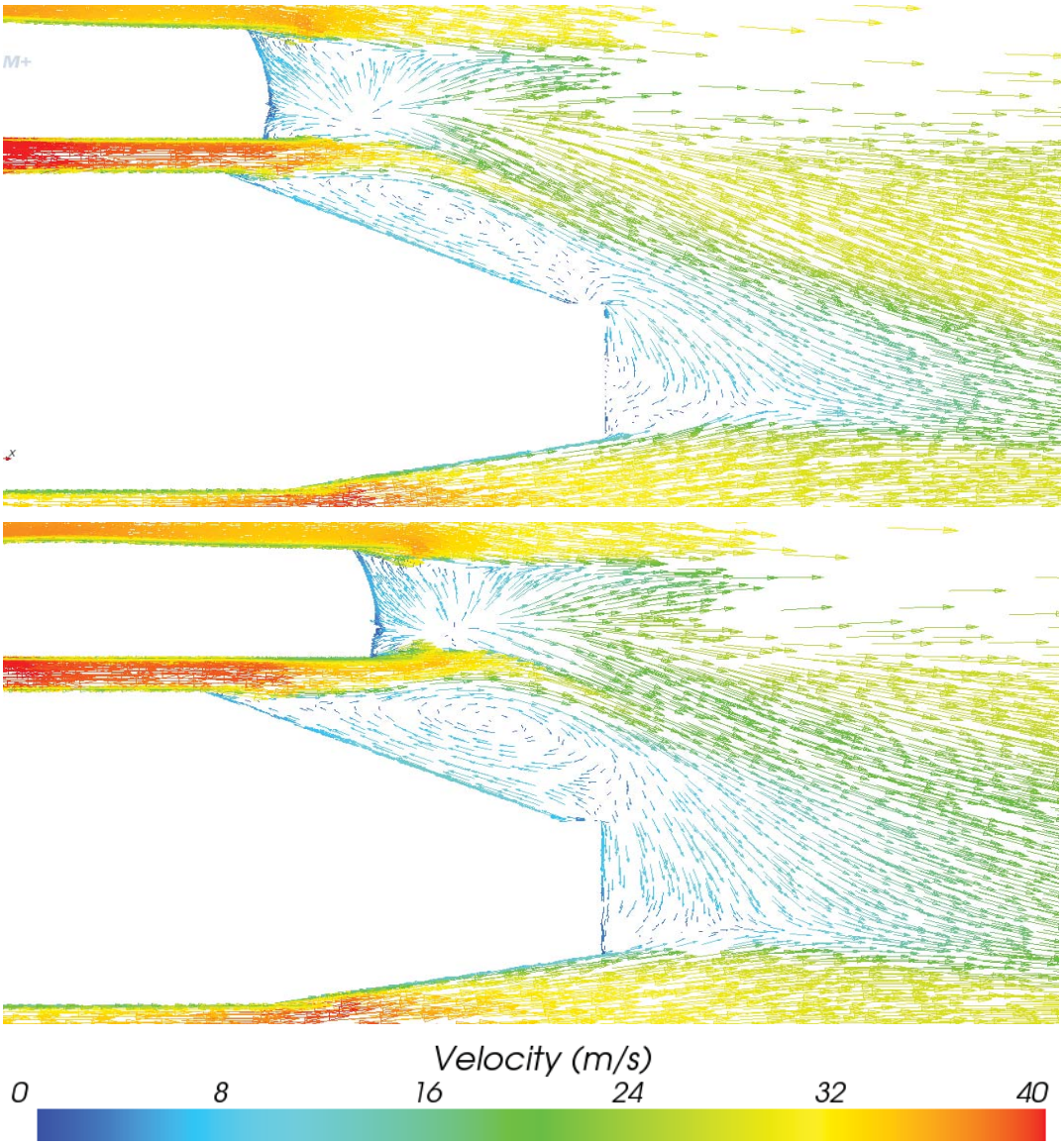

Figure 44: Comparison in wake region when the box was placed at extremes

While positioning the box to the front from datum position, the force acting on the car and box decreases. C_D value due to car with roof box was 30% higher than fastback car without roof box, when the roof box was placed at extreme front position. Nearly one-fourth of the overall drag was contributed due to roof box. When the box shifts toward the rear by 200mm from datum position, overall C_D increases when compared

to extreme front position (44 counts). In this case, most of the drag was due to car. Thus the effect on car due to box was higher than that of roof box at extreme front position. When the box was placed at extreme rear position, the smooth flow above the car was disturbed. The size of low pressure region over the rear wind shield of fastback car increases. The pressure difference around the car was higher when compared to car without roof box. Thus overall C_D value increases.

The car always pitches towards front due to roof box. The flow through the gap between the box and the car continues to some distance and merges with the free stream flow, when the box was placed at extreme front position. When the box was positioned at extreme rear position, the air flow through the gap travels to some distance with the same velocity and diminishes into the low pressure region. When the box was placed at front position, two small vortices on the sides, one near to the bottom portion of roof box and another along the rain guard were generated. These were generated from the front of the box. It was one of the factors in increasing the C_D on the box. This vortex flow makes little disturbance in the rear flow of the car. When the box positioned toward rear, side vortices disappear.

Figure 45 below provides the information of C_P on the upper side of the box in three different positions.

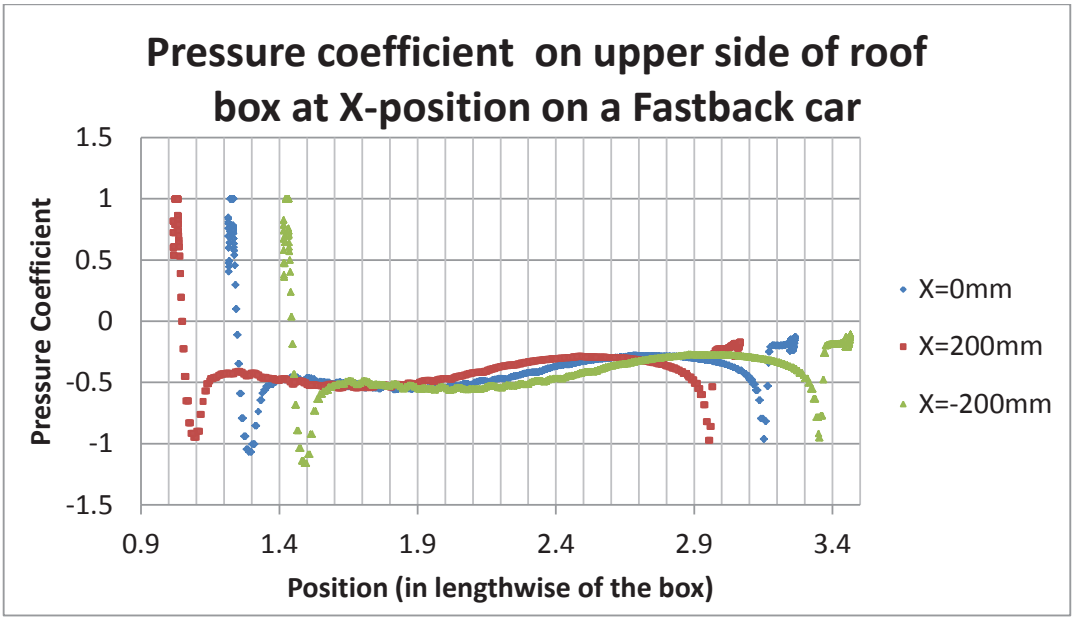

Figure 45: C_P on roof box upper side at different position on fastback car

The initial peak in the graph represents the stagnation points. Most of the points generated in the above mentioned graph were below zero. The pressure coefficient reaches the maximum at beginning (stagnation area) and suddenly drops to -1. The rapid decrease in C_P value shows that velocity obtained in that portion was much higher than free stream velocity. The C_P value decreases at the end of roof box. This was due to the reverse flow behind the box. All other areas of the plots shows same trend.

5.1.2. Y Direction

Figure 46 shows the streamlines and vortex around fastback car and roof box at 3 different Y positions (Y=0mm, -75mm, -150mm) when X=0mm and Z=50mm.

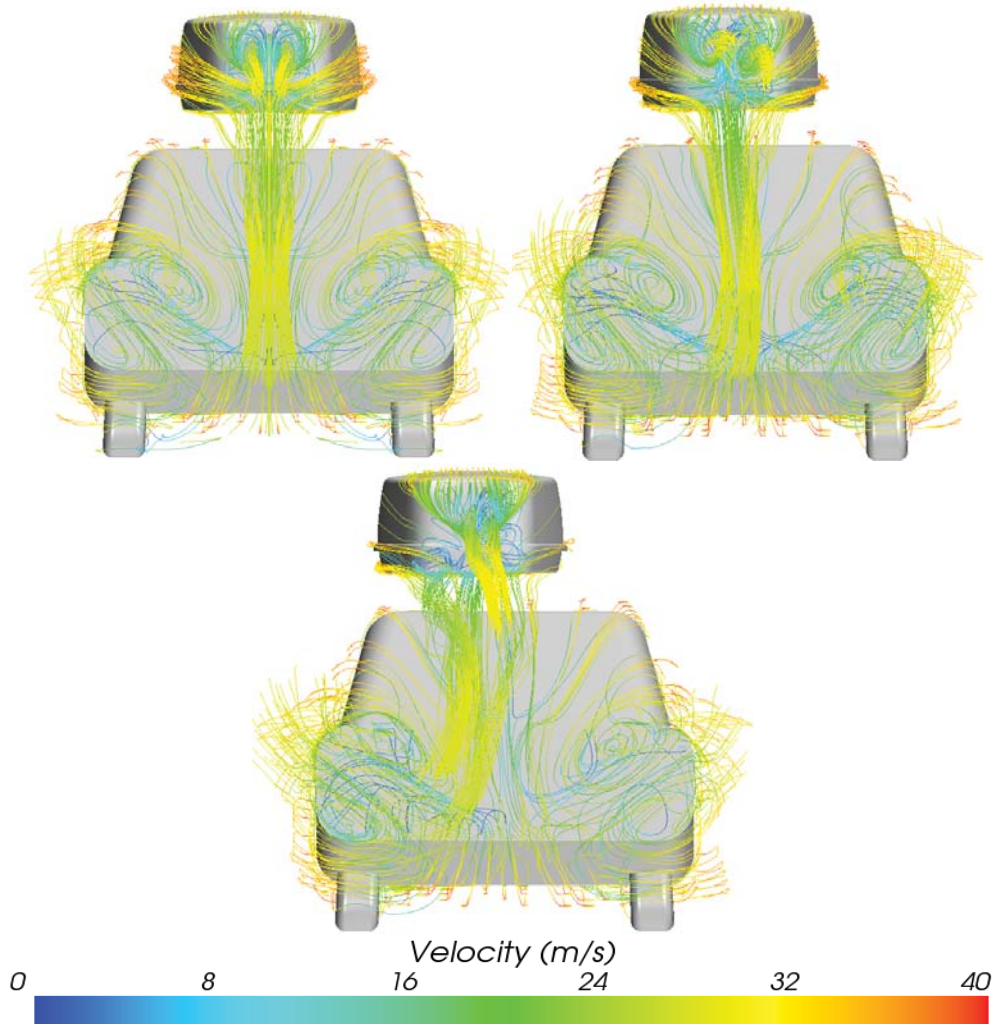

Figure 46: Vortex generation in three different positions when X= 0mm, Z=50mm and Y position varies, box was placed at datum position (top left), box was shifted by 75mm to the left (top right) and box was shifted by 150mm to the left (bottom)

When the box was placed at datum position, the flow over the box and car was symmetry along ZX plane. Due to the positioning of the box, the vortex was slightly shifted to the left of the car. When the box was positioned towards left, the size of the vortex generated in that side reduces compared to other. The flow structure was no longer symmetry along Y axis as the box was positioned to either side. When the roof box was placed to the farthest position, the flow deflects away from the centre line. When the box was positioned to extreme left, the flow on the right side over the car was not much affected. Hence drag coefficient reduces.

The car was always pitching downwards because all the values recorded were negative. The car will tend to roll to the left when the box was positioned to that side. The magnitude of pitching moment coefficient decreases when the box placed to the left side of the car. The pitching moment coefficient was considerably high when compared to rolling and yaw moment coefficient. The rolling and yaw moment coefficient was negligible since it was in the order of 10^{-3}.

Figure 47 shows the 3-D graphs of fastback car and roof box at various positions by considering the variations in X and Y when Z was constant.

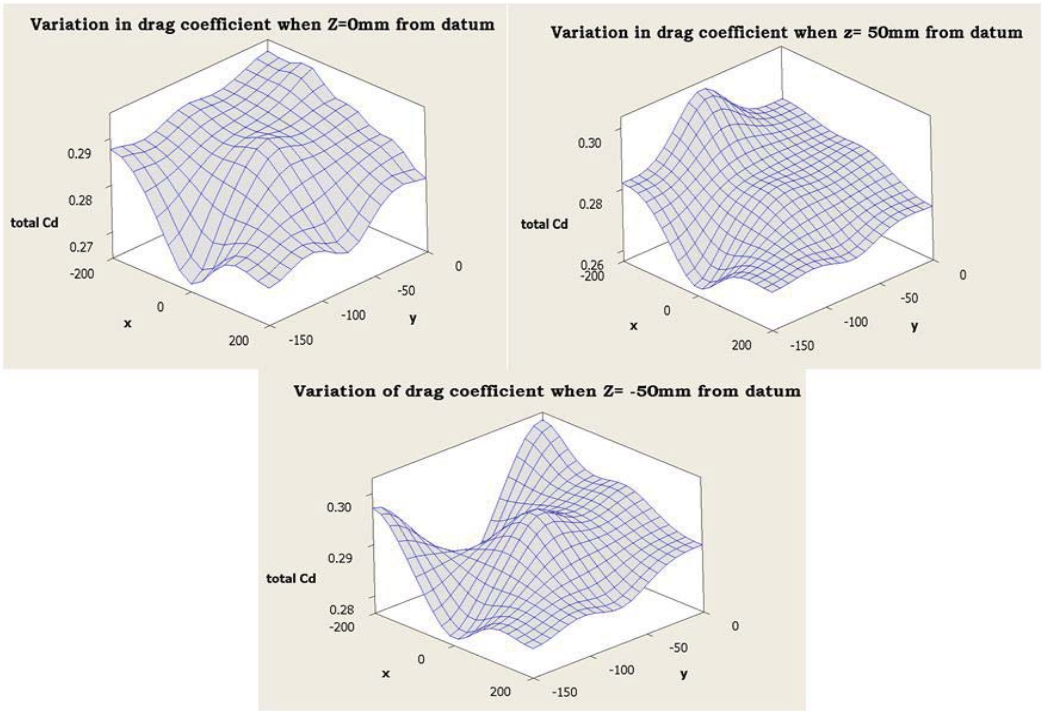

Figure 47: Variation in C_D at different Z positions of roof box over fastback car

By analysing the above picture, the position of roof box with lowest and highest drag coefficient can be clearly identified. The maximum C_D value was obtained at

(-200,0,-50) and the lowest value obtained was placed at (0,-150,50). There was no similar trends in the three graphs mentioned in the above figure.

Figure 48 below shows total pressure coefficient obtained when the box was placed at (-200, 0,-50) and (0, -150, 50) away from datum position.

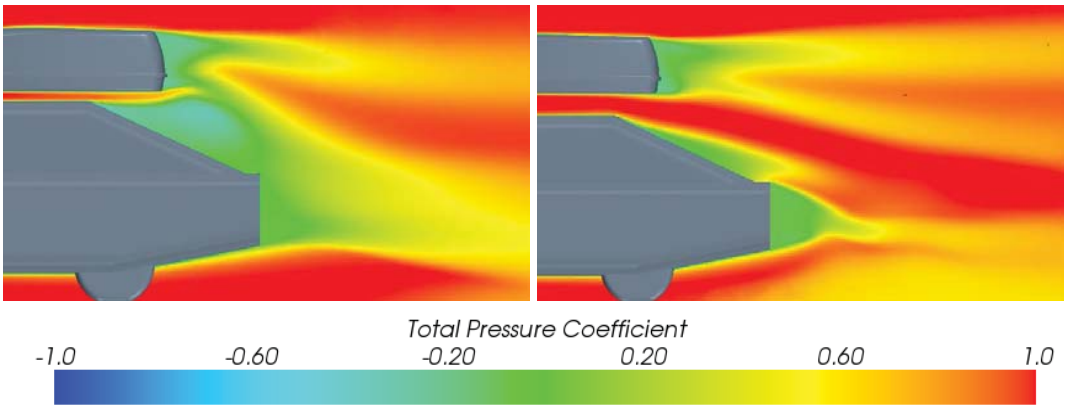

Figure 48: Total pressure coefficient obtained when the box was placed at (-200, 0,-50) and (0, -150, 50)

When the box was placed at (-200,0,-50), approximately half of the rear wind shield was covered with the box. This will enhance low pressure region above the rear wind shield. The flow will detach at the point where the rear wind shield starts. The low pressure region behind the car at (-200,0,-50) was much higher than that of (0,-150,50). Overall pressure difference between the front and rear of the car with roof box at (-200,0,-50) was much higher than car without roof box. Hence, drag coefficient on the car increases by 84 counts from car without roof box. This was due to large wake region behind the car and box. From the above figure, the position of the roof box was also critical in terms of aerodynamics.

5.1.3. Z Direction

When the box was placed away from the car's roof, more air will flow through the gap. The velocity of flow was higher than free stream velocity and then decreases when compared to datum position. This air flow will try to supress the low pressure region and hence the drag coefficient was low when compared to the position where the roof box was near to the car. A difference of 5-7% (15 counts) drag was obtained between two extremes. When the box was positioned away from the roof of the car, drag coefficient decreases. When individual results on the car and the box were considered, the C_D value was reduced on the car and increased on the box.

Figure 49 shows the variation in pressure coefficient on fastback car and box. The colour bar ranges from -1 to 1. The zone in which green colour indicates reference pressure.

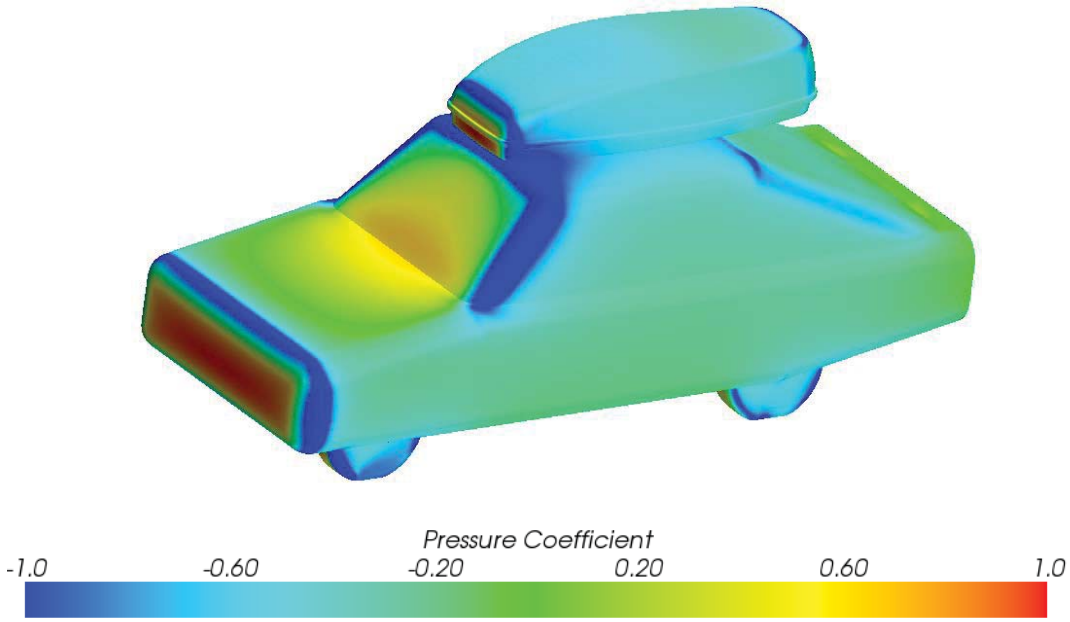

Figure 49: Pressure coefficient when the box was placed at extreme rear position and near to the car

A stagnation area can be identified in the front of car and box. A low pressure region can be identified over the front curvatures of roof box, A- and C-pillar curvatures. When the box was placed near to the roof of the car, the gap between the car and box reduces. Hence, the velocity of flow increases through the gap. As the flow continues through the gap, the velocity of flow decelerates because of the viscous effects due to the surface of car and box. When the drag coefficient due to the box and car were analysed individually, one can find an opposite trend in the values of box and car. When the box was placed away from the roof of the car, drag on the box increases. The effect on car due to box was decreasing as it placed away from the roof of the car. The contribution of drag due to roof box to total C_D was the same when the box was positioned at five locations along Z direction at datum position. Similar trend can be identified when the box was placed at extreme rear position

5.2. Notchback Car

5.2.1. X Direction

Figure 50 below shows the % total deviation in drag coefficient of car with and without roof box.

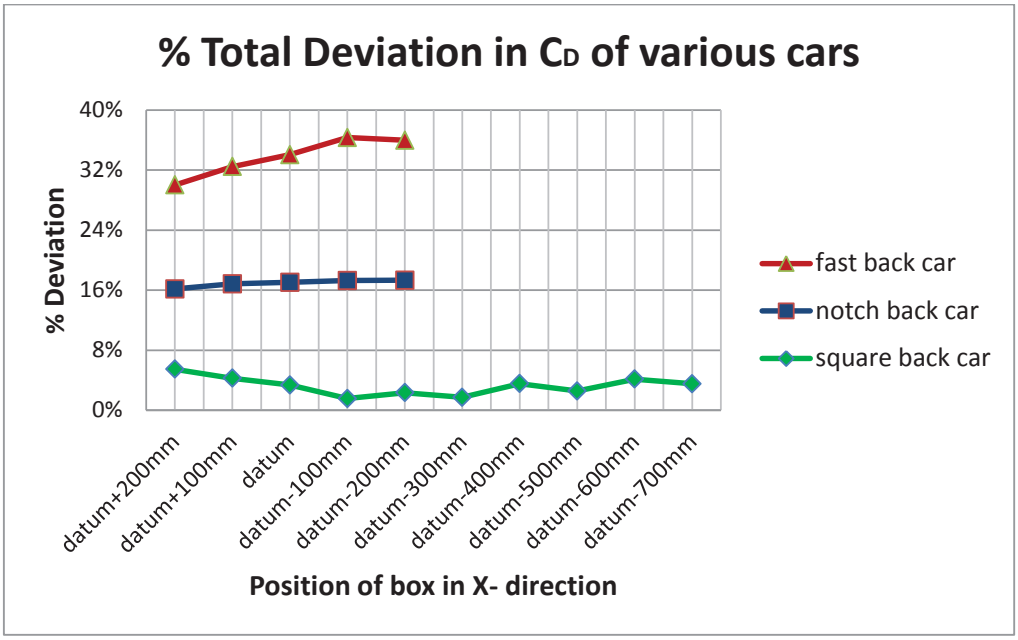

Figure 50: % Total deviation in C_D

.The actual deviation from notchback car with and without roof box was in the range of 40-44 counts of drag. Even if the total C_D value for notchback car was higher than fastback car, % deviation for notchback car with roof box was 15-20% lesser than fastback car with roof box. The total deviation of squareback car due to roof box was in the range of 0-8%.

The deviation in drag for notchback car with roof box was almost constant when compared to and fastback car. A blue colour curve in the above graph represents drag deviation in notchback car when a roof box was placed on various positions in X direction. When analysing the drag coefficient individually, the car and the box shows opposite trend. When the box was placed at extreme front position, the drag coefficient obtained due to car was less when compared to extreme rear position. Nearly 40 counts of drag coefficient were increased due to the box at extreme front position. While placing the roof box at rear position, more drag was generated due to the car. Only 11 counts of drag were generated due to the box at this position.

Figure 51 represents the wake structure behind notchback car without roof box and the box was positioned at extreme front position.

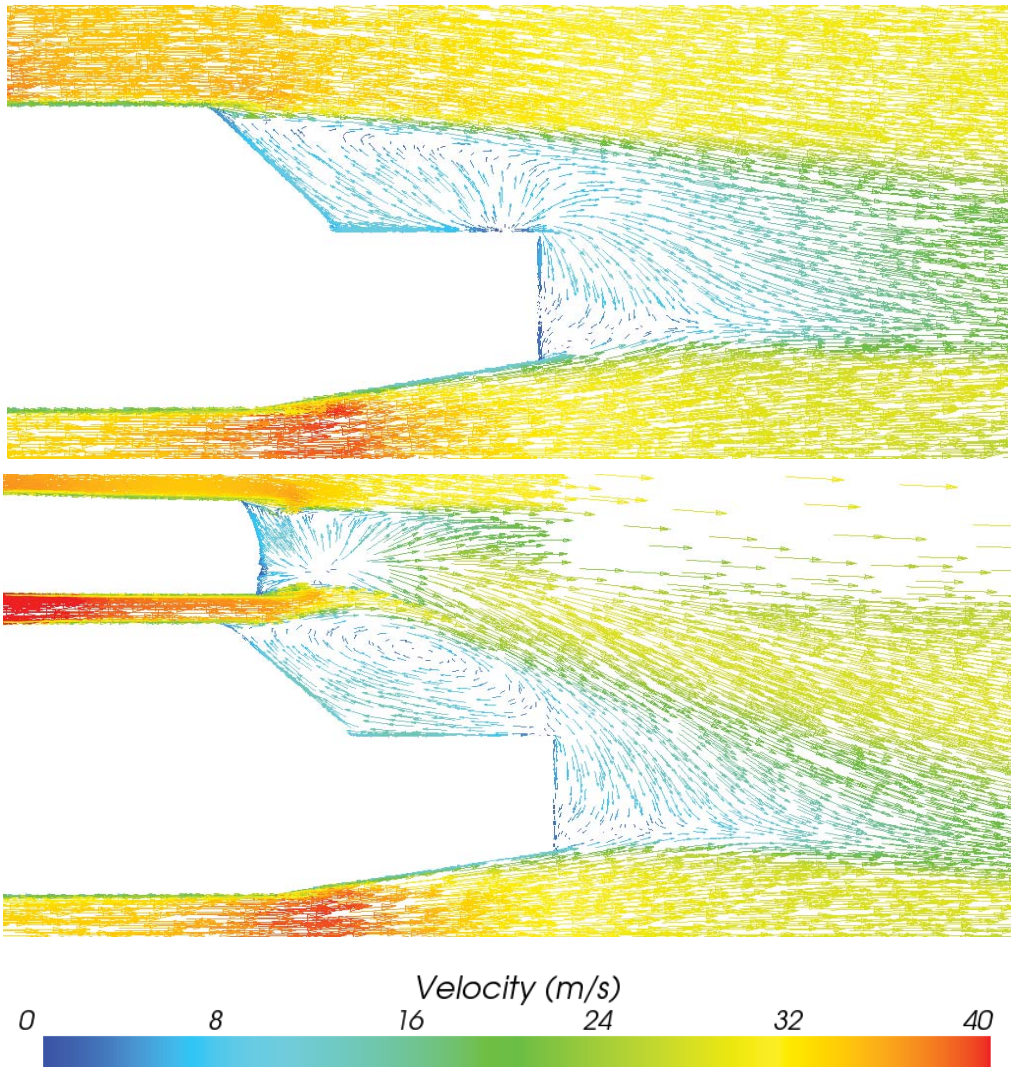

Figure 51: Wake structure behind notchback car without roof box and the box was positioned at extreme front position

First vector scene in the above figure shows the low pressure region at the rear end of the car without roof box. Second one indicates the wake formation when the box was placed at extreme front position in X direction. The vector scene of car without roof box shows that flow separation in the rear end originates from the point where rear wind shield starts. The free stream flow tries to supress the low pressure region and continues along the flow to a certain distance. There was a minor difference in the wake structure between extreme front and rear positions.

Figure 52 shows the vortices generated behind the notchback car and roof box. Also, the vortices created at the sides of roof box.

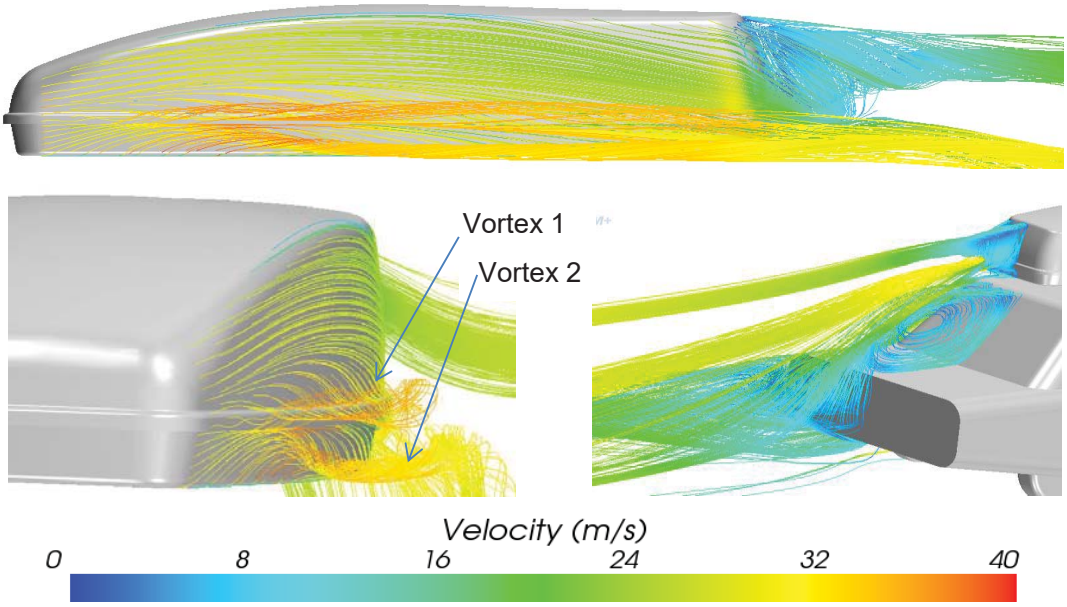

Figure 52: Vortices around roof box and car

There was a region behind the roof box where the pressure was larger than atmosphere. This may be due to the impact of air flow from the roof and sides of the box. Two vortices were generated on either side of the box. This phenomenon can be seen when the roof box was positioned towards extreme front position. This was one of the main reasons for increase in drag on roof box. The strength of the vortices gets diminished when the box was positioned at datum position and no vortex was generated when the box was placed at extreme rear position.

5.2.2. Y Direction

The position of roof box in which the lowest and highest drag coefficient for fastback and notchback car was entirely different. For fastback car, the lowest drag coefficient occurs when the box was placed at (0,-150,50) and for notchback car, it was positioned at (200,-75,50) and (200,-150,50). There was a difference of 30 counts of drag on the car when the box was placed at the position where the lowest and the highest drag coefficient occur. Like fastback car, the rolling and yaw moment coefficients were small when compared to pitching moment and the effect of those moments on the car due to box were negligible. When the box was positioned along Y direction from datum plane, the pitching moment reduces. The notchback car always pitches to the front when the roof box was kept over the car.

Figure 53 shows % effect on notchback car and roof box when the box was placed at X=0 mm and different Z positions. The dark line shows the effect on car due to box at various positions and transparent line shows the effect on box due to car when the box was placed at different positions.

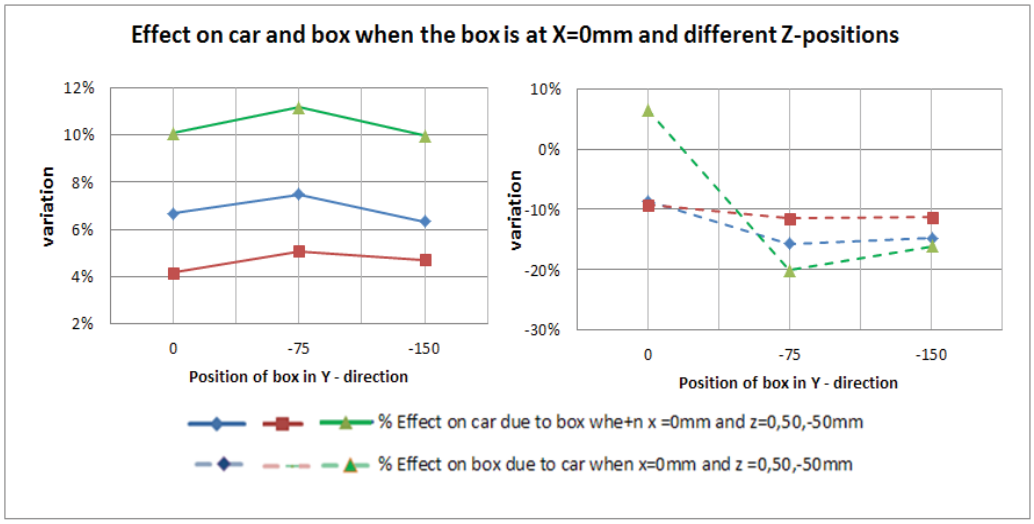

Figure 53: % Effect on car and box when the box was placed at X=0 mm and different Z positions

When the box was positioned near to the roof of the car, overall drag coefficient increases. When the box was placed at extreme top position, the effect on car was the lowest. When the box was positioned at datum position, the effect of notchback car on roof box was positive. In all other positions, the effect on box was negative in nature. It shows that the actual drag obtained on these cases was less than the indicated value when the box was tested without the car.

Figure 54 shows the total pressure coefficient on symmetry plane when the total drag coefficient was lowest and highest.

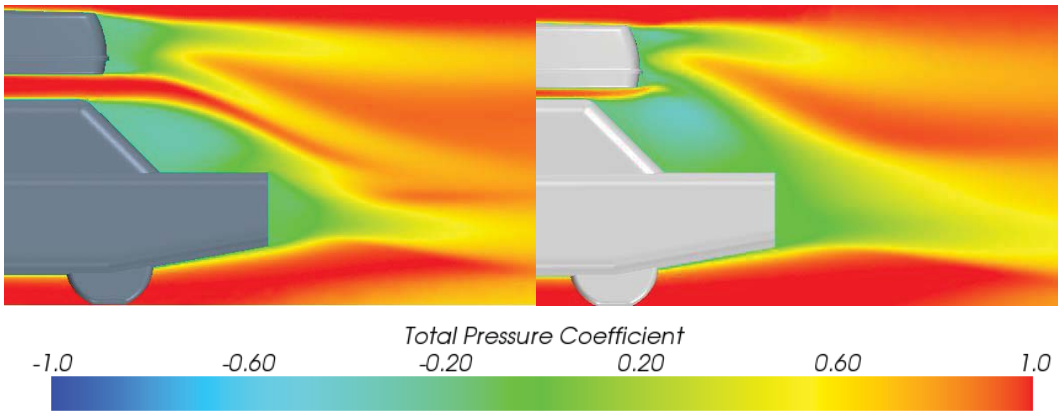

Figure 54: Total C_P symmetry plane when the overall drag was lowest and highest

Pressure distribution on symmetry wall in the front side of car and box in both cases was almost same. There was a high pressure region occurs behind the roof box. This may be due to the collision of the flow. When the flow through the gap reaches the rear side of the box, the high pressure region expands. As the pressure behind the box decreases, the overall pressure difference between the front and rear side of the box increases. Thus the drag on the box increases. When the box was placed at extreme top position from the car, more air flows through the gap. The interaction between notchback car and box was less when compared to the position of the box near to the roof of the car. Hence, overall drag reduces.

Figure 55 represents the variation in C_D in various Z positions of car and roof box over a notchback car.

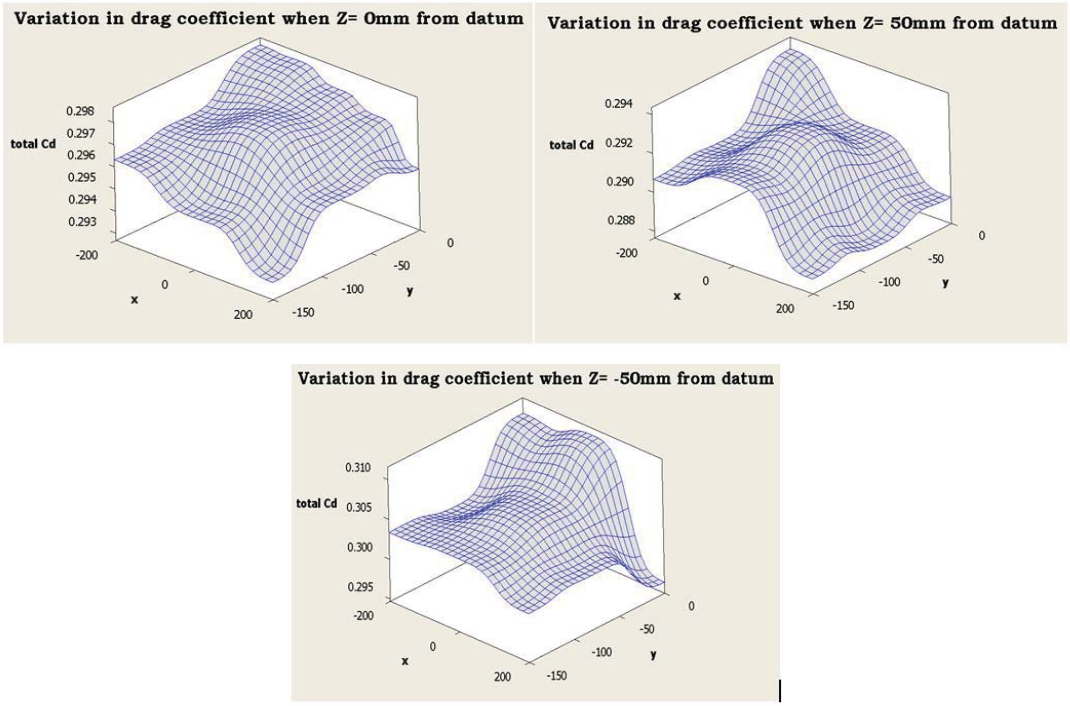

Figure 55: Variation in C_D in various Z positions of roof box over a notchback car

From the above figure, the lowest and highest drag generated on notchback car and roof box can be easily identified.

5.2.3. Z Direction

When the box was positioned at extreme front position and placed along Z direction, the drag remains almost constant. When the box was placed at extreme front top position, the drag decreases by 2.5% (7 counts) compared to extreme front bottom

position. Stream lines and vortices around notchback car and roof box at different Z positions were shown Figure 56.

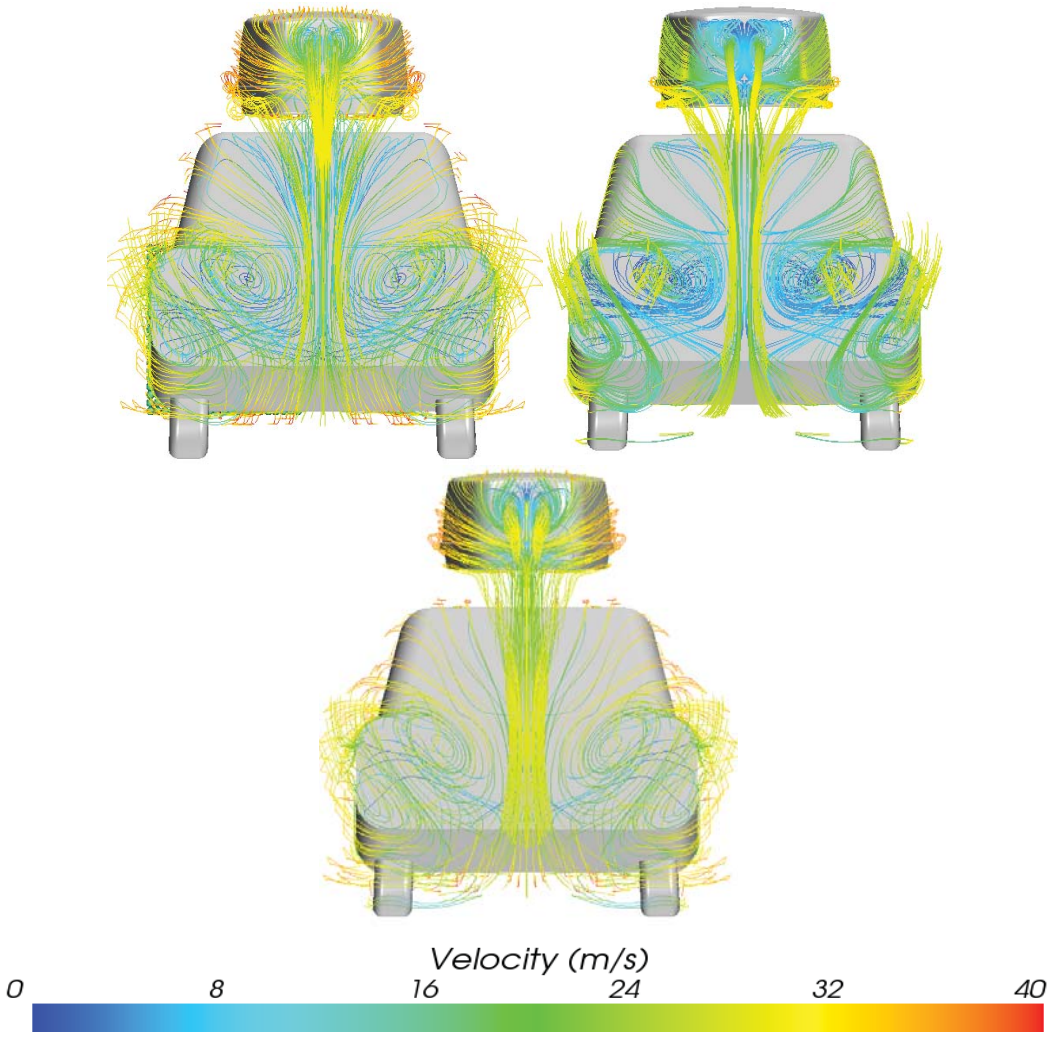

Figure 56: Vortex generation on car and box at various Z positions when the box was at datum plane normal to the flow direction over notchback car

When the roof box was placed near to the car, the strength of the vortex generated near to the box was high. The contribution of drag due to box was less, but the effect on car due to box was much higher than any other positions. When the box was placed at datum position, the strength of the vortex was less than that of the former position. The drag was increased by 13 counts between the above mentioned positions. When the roof box was placed at extreme top position, the strength of vortex around the roof box diminishes. The effect due to roof box on notchback car at this position was lower than other two positions. Hence the overall drag reduces by 26 counts between the nearest and farthest position of roof box from the roof of the car.

5.3. Squareback Car

5.3.1. X Direction

Figure 57 below shows the effect on car due to roof box on fastback, notchback and squareback geometries.

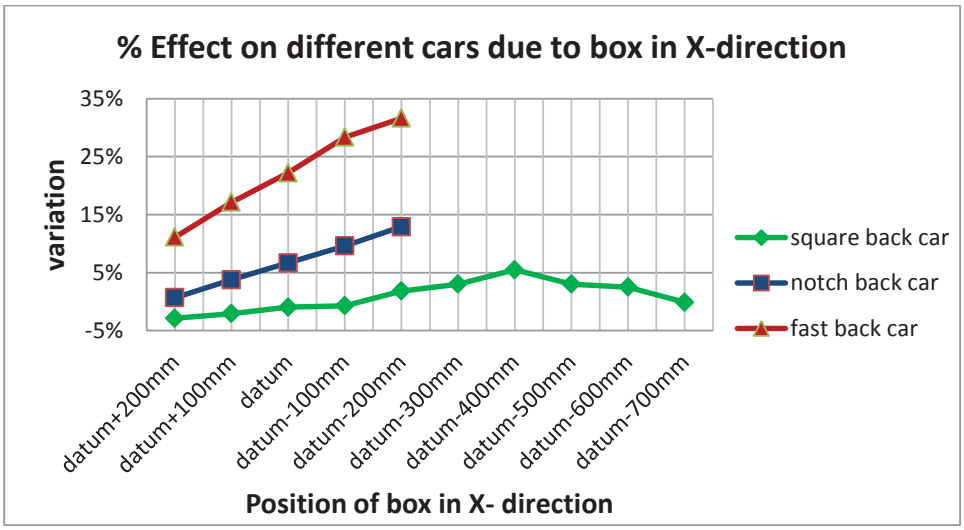

Figure 57: % Effect on different cars due to box in X direction

For fastback and notchback cars, when the box was positioned from extreme front to extreme rear, the effect on car due to box increases. For fastback car, this value varies the maximum (20%). A zero effect on notchback car can be identified when the roof box was placed at extreme front position. There was a negative effect on squareback car when the box was placed at extreme front position and this effect continues till the box was positioned 100mm towards rear side from datum position in X direction. This variation increases till the box reaches (-400,0,0) and it reduces beyond that position. The actual deviation was 5-18 counts from squareback car without roof box. When compared to other cars, lowest deviation was generated due to roof box on squareback car.

Figure 58 shows the re-circulating flow behind squareback car and roof box at (200,0,0) and (-400,0,0).

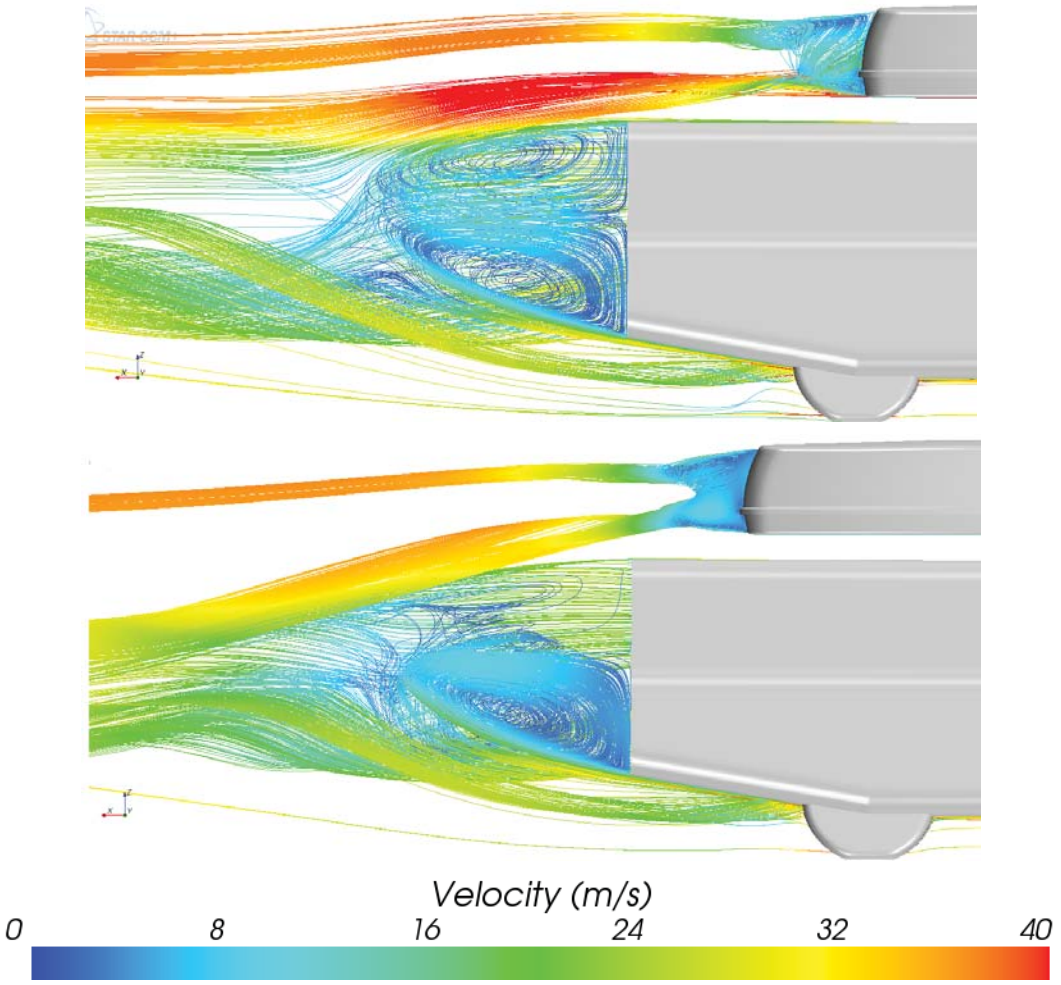

Figure 58: Re-circulated flow at (200, 0, 0) and (-400, 0, 0)

There were two recirculated flows obtained behind the squareback car. The strength of the top re-circulating flow diminishes when the box was positioned from front to rear (till datum-400mm). The position where the lowest drag generated was placed at 100mm away from datum position towards rear side. The flow from rear side of roof box will try to supress the top re-circulating flow behind the car. This was one of the reasons for reduction in drag coefficient by 6 counts when compared to the box at extreme front position. As the box was placed further backward, top re-circulated flow regains its strength, and the bottom become weaker. When the box was placed at 700mm away from datum position towards rear side, the two recirculating flow shows almost equal strength.

Figure 59 shows the wake generated behing squareback car and roof box at three different X positions.

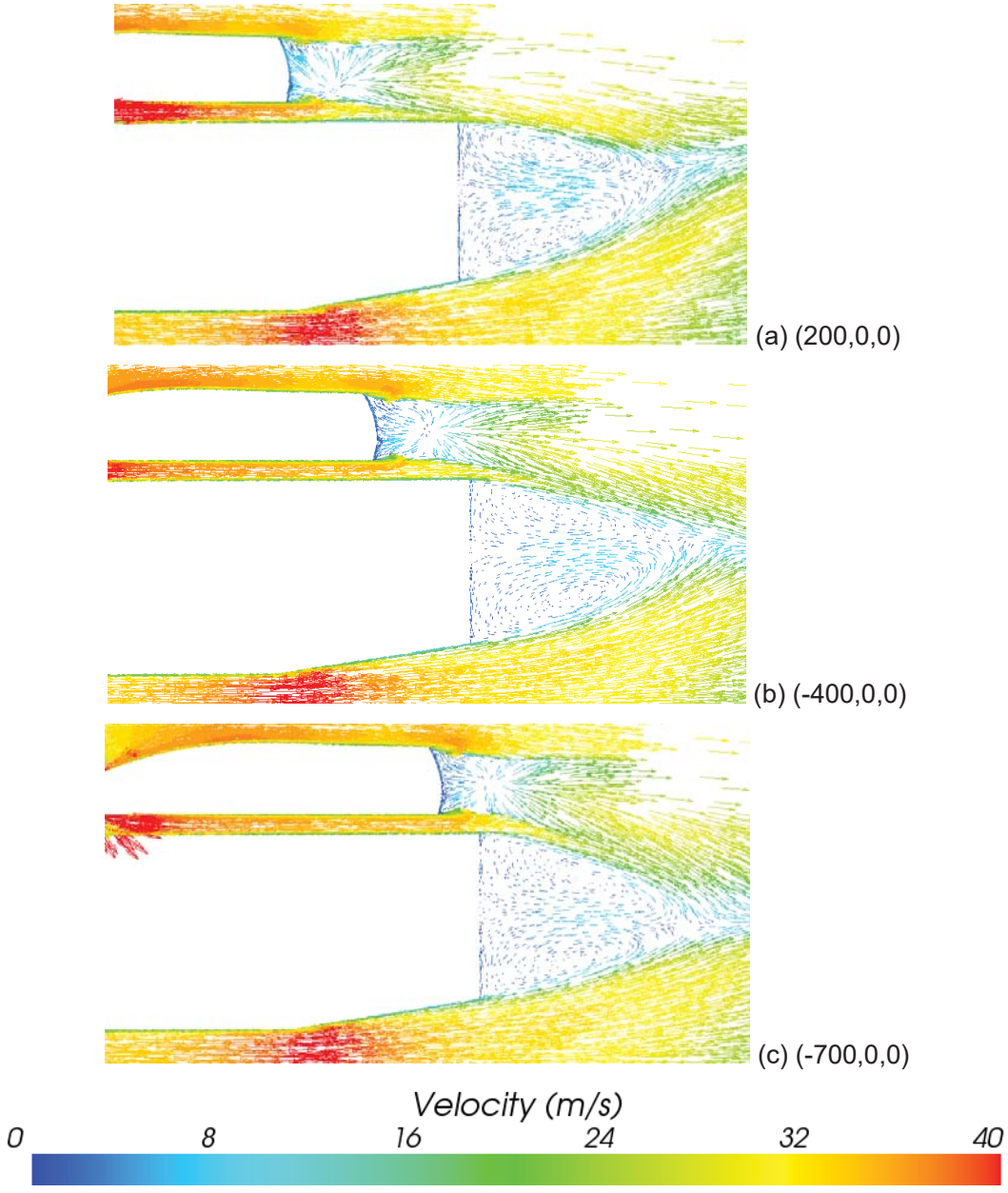

Figure 59: Wake structure of squareback car with roof box

The wake generated behind the roof box over squareback car was almost similar in shape. Due to the two re-circulating flows, a horizontal V-notched shape was created behind the car. When the squareback car without roof box was analysed, the wake region behind the car was almost parallel to top surface. The low pressure region was shaped according to the diffuser angle at rear bottom side of the car. When a roof box

was placed over the squareback car at extreme front position in figure-59 (a), the flow past the roof box tries to push down the low pressure region. The flow along the diffuser of the car will try to lift this region. Hence the notched shape was occurred as wake region. The tail of this region was lifted to some extent because of flow velocity. When the box was positioned by a distance of 600mm to the rear side from extreme front position, the shape of wake region remains the same. But the tail of this region pointed downwards. When the box was placed at extreme rear position, wake region was pushed down furthermore when compared to that of (-400,0,0).

5.3.2. Y Direction

Figure 60 below shows the variation in C_D value at different Z positions of roof box over a squareback car. Three 3-D graphs which include the corrected drag of all positions over squareback car.

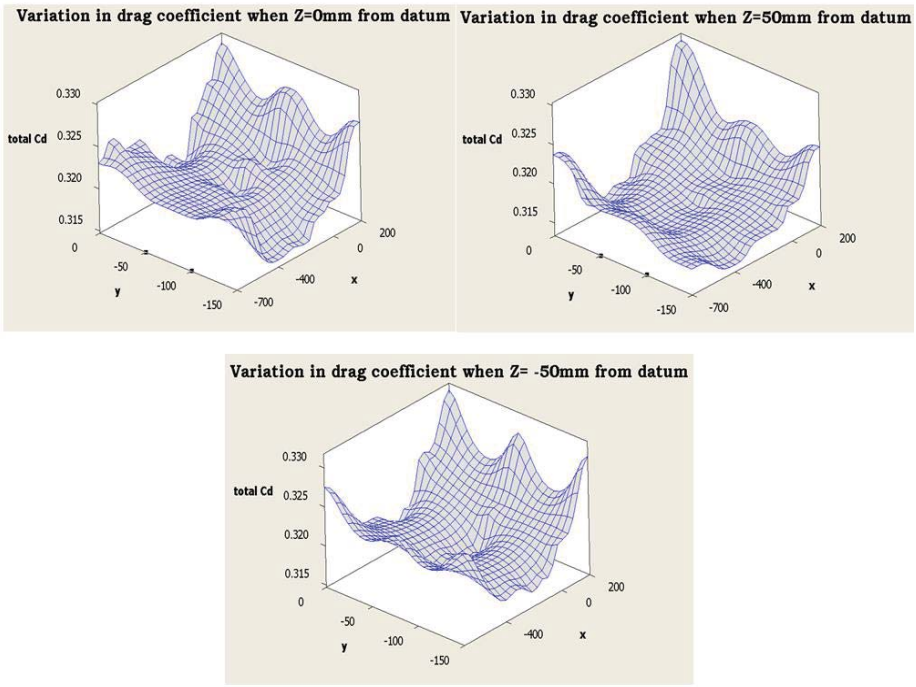

Figure 60: Variation in C_D in different Z positions of roof box over a squareback car

There was a common trend in all three graphs. The drag decreases as X varies from extreme front position to the position where the box was 400mm towards rear side from datum position. The drag then increases as the box was placed beyond this position. In some X positions, when the box was positioned apart from the centre plane to the side, the drag initially decreases and regain to the same value or continuously decrease when it reaches farthest position. Pitch, roll and yaw moment coefficient for all positions

of box were in the order of 10^{-2} or 10^{-3}. So these effects due to box on car can be neglected.

5.3.3. Z Direction

Figure 61 shows the pressure coefficient on symmetric plane at lowest and highest drag coefficient positions when the box was placed on squareback car.

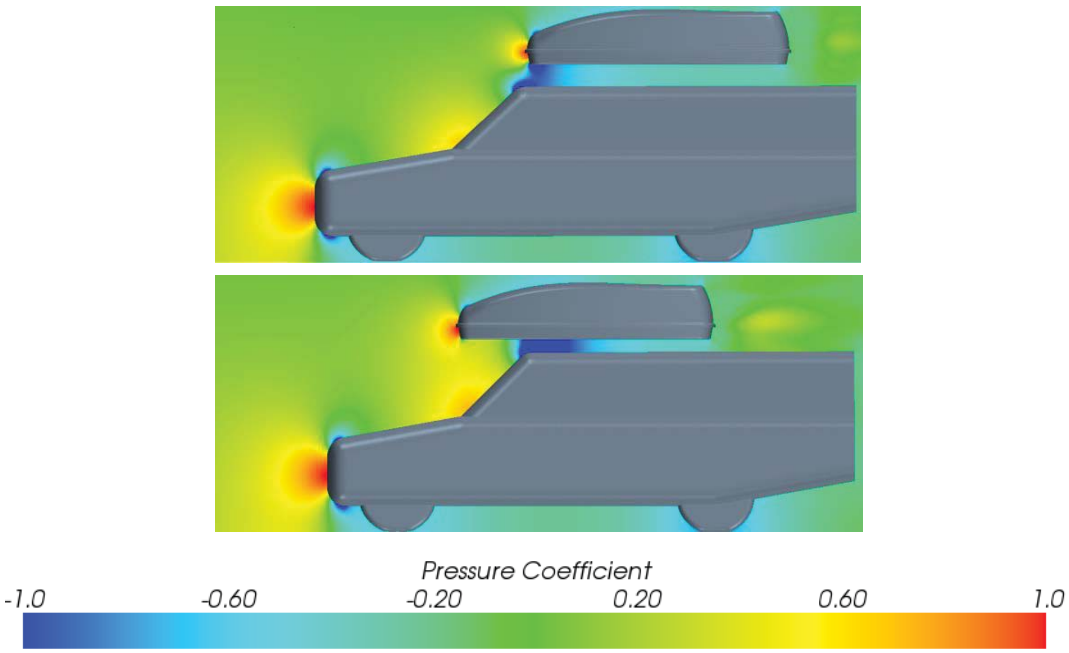

Figure 61: C_P of lowest and highest drag positions when the box was placed on squareback car

When analysing pressure coefficient, the drag obtained was roughly equal on car and box. When the box was placed in extreme front position, a high pressure area was generated over the hood and wind screen. This pressure difference will affect the drag on roof box. A pale red colour in front of wind screen and hood shows high pressure region in the former picture. A high pressure region was generated behind the roof box. When the roof box was positioned from front to rear, strength of this region got diminished. The pressure variation around car and box was less in second picture. Hence overall drag was less for first case when compared to the second positions.

5.4. Analysis of different roof box

Figure 62 shows the pressure coefficient on symmetric plane of different designs of roof box.

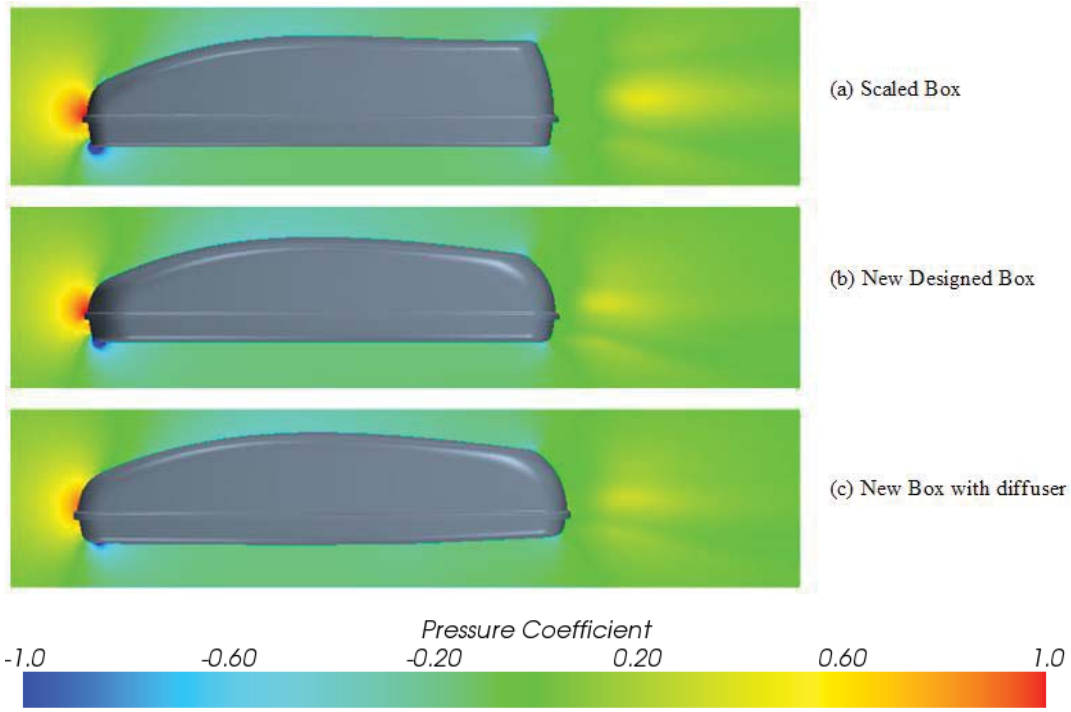

Figure 62: C_P on different designs of roof box

In this section, three design of roof box and the results from those simulations were analysed. The drag coefficient of scaled box was less than full roof box by 15 counts. Out of these, 40% for drag variation was due to friction and remaining was due to pressure difference. When overall drag was considered, this variation can be neglected (0.1% approximately). So the size of the roof box will not affect the drag coefficient. When modified box was tested alone, the drag generated on the box was higher than the scaled box by 30%. The new box was well shaped by improving different curvatures. When the new box was simulated with different cars, there was some improvement in the results.

In all three figures, a high pressure region was obtained just behind the roof box. The flow from the bottom and top of the box tend to circulate behind the box since radius of curvature was less in figure (a). In Figure 60 (a), area covered by high pressure behind the roof box was more than scaled or newly designed box. While investigating the results of new design of the box with a taper, the drag decreases by 24 counts from scaled re-designed box without taper. No vortex was generated in the sides of roof box

when the box without car was simulated. The main concept of the taper was to increase the pressure and reduce the effect of low pressure behind the box.

Figure 63 shows the variation of pressure coefficient along the bottom surface of roof box. The graph includes the pressure coefficient variation due to taper underneath the roof box.

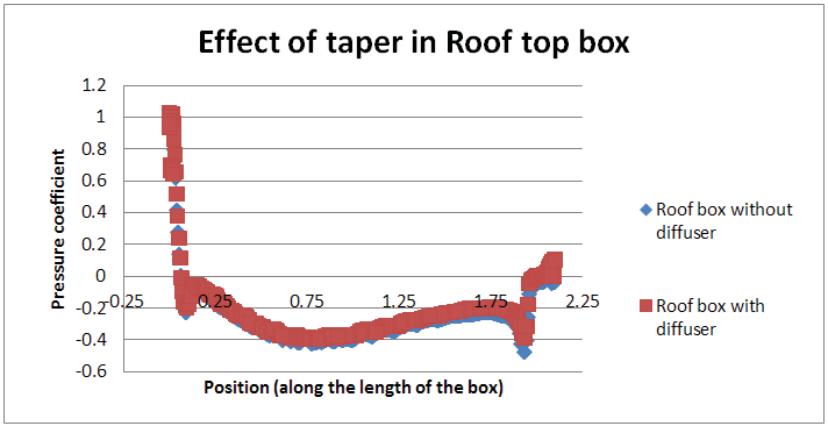

Figure 63: Effect of 2^0 taper angle in Roof box

There was a slight variation in pressure behind the roof box. This increase in pressure reduces the drag on the box. The effect of box on car was also reduced due to taper. The results of tapering on roof box were shown in Appendix III.

The flow around the re-designed box with taper and various cars can be compared using the vector scenes. They were shown in Appendix I. The flow over the box follows the curvature of roof box. This will help to reduce the size of low pressure region behind the car and box. For a fastback car, the flow was attached along rear wind shield of the car and the flow separates as seen in fastback car without the roof box. When a re-designed box with taper was attached at extreme front bottom position over a fastback car, the size of re-circulating flow above the rear wind shield diminishes. The flow was almost attached to the body of the car. Hence, drag coefficient decreases. For notchback car and squareback car with re-designed box, similar trend of fastback car can be identified. Hence overall drag coefficient decreases.

6. Discussion

6.1. MINITAB Validation

In order to validate MINITAB using the results of various simulations, full factorial and Taguchi designs were used. This software was mainly used to optimize the number of simulations using DOE by considering three independent variables (X,Y,Z). Initially car was considered as an independent variable. Different levels and factors used in this research were shown in Table 31. The prediction using Taguchi method was represented in Figure 64.

Levels/Factors	Car	X	Y	Z
1	Fastback	-200	-150	-50
2	Notchback	0	-75	0
3	Squareback	200	0	50

Table 31: Levels and Factors

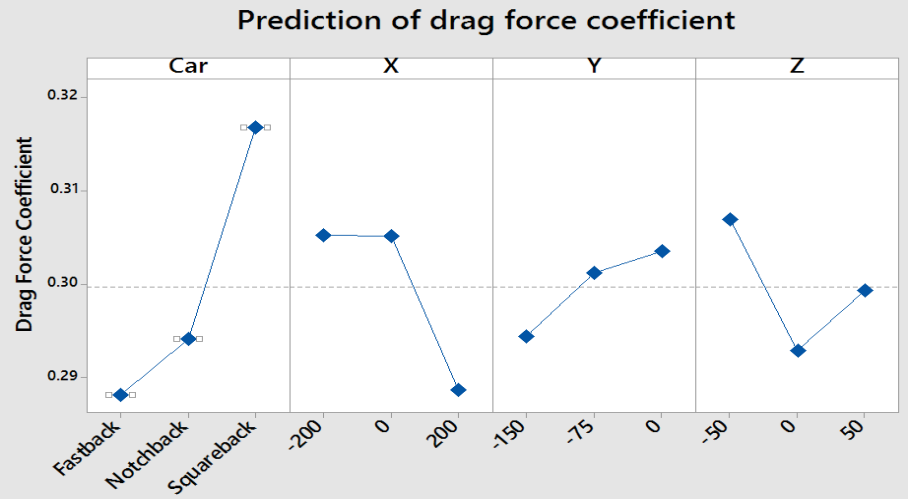

Figure 64: Prediction of C_D using MINITAB

Drag coefficient was lowest on fastback car when compared to other car models and it was easily predicted by MINITAB. The actual drag for fastback car with roof box was in the range of 0.25-0.305. The drag recorded in the graph was just below 0.29. When notchback car was considered, this value ranges from 0.288 to 0.311. The graph denotes the value as 0.295. When roof box was kept on a squareback car, actual drag ranges from 0.314 to 0.333. The predicted drag was just below 0.32 and these results were acceptable. On each car, each independent variable shows different trends. To find out the trends with other independent variables, results from more number of experiments were analysed.

6.1.1. Fastback Car

Figure 65 shows the trends in predicting drag coefficient when the box was placed on fastback car.

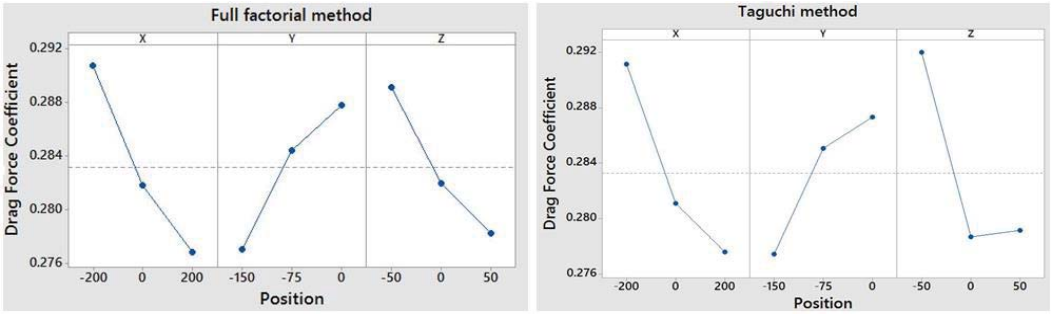

Figure 65: Trends in predicting C_D when the box was placed on fastback car

There was some matching of trends between Taguchi and full factorial method in X and Y directions. Out of 9 rows of simulations in X direction, 5 shows similar trend. When the box was placed at rear side of datum position on fastback car, drag coefficient shows the highest value. None of the designs were following the actual trend. When Y position variation was considered, both designs follow the same trend. But the drag coefficient was different. The actual trend in Z direction was properly predicted by full factorial method and the performance was satisfactory with Taguchi design. Even if the trends were slightly different, the position for highest drag predicted by both methods was almost same. The prediction for lowest drag by Taguchi method is similar to that of full factorial method except in X and Z direction. The lowest drag coefficient obtained due to roof box on a fastback car is at (0,-150,50). But the above graphs show that the lowest drag obtained is at extreme front position. Further investigation is required in X and Z directions if Taguchi method is used.

6.1.2. Notchback Car

Figure 66 shows the trends in predicting drag coefficient when the box was placed on notchback car.

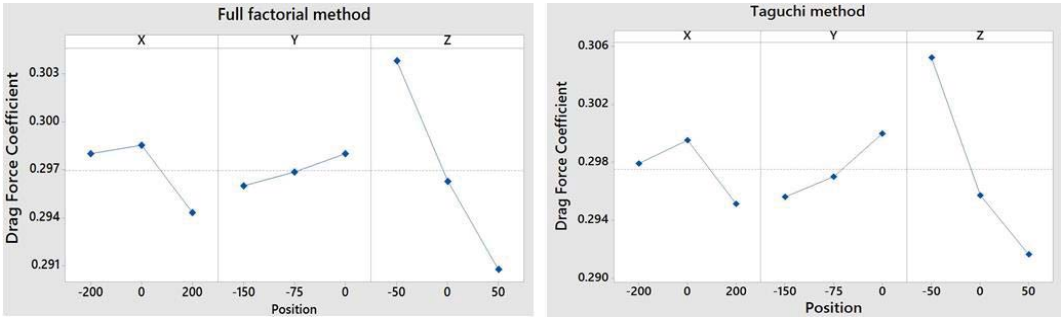

Figure 66: Trends in predicting C_D when the box was placed on notchback car

Taguchi method always over-predicts the results when compared to full factorial method. The trend of both methods in all directions was almost similar in shape. When the box was placed from extreme rear to front on a notchback car, the drag initially increases and reaches the maximum at datum position and then decreases. In Y direction, both methods show same trend and almost same drag coefficient. Out of 9 set of simulations, 5 have same tendency of decrease in drag coefficient when the roof box was positioned towards left. Further investigation was required to analyse the roof box in X direction over notchback car since it does not predicts the exact position.

6.1.3. Squareback Car

Figure 67 shows the trends in predicting drag coefficient when the box was placed on squareback car.

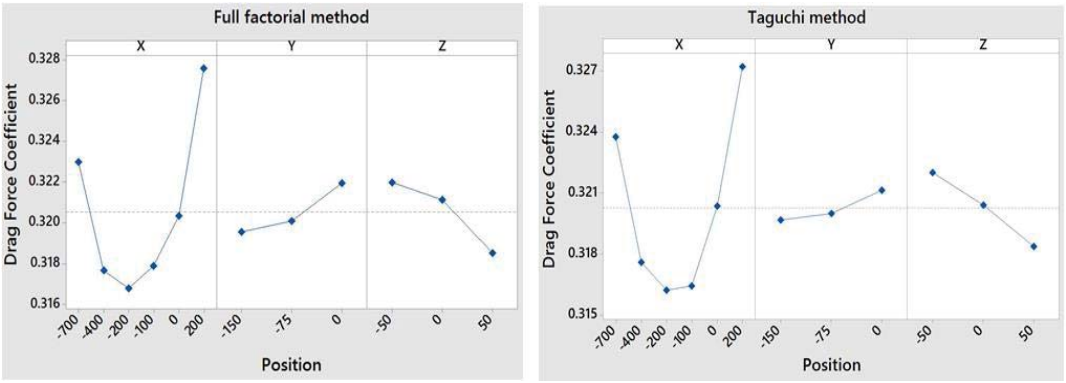

Figure 67: Trends in predicting C_D when the box was placed on squareback car

The trends followed by both the methods were the same in all directions. The overall drag decreases when the box was positioned from extreme front to rear in X direction. In the case of Y and Z direction, both methods follow almost same trend when compared to CFD results. The position where lowest drag coefficient obtained was at (-200,-150,50) from the above graph. But the CFD result shows that the lowest value was generated when X = -100mm from datum position. Hence Taguchi method almost predicts the position of roof box in the case of squareback car except in X direction. Both predict the same position for highest drag coefficient.

6.2. Estimation of Excess Power consumption due to Roof box

The maximum weight of a fully loaded box was assumed as 100 kg. In order to pull the car moving at a speed of 30 m/s with roof box, engine requires an additional power. The variation of excess power consumed by the engine against C_D*A for three MIRA cars were represented in Figure 68.

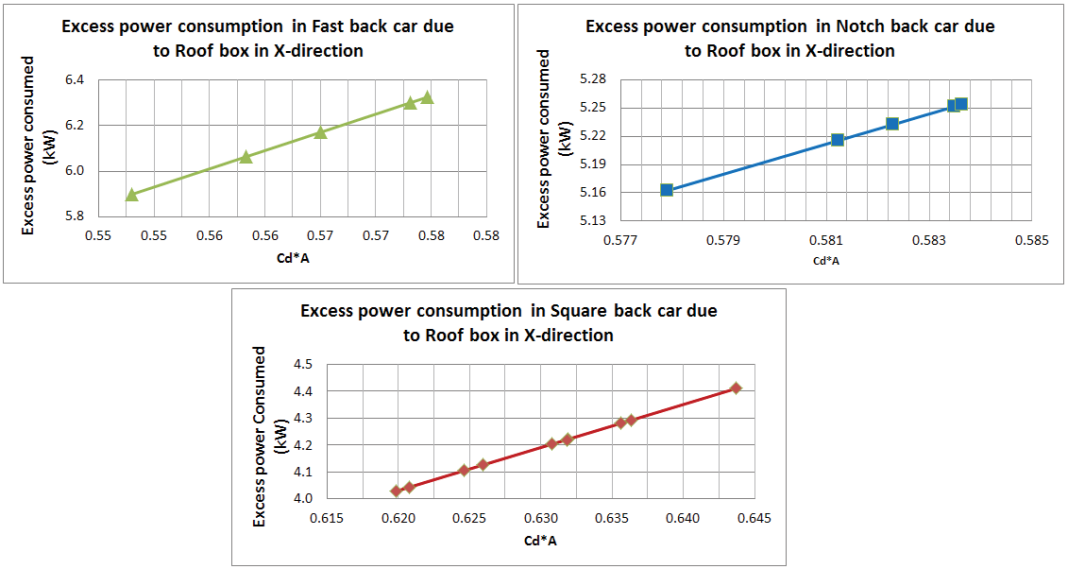

Figure 68: Excess power consumption due to roof box

To pull a weight of 100kg, engine requires an extra power of 3.88kW to maintain the speed of the car. Remaining power consumption was due to aerodynamic resistance on the box. Excess power consumed on a fastback car due to roof box was higher than other cars since the variation from car without roof box was higher for fastback car. When the roof box was placed at extreme front position, C_D*A value was recorded the lowest. To overcome aerodynamic resistance generated on the box and car, an additional 2kW engine power was required to compensate the speed reduction. There was an increase of 0.5kW when the box was placed towards the rear. On a notchback car, lowest aerodynamic resistive power was 1.3kW. There was minor variation in drag coefficient when the box was positioned towards the rear. Only 0.15kW engine power was required to overcome air resistance of roof box when it was kept on a squareback car. So less power was required to pull a roof box over a squareback car than other type of cars.

7. Conclusion and Recommendations

The baseline design of roof box and its design variations was modelled and analysed at various positions in three perpendicular directions over different MIRA car geometries. The drag force coefficient was mainly analysed throughout the project and there were so significant developments while positioning of roof box over different MIRA car. There was a minor variation in lift force coefficient of car with and without roof box. When the weight of roof box and its belongings were considered, the change in lift coefficient will be smaller than actual variation. Hence the analysis of lift coefficient was neglected in this project. Table 32 below shows three different positions where the drag coefficient is lowest.

Car	1st preference	2nd preference	3rd preference
Fastback car	(0,-150,50)	(0,-150,0)	(200,-75.50)
Notchback car	(200,-75,50)	(200,-150,50)	(200,0,50)
Squareback car	(-400,-150,50)	(-400,0,50)	(-400,-150,0)

Table 32: Probable positions of larger roof box

The above positions of roof box on the car may or may not be stable. In order to identify the exact stable position, field tests need to be conducted. When the roof box was placed at extreme front position notchback car and rear position of squareback car, drag coefficient recorded the lowest. In the case of fastback car, the drag coefficient was at the datum position. There was a deviation of 3% in overall drag between first two preferred positions when the roof box was placed over fastback car. So, one can clearly suggest that (0,-150,0) was the best position for roof box on a fastback car for full scaled roof box. There was no drag variation between first two positions when the box was placed over notchback car. For a squareback car, lowest drag coefficient was obtained at (-400,-150,50). There was a minor change in drag coefficient among three preferred positions.

When scaled box was analysed, the drag coefficient was lowest at the front position of fastback and notchback car. For a squareback car with scaled box, the position of roof box changes to extreme rear end. The roof box was scaled in 3 dimensions and the final volume was 270 litres. For full scaled box, the internal volume was 450 litres. The frontal area of the roof box was reduces by 32% when compared to full scaled box and the drag coefficient reduces accordingly. When the size of the roof box reduces, the interaction between the car and roof box reduces. Hence the drag acting on the car reduces when compared to full scaled box. Manual shape optimization of roof box was

done effectively. The drag coefficient reduces when a box with a taper at its rear bottom was placed over all three geometries. As the taper angle increases, the drag reduces. The total volume of roof box was reduced by less than 1% per degree of taper. When a taper was added on the roof box, a reduction of 2-5% drag coefficient occurs when compared to fastback car with no taper angle. The taper angle on roof box was effective when the box was placed on a fastback and notchback car at extreme front position.

The excess power required to maintain same speed for squareback car with roof box was less than other type of cars. For a squareback car, excess power required to pull the car with roof box was 4-4.5kW. The fastback car requires 2kW excess engine power to carry roof box than that of squareback car.

In order to reduce the overall experiment cost, CFD toolbox (Star-CCM+) was used to analyse this problem. Since the free stream velocity generates turbulence due to the interaction of car and roof box, the problem was considered as turbulent. k-ε turbulence model was chosen because it shows better results when compared to other turbulence models. The computational time required to solve this problem using k-ε model was less than other models. The CFD results obtained was under-predicted by 5-10% when compared to reference car drag coefficient. To reduce the error obtained due to turbulence model, more realistic models like LES and DNS can be applied. Since the computational power required is much higher, it can be used once or twice to prove the results. Meshing plays an important role in predicting the results. Fine mesh generates better results and in this case it was not different. The MIRA car geometry provided for this research has many flaws like sharp edges on car surfaces, non-cylindrical tyres and tyres were inclined by some angle. Due to this reason, there were some errors in CFD results.

MINITAB validation was successfully completed using the results from various simulations of full scaled roof box. Taguchi method can be recommended in future to reduce the number of experiments except in analysing the roof box in X direction. All the results obtained (drag coefficient) was used to validate DOE in MINITAB. Upon comparing both DOE methods, Taguchi method follows the same trend of general full factorial method. Taguchi method over-predicts the drag coefficient in a smaller amount.

The modified design of roof box with taper at its bottom shows good result. Due to the better curvature on the top of the roof box, the wake generated behind the car and roof box was supressed when compared to the baseline design. The vector scenes were shown in Appendix I. Overall; the objectives of the project were met. A meaningful amount of beneficial data was generated through this research.

8. Future Works

Since this research covers aerodynamic designing and positioning of roof box, further works and development of roof box are vast. The possible works beyond this research are highlighted below.

- Further analysis of roof box due to crosswinds.
- Study on the effect of roof box when the car is in convoy.
- Detailed material design and manufacturing technique can be done. These topics were generalised in this research.
- Field test can be conducted for proper analysis of fuel and power consumption and fuel emission due to roof box.
- Wind tunnel test can be done to calculate the drag due to car and box and study their interactions.
- Study of effect on roof box and car when a roof rack attached between them.
- Study of more than one add-on on the roof of the car and their effects.
- Study on the effect of variation in slant distance of taper underneath the roof box.

References

AdrianHi (2011) *Roof Boxes and Fuel Economy*. [2011] available from <http://forums.moneysavingexpert.com/showthread.php?t=3209720> [February 12]

Andersson, B. (2012) *Computational Fluid Dynamics for Engineers*. Cambridge: Cambridge University Press.

Barnard, R. H. (2001) *Road Vehicle Aerodynamic Design*. 2nd edn. St. Albans: MechAero.

Browand, F. (ed.) (2005) *Reducing Aerodynamic Drag and Fuel Consumption*. 'Global Climate and Energy Project'. held October 10 - 11 at Stanford University. Southern California: University of Southern California.

CD-Adapco. (2012) *Star CCM+ 7.06 User Guide*. 7.06th edn: CD Adapco.

CFD online. (1994) *Standard k - Epsilon Model*. [1994] available from <http://www.cfd-online.com/> [June 15 2013]

Chowdhury, H., Alam, F., Khan, I., Djamovski, V., and Watkins, S. (2012) *Impact of Vehicle Add-Ons on Energy Consumption and Greenhouse Gas Emissions*. http://www.sciencedirect.com/science/article/pii/S1877705812047972 Melbourne: Elsevier.

European Research Community on Flow Turbulence and Combustion (2000) *Best Practice Guidelines*. Version 1.0.: ERCOFTAC.

Fluent User Guide. (2006) *Fluent User Guide 6.3*. 6.3rd edn: Ansys.

Franke, J., Hellsten, A., Schlunzen, H., and Carrisimo, B. (2007) 'Best Practice Guideline for the CFD Simulation of Flows in the Urban Environment', 26.

Happian-Smith, J. (ed.) (2001) *An Introduction to Modern Vehicle Design.* Oxford; London: Oxford: Butterworth-Heinemann.

Holloway, S., Leylek, J. H., York, W. D., and Khalighi, B. (2009) *Aerodynamics of a Pickup Truck: Combined CFD and Experimental Study*. http://digitallibrary.sae.org/content/2009-01-1167. United States of America: SAE International.

Hucho, W. (1998) 'Aerodynamic Drag of Passenger Cars'. in *Aerodynamics of Road Vehicles*. ed. by Hucho, W. Warrendale, Pa.: Society of Automotive Engineers, 131-229.

Kasravi, K. (2013) *Body Structure 1* [online] available from <http://www.kasravi.com/cmu/tec452/index.htm> [March 12 2014]

Krastev, V. K. and Bella, G. (2011) *On the Steady and Unsteady Turbulence Modeling in Ground Vehicle Aerodynamic Design and Optimization*. http://digitallibrary.sae.org/content/2011-24-0163. University of Rome Tor Vergata: SAE International.

Lopes, A. M. G. and Carvalheira, P. (2003) *On the Application of Numerical Methods for the Calculation of the External Aerodynamics of a Streamlined Car Body'*. http://digitallibrary.sae.org/content/2003-01-1249. Warrendale, PA: SAE International.

Marur, S. R. (2013) 'Plastics Application Technology for Safe and Lightweight Automobiles', 247-253.

Mathews, P. G. (2005) *Design of Experiments with MINITAB*. Milwaukee, WI: Milwaukee, WI: ASQ Quality Press.

McBeath, S. (2006) *Competition Car Aerodynamics*. 1st edn. Somerset: Haynes Publication.

McDonald, A. T., Kreith, F., and Berger, S. A. (1999) 'External Incompressible Flows'. in *Fluid Mechanics*. ed. by Kreith, F. Boca Raton: CRC Press LLC, 3-71-3-71 - 3-80.

Minitab (2005) *Design of Experiments* [online] available from <http://cms3.minitab.co.kr/board/minitab_data/7.%20DesignofExperimentsAllTopics.pdf > [March / 10 2014]

Minitab (2014) *Taguchi Designs* [online] available from <http://support.minitab.com/en-us/minitab/17/topic-library/modeling-statistics/doe/taguchi-designs/taguchi-designs/> [October 17 2014]

Norbye, J. P. (1984) 'Body Engineering and Materials'. in *Car Design - Structure and Architecture*. United States of America: TAB Books Inc., 114-119.

Peric, M. and Ferguson, S. *The Advantage of Polyhedral Meshing* [online] available from <http://www.plmmarketplace.com/upload/Temp/The_Advantage_of_polyhedral.pdf> [February 12 2014]

Perzon, S., Janson, J., and Hoglin, L. (1999) *'On Comparison between CFD Methods and Wind Tunnel Tests on a Bluff Body*. United States of America: SAE International.

Piatek, R. and Schmitt, J. (1998) 'Aerodynamic Drag of Passenger Cars'. in *Aerodynamics of Road Vehicles*. ed. by Hucho, W. Warrendale, Pa.: Society of Automotive Engineers, 311-324, 330 – 337.

Raymond, J. (2012) *Horsepower Design Equations and Formulas Calculator* [online] available from <http://www.ajdesigner.com/phphorsepower/horsepower_equation_trap_speed_method_horsepower.php#ajscroll> [February 25 2014]

Rowell G.H. and Duffey M. (2004) *Introduction to Minitab* [online] available from <https://www.causeweb.org/repository/Minitab/Minitab.pdf> [June 10 2014]

Ryan, B. F., Joiner, B. L., and Cryer, J. D. (2005) *Minitab Handbook: Updated for Release 14*. 5th edn. Belmont, CA: Belmont, CA: Thomson Brooks/Cole.

SAE Dummy Testing Equipment Subcommittee (1994) *Surface Vehicle Information Report* [online] available from <https://law.resource.org/pub/us/cfr/ibr/005/sae.j1733.1994.html> [July 8 2014]

Saxena A. (2014) *Esi-Cfd Support* [online] available from <http://support.esi-cfd.com/esi-users/turb_parameters/> [2015]

Scheunert, D., DaimlerChysler, A., and Sindelfingen. (2004) 'Vehicle Bodies'. in *Automotive Handbook*. Plochingen. Germany: Robert Bosch, 884-886-895.

Stargazer, P. (2007) *Roof Box and Fuel Economy*. [2007] available from <http://www.honestjohn.co.uk/forum/post/index.htm?t=56521> [February 12]

The Roof Box Company (2014) *The Roof Box Company* [online] available from <http://www.roofbox.co.uk/roof-boxes/> [May/16 2013]

Thule (2014) [online] available from <http://www.thule.com.au/details.php?p_id=318> [March/5 2014]

CES EduPack (2013) *University of Cambridge 2013 Version 12.2.13* [online] [March 5 2014]

University of Texas [online] available from <http://www.ce.utexas.edu/prof/Novoselac/classes/ARE372/Notes/372_NO06_ReynoldsEq.ppt> [March 9 2014]

Versteeg, H. K. and Malalasekara, W. (2007) *An Introduction to Computational Fluid Dynamics*. 2nd edn. Essex: Peardon Education Limited.

WeinKauf, T. (2012) *Characteristic Curves of Vector Fields* [online] available from <http://feature.mpi-inf.mpg.de/2012/characteristiccurves> [March 8 2014]

White, F. M. (ed.) (2011) *Flow Past Immersed Bodies.* 7th edn. The United States of America: McGraw Hill Companies Inc.

Wilcox, D. C. (2006) *Turbulence Modeling for CFD*. 3rd edn. trans. by Craft, T. J. La Canada, Calif.: La Canada, Calif. : DCW Industries.

APPENDIX I

Vectors scenes of lowest drag position of box with design variation and car without roof box

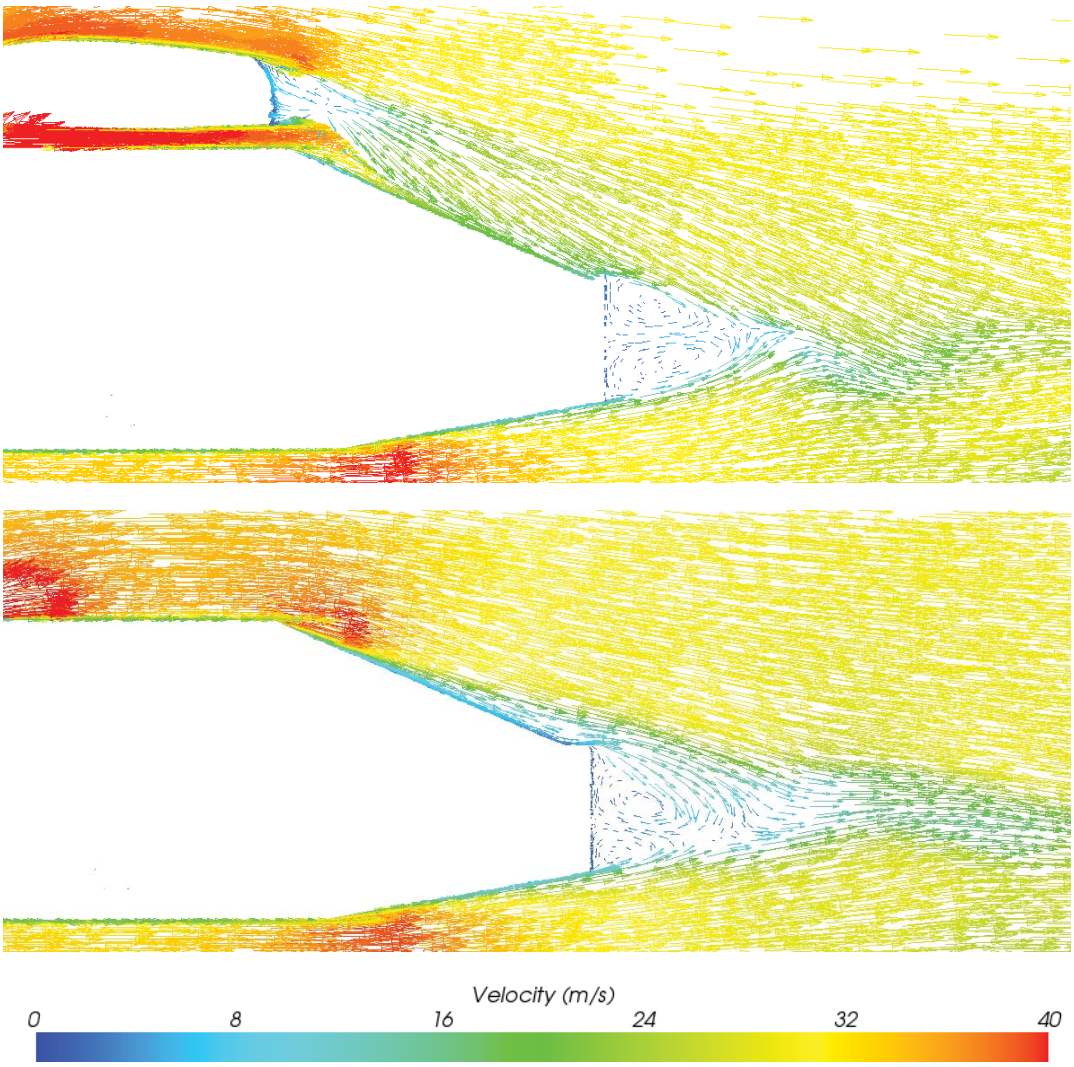

Figure 69: Flow around fastback car at lowest drag position and car without roof box

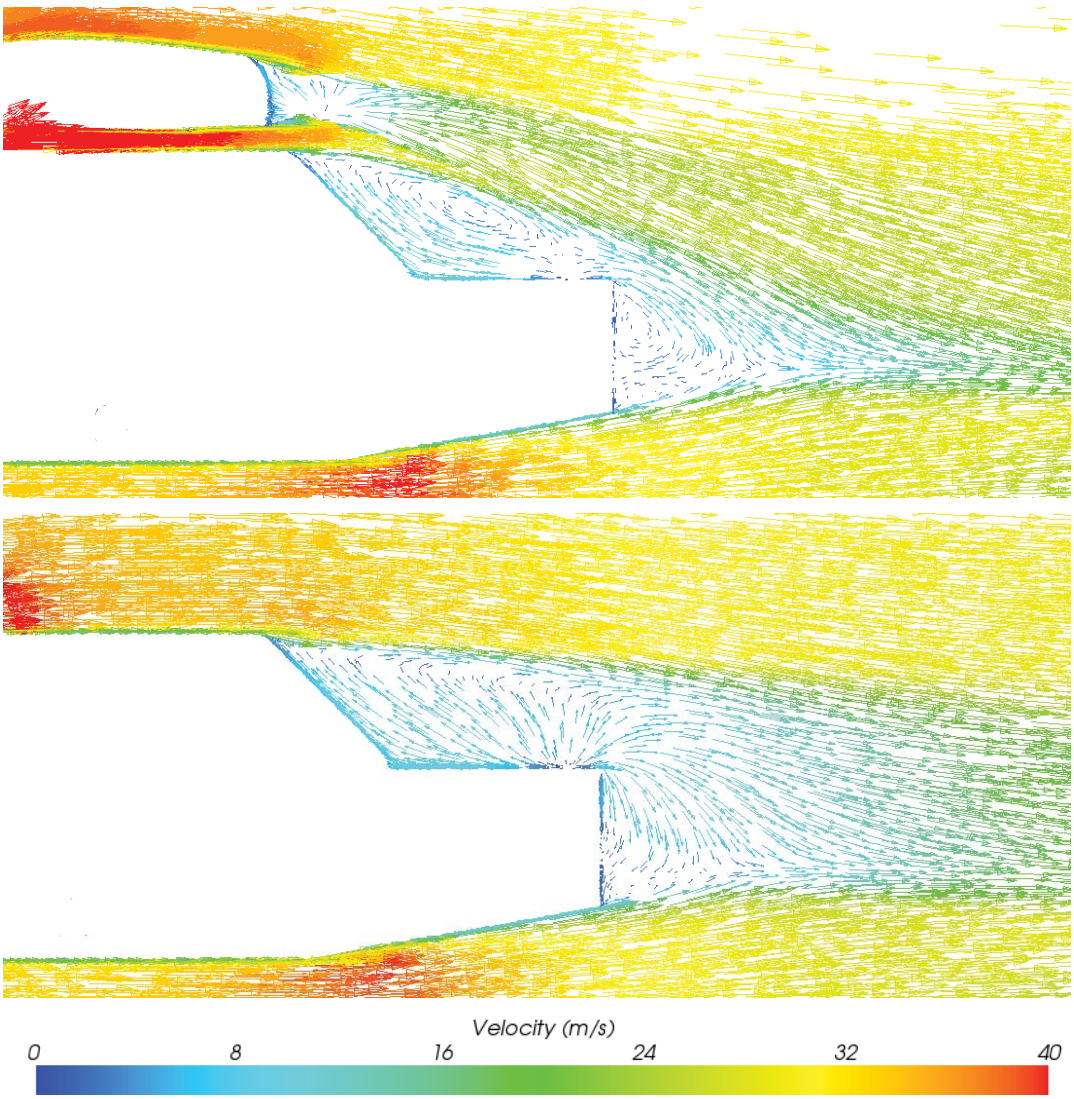

Figure 70: Flow around notchback car at lowest drag position and car without roof box

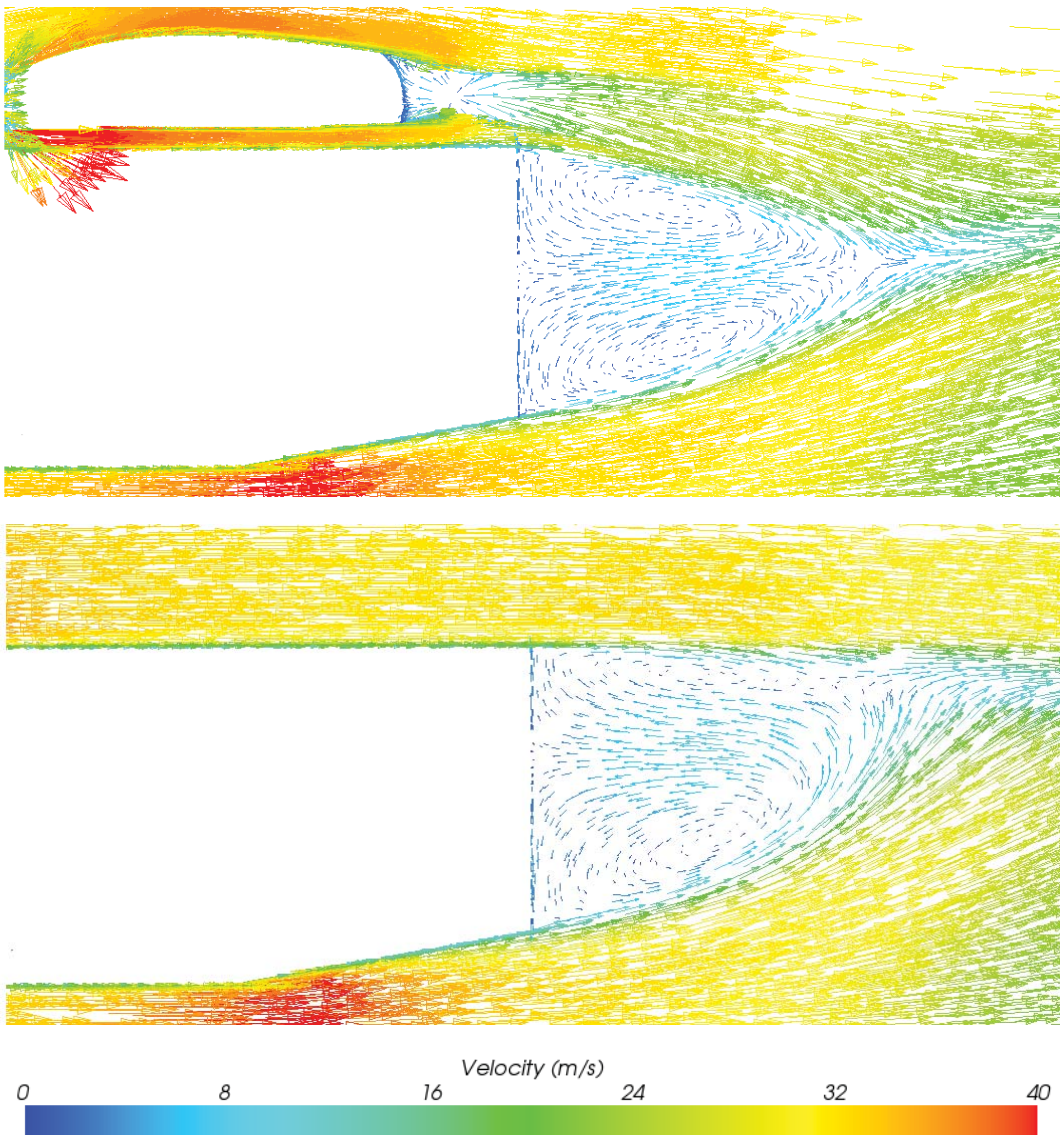

Figure 71: Flow around squareback car at lowest drag position and car without roof box

APPENDIX II

General Materials and its Properties Used for Roof Box

↓ Properties Material →	ABS	PS	PMMA	PC	PE	PET
Density (kg/m^3)	1.01-1.21	1.04-1.05	1.16-1.22	1.14 - 1.21	0.94 - 0.96	1.29 - 1.4
Price (GBP/kg)	1.79 - 1.97	2.18 - 2.4	1.73 - 1.91	2.58 - 2.84	1.11 - 1.22	1.3 - 1.44
Young's modulus (GPa)	1.1 - 2.9	1.2 - 2.6	2.24 - 3.8	2 - 2.44	0.62 - 0.9	2.76 - 4.14
Shear modulus (GPa)	0.32 - 1.03	0.5 - 0.9	0.8 - 1.37	0.79 - 0.87	0.22 - 0.31	0.99 - 1.49
Yield strength (Mpa)	18.5 - 51	28.7 - 56.2	53.8 - 72.4	59 - 70	18 - 29	56.5 - 62.3
Tensile strength (MPa)	27.6 - 55.2	35.9 - 56.5	48.3 - 79.6	60 - 72.4	20.7 - 44.8	48.3 - 72.4
Fracture toughness (Mpa.m^0.5)	1.19 - 4.29	0.7 - 1.1	0.7 - 1.6	2.1 - 4.6	1.44 - 1.72	4.5 - 5.5
Maximum service temperature (^{0}C)	62 - 77	77 - 103	42 - 57	101 - 144	90 - 110	67 – 87

Table 33: Commonly used materials and their general properties (University of Cambridge 2013)

Properties/Material	ABS	ABS	ABS	ABS
Filler material	Stainless steel	Carbon fibre	Glass fibre	Aluminium flake
% of filler material	10	20	20	40
Density (kg/m^3)	1.13 - 1.15	1.13 - 1.14	1.18 - 1.22	1.56 - 2.49
Price (GBP/kg)	2.63 - 2.88	5.47 - 6.02	2.29 - 2.55	2.26 - 2.49
Young's modulus	2.69 - 2.83	12.4 - 13.8	5.1 - 6.07	2.49 - 2.61
Shear modulus	0.964 - 1.01	4.61 - 5.13	1.86 - 2.21	0.89 - .934
Yield strength (Mpa	37.3 - 41.1	82.4 - 88	57.9 - 71.7	18.2 - 23.2
Tensile strength	46.6 - 51.4	103 - 110	72.4 - 89.6	22.8 – 29
Fracture toughness (Mpa.m^0.5)	1.99 - 2.39	3.23 - 3.98	2.82 - 3.38	0.878 - 2.29
Maximum service temperature (^{0}C)	67 - 87	67 - 87	67 - 87	67 – 87

Table 34: ABS composites and its properties (University of Cambridge 2013)

Properties / Material	PC	PC	PC
Filler material	**Stainless steel**	**Carbon fibre**	**Glass fibre**
% of filler material	6	20	20
Density (kg/m^3)	1.27 - 1.29	1.27 - 1.29	1.43 - 1.5
Price (GBP/kg)	3.36 - 3.7	6.15 - 6.77	3.88 - 4.37
Young's modulus (GPa)	2.76 - 2.9	13.5 - 14.1	8.07 - 8.48
Shear modulus (GPa)	0.99 - 1.04	5.03 - 5.25	2.96 - 3.12
Yield strength (Mpa)	51.5 - 56.7	99.2 - 110	66.2 - 82.4
Tensile strength (MPa)	64.4 - 70.9	124 - 138	82.7 – 103
Fracture toughness (Mpa.m^0.5)	2.07 - 3.52	4.29 - 5.33	3.31 - 5.15
Maximum service temperature (^{0}C)	117 - 133	111 - 126	107 – 122

Table 35: PC composites and its properties (University of Cambridge 2013)

APPENDIX III - Results

Position variation of Roof Box on Fastback Car in X direction

Position	C_D		Total C_D	Corrected C_D	Deviation	% deviation	C_{PM}
	Car	Box	-	-	-	%	-
(200,0,0)	0.240	0.220	0.237	0.280	0.065	30.01	-0.045
(100,0,0)	0.253	0.179	0.241	0.285	0.070	32.45	-0.061
(0,0,0)	0.263	0.138	0.244	0.289	0.073	34.04	-0.072
(-100,0,0)	0.277	0.093	0.248	0.294	0.078	36.32	-0.087
(-200,0,0)	0.284	0.051	0.247	0.293	0.078	35.96	-0.090

Table 36: Position variation of roof box in X direction on fastback car

Position variation of Roof Box on Notchback Car in X direction

Position	C_D		Total C_D	Corrected C_D	Deviation	% deviation	C_{PM}
	Car	Box	-	-	-	%	-
(200,0,0)	0.256	0.213	0.249	0.295	0.041	16.16%	-0.050
(100,0,0)	0.264	0.180	0.251	0.297	0.043	16.83%	-0.062
(0,0,0)	0.271	0.143	0.251	0.298	0.043	17.04%	-0.074
(-100,0,0)	0.279	0.106	0.252	0.298	0.044	17.28%	-0.084
(-200,0,0)	0.287	0.061	0.252	0.298	0.044	17.31%	-0.087

Table 37: Position variation of roof box in X direction on notchback car

Position variation of Roof Box on Squareback Car in X direction

Position	C_D		Total C_D	Corrected C_D	Deviation	% deviation	C_{PM}
	Car	Box	-	-	-	%	-
(200,0,0)	0.303	0.141	0.278	0.329	0.017	5.47%	0.070
(100,0,0)	0.306	0.107	0.275	0.325	0.013	4.26%	0.060
(0,0,0)	0.309	0.073	0.272	0.323	0.011	3.35%	0.046
(-100,0,0)	0.310	0.039	0.268	0.317	0.005	1.56%	0.032
(-200,0,0)	0.318	0.009	0.270	0.319	0.007	2.34%	0.020
(-300,0,0)	0.321	-0.022	0.268	0.317	0.005	1.72%	0.009
(-400,0,0)	0.329	-0.033	0.273	0.323	0.011	3.54%	0.000
(-500,0,0)	0.321	-0.008	0.270	0.320	0.008	2.56%	-0.012
(-600,0,0)	0.320	0.028	0.274	0.325	0.013	4.14%	-0.017
(-700,0,0)	0.312	0.061	0.273	0.323	0.011	3.52%	-0.026

Table 38: Position variation of roof box in X direction on Squareback car

Position variation of Roof Box on Fastback Car

Position variation in Y Direction

In datum position

Position	C_D		Total C_D	Corrected C_D	Deviation	% deviation
-	Car	Box	-	-	-	%
(0,0,0)	0.263	0.133	0.269	0.287	0.072	33.29%
(0,-75,0)	0.262	0.146	0.270	0.289	0.074	34.24%
(0,-150,0)	0.242	0.131	0.249	0.266	0.051	23.46%
(0,0,50)	0.257	0.142	0.265	0.283	0.068	31.33%
(0,-75,50)	0.255	0.148	0.264	0.282	0.066	30.81%
(0,-150,50)	0.234	0.135	0.242	0.259	0.044	20.18%
(0,0,-50)	0.271	0.132	0.276	0.295	0.080	37.04%
(0,-75,-50)	0.270	0.142	0.277	0.297	0.081	37.59%
(0,-150,-50)	0.256	0.120	0.260	0.278	0.063	29.03%

Position	Pitching moment coefficient	Rolling moment coefficient	Yaw moment coefficient
(0,0,0)	-0.069	-0.001	0.000
(0,-75,0)	-0.063	0.000	-0.001
(0,-150,0)	-0.050	-0.002	0.001
(0,0,50)	-0.066		
(0,-75,50)	-0.058	-0.002	0.001
(0,-150,50)	-0.044	-0.002	0.001
(0,0,-50)	-0.072		
(0,-75,-50)	-0.066	-0.001	0.001
(0,-150,-50)	-0.060	-0.004	0.003

Table 39: Position variation of roof box in Y direction datum position on fastback car

In datum +200mm (Extreme front position)

Position	C_D		Total C_D	Corrected C_D	Deviation	% deviation
-	Car	Box	-	-	-	%
(200,0,0)	0.240	0.220	0.262	0.280	0.065	30.01%
(200,-75,0)	0.231	0.224	0.255	0.272	0.057	26.26%
(200,-150,0)	0.230	0.230	0.255	0.272	0.057	26.40%
(200,0,50)	0.234	0.217	0.256	0.274	0.059	27.16%
(200,-75,50)	0.229	0.214	0.251	0.268	0.053	24.36%
(200,-150,50)	0.229	0.220	0.252	0.26	0.054	24.83%
(200,0,-50)	0.249	0.222	0.271	0.290	0.074	34.46%
(200,-75,-50)	0.244	0.212	0.265	0.284	0.068	31.59%
(200,-150,-50)	0.243	0.216	0.264	0.282	0.067	31.04%

Position	Pitching moment coefficient	Rolling moment coefficient	Yaw moment coefficient
(200,0,0)	-0.045		
(200,-75,0)	-0.027	-0.003	0.002
(200,-150,0)	-0.024	-0.005	0.005
(200,0,50)	-0.043		
(200,-75,50)	-0.034	-0.001	0.001
(200,-150,50)	-0.032	-0.002	0.003
(200,0,-50)	-0.048		
(200,-75,-50)	-0.042	-0.003	0.003
(200,-150,-50)	-0.039	-0.004	0.006

Table 40: Position variation of roof box in Y direction datum +200mm position on fastback car

In datum -200mm (Extreme rear position)

Position	C_D		Total C_D	Corrected C_D	Deviation	% deviation
-	Car	Box	-	-	-	%
(-200,0,0)	0.284	0.051	0.274	0.293	0.078	35.96%
(-200,-75,0)	0.283	0.039	0.271	0.290	0.074	34.45%
(-200,-150,0)	0.280	0.041	0.269	0.288	0.072	33.48%
(-200,0,50)	0.276	0.057	0.268	0.287	0.071	32.94%
(-200,-75,50)	0.294	0.040	0.282	0.301	0.086	39.72%
(-200,-150,50)	0.273	0.051	0.264	0.282	0.067	30.87%
(-200,0,-50)	0.295	0.035	0.282	0.302	0.086	39.92%
(-200,-75,-50)	0.273	0.026	0.260	0.278	0.063	29.01%
(-200,-150,-50)	0.292	0.031	0.278	0.297	0.082	37.88%

Position	Pitching moment coefficient	Rolling moment coefficient	Yaw moment coefficient
(-200,0,0)	-0.090		
(-200,-75,0)	-0.087	-0.003	0.000
(-200,-150,0)	-0.088	-0.005	0.002
(-200,0,50)	-0.080		
(-200,-75,50)	-0.105	-0.032	0.035
(-200,-150,50)	-0.074	-0.003	0.001
(-200,0,-50)	-0.098		
(-200,-75,-50)	-0.126	0.027	0.012
(-200,-150,-50)	-0.095	0.000	0.000

Table 41: Position variation of roof box in Y direction datum -200mm position on fastback car

Position variation in Z Direction

Position	C_D		Total C_D	Corrected C_D	Deviation	% deviation	C_{PM}
-	Car	Box	-	-	-	%	-
datum							
(0,0,-50)	0.271	0.132	0.249	0.295	0.080	37.04%	-0.072
(0,0,-25)	0.267	0.138	0.247	0.293	0.077	35.75%	-0.074
(0,0,0)	0.263	0.138	0.244	0.289	0.073	34.04%	-0.072
(0,0,25)	0.261	0.139	0.242	0.286	0.071	32.84%	-0.070
(0,0,50)	0.257	0.142	0.239	0.283	0.068	31.33%	-0.066
Datum + 200mm							
(200,0,-50)	0.249	0.222	0.245	0.290	0.074	34.46%	-0.048
(200,0,-25)	0.243	0.222	0.240	0.284	0.069	31.86%	-0.044
(200,0,0)	0.240	0.220	0.237	0.280	0.065	30.00%	-0.045
(200,0,25)	0.235	0.217	0.233	0.276	0.060	27.85%	-0.043
(200,0,50)	0.234	0.217	0.231	0.274	0.059	27.16%	-0.043
Datum - 200mm							
(-200,0,-50)	0.295	0.035	0.255	0.302	0.086	39.92%	-0.098
(-200,0,-25)	0.289	0.042	0.251	0.297	0.082	37.88%	-0.093
(-200,0,0)	0.284	0.044	0.246	0.292	0.076	35.43%	-0.090
(-200,0,25)	0.280	0.050	0.244	0.289	0.074	34.23%	-0.086
(-200,0,50)	0.276	0.057	0.242	0.287	0.071	32.94%	-0.080

Table 42: Position variation of roof box in Z direction on fastback car

Position variation of Roof Box on Notchback Car

Position variation in Y Direction

In datum position

Position	C_D		Total C_D	Corrected C_D	Deviation	% deviation
-	Car	Box	-	-	-	%
(0,0,0)	0.271	0.143	0.278	0.298	0.043	17.04%
(0,-75,0)	0.273	0.132	0.278	0.298	0.043	17.05%
(0,-150,0)	0.271	0.133	0.276	0.295	0.041	16.01%
(0,0,50)	0.265	0.142	0.272	0.291	0.037	14.48%
(0,-75,50)	0.267	0.138	0.274	0.293	0.038	15.11%
(0,-150,50)	0.266	0.139	0.273	0.292	0.038	14.79%
(0,0,-50)	0.280	0.167	0.291	0.311	0.056	22.17%
(0,-75,-50)	0.283	0.125	0.286	0.306	0.051	20.22%
(0,-150,-50)	0.280	0.131	0.284	0.304	0.050	19.49%

Position	Pitching moment coefficient	Rolling moment coefficient	Yaw moment coefficient
(0,0,0)	-0.074		
(0,-75,0)	-0.067	-0.012	0.004
(0,-150,0)	-0.069	0.007	-0.001
(0,0,50)	-0.072		
(0,-75,50)	-0.069	0.007	-0.002
(0,-150,50)	-0.066	0.006	-0.001
(0,0,-50)	-0.067		
(0,-75,-50)	-0.063	0.011	-0.004
(0,-150,-50)	-0.060	-0.013	0.006

Table 43: Position variation of roof box in Y direction datum position on notchback car

In datum +200mm (Extreme front position)

Position	C_D		Total C_D	Corrected C_D	Deviation	% deviation
-	Car	Box	-	-	-	%
(200,0,0)	0.256	0.213	0.276	0.295	0.041	16.16%
(200,-75,0)	0.257	0.209	0.277	0.296	0.041	16.27%
(200,-150,0)	0.255	0.209	0.275	0.294	0.039	15.38%
(200,0,50)	0.251	0.206	0.270	0.289	0.035	13.63%
(200,-75,50)	0.250	0.207	0.270	0.288	0.034	13.39%
(200,-150,50)	0.250	0.211	0.270	0.288	0.034	13.39%
(200,0,-50)	0.257	0.213	0.277	0.296	0.042	16.42%
(200,-75,-50)	0.264	0.206	0.282	0.302	0.047	18.57%
(200,-150,-50)	0.262	0.213	0.281	0.301	0.047	18.28%

Position	Pitching moment coefficient	Rolling moment coefficient	Yaw moment coefficient
(200,0,0)	-0.051		
(200,-75,0)	-0.039	0.007	-0.002
(200,-150,0)	-0.040	0.006	0.001
(200,0,50)	-0.053		
(200,-75,50)	-0.051	0.006	-0.002
(200,-150,50)	-0.047	0.005	0.001
(200,0,-50)	-0.050		
(200,-75,-50)	-0.032	-0.012	0.005
(200,-150,-50)	-0.036	-0.012	0.007

Table 44: Position variation of roof box in Y direction datum +200mm position on notchback car

In datum -200mm (Extreme rear position)

Position	C_D		Total C_D	Corrected C_D	Deviation	% deviation
-	Car	Box	-	-	-	%
(-200,0,0)	0.287	0.061	0.279	0.298	0.044	17.31%
(-200,-75,0)	0.287	0.055	0.278	0.297	0.042	16.65%
(-200,-150,0)	0.286	0.059	0.277	0.296	0.042	16.50%
(-200,0,50)	0.281	0.069	0.275	0.294	0.039	15.50%
(-200,-75,50)	0.279	0.064	0.272	0.291	0.037	14.35%
(-200,-150,50)	0.279	0.065	0.272	0.291	0.036	14.28%
(-200,0,-50)	0.294	0.085	0.290	0.310	0.054	21.78%
(-200,-75,-50)	0.295	0.040	0.283	0.3024	0.048	18.91%
(-200,-150,-50)	0.295	0.044	0.284	0.3034	0.049	19.28%

Position	Pitching moment coefficient	Rolling moment coefficient	Yaw moment coefficient
(-200,0,0)	-0.088		
(-200,-75,0)	-0.089	0.008	-0.004
(-200,-150,0)	-0.084	-0.009	0.004
(-200,0,50)	-0.081		
(-200,-75,50)	-0.086	-0.011	0.002
(-200,-150,50)	-0.080	-0.009	0.003
(-200,0,-50)	-0.082		
(-200,-75,-50)	-0.092	0.011	-0.004
(-200,-150,-50)	-0.082	0.002	0.001

Table 45: Position variation of roof box in Y direction datum -200mm position on notchback car

Position variation in Z Direction

Position	C_D		Total C_D	Corrected C_D	Deviation	% deviation	C_{PM}
-	Car	Box	-	-	-	%	-
datum							
(0,0,-50)	0.280	0.167	0.262	0.311	0.056	22.17%	-0.067
(0,0,-25)	0.274	0.161	0.257	0.304	0.050	19.57%	-0.067
(0,0,0)	0.271	0.143	0.251	0.298	0.043	17.04%	-0.074
(0,0,25)	0.268	0.144	0.248	0.294	0.040	15.59%	-0.072
(0,0,50)	0.265	0.141	0.246	0.291	0.030	14.48%	-0.072
Datum + 200mm							
(200,0,-50)	0.257	0.213	0.250	0.296	0.042	16.42%	-0.050
(200,0,-25)	0.255	0.213	0.249	0.295	0.040	15.82%	-0.051
(200,0,0)	0.256	0.213	0.249	0.295	0.041	16.16%	-0.050
(200,0,25)	0.254	0.210	0.247	0.292	0.038	14.96%	-0.054
(200,0,50)	0.251	0.206	0.244	0.289	0.035	13.63%	-0.053
Datum - 200mm							
(-200,0,-50)	0.294	0.085	0.261	0.310	0.055	21.75%	-0.082
(-200,0,-25)	0.291	0.059	0.255	0.302	0.048	18.66%	-0.091
(-200,0,0)	0.287	0.061	0.252	0.298	0.044	17.31%	-0.088
(-200,0,25)	0.283	0.065	0.249	0.295	0.041	15.98%	-0.088
(-200,0,50)	0.281	0.069	0.248	0.294	0.039	15.50%	-0.081

Table 46: Position variation of roof box in Z direction on notchback car

Position variation of Roof Box on Squareback Car

Position variation in Y Direction

In datum +200mm (Extreme front Position)

Position	C_D		Total C_D	Corrected C_D	Deviation	% deviation
-	Car	Box	-	-	-	%
(200,0,0)	0.303	0.141	0.308	0.329	0.017	5.47%
(200,-75,0)	0.302	0.138	0.306	0.327	0.015	4.82%
(200,-150,0)	0.301	0.136	0.305	0.327	0.014	4.62%
(200,0,50)	0.302	0.149	0.308	0.329	0.017	5.58%
(200,-75,50)	0.296	0.146	0.302	0.323	0.011	3.44%
(200,-150,50)	0.296	0.146	0.303	0.323	0.011	3.65%
(200,0,-50)	0.308	0.124	0.310	0.331	0.019	6.06%
(200,-75,-50)	0.307	0.119	0.308	0.329	0.017	5.49%
(200,-150,-50)	0.307	0.123	0.309	0.330	0.018	5.72%

Position	Pitching moment coefficient	Rolling moment coefficient	Yaw moment coefficient
(200,0,0)	0.070		
(200,-75,0)	0.074	-0.001	0.002
(200,-150,0)	0.073	-0.001	0.004
(200,0,50)	0.03		
(200,-75,50)	0.069	-0.001	0.001
(200,-150,50)	0.073	-0.001	0.004
(200,0,-50)	0.073		
(200,-75,-50)	0.075	0.001	0.001
(200,-75,-50)	0.053	0.000	0.005

Table 47: Position variation of roof box in Y direction- datum +200mm position on squareback car

In datum position

Position	C_D		Total C_D	Corrected C_D	Deviation	% deviation
-	Car	Box	-	-	-	%
(0,0,0)	0.309	0.073	0.302	0.323	0.011	3.35%
(0,-75,0)	0.306	0.071	0.299	0.319	0.007	2.37%
(0,-150,0)	0.306	0.073	0.298	0.319	0.007	2.26%
(0,0,50)	0.303	0.091	0.299	0.319	0.007	2.36%
(0,-75,50)	0.301	0.088	0.297	0.317	0.005	1.60%
(0,-150,50)	0.302	0.090	0.298	0.318	0.006	1.95%
(0,0,-50)	0.317	0.044	0.304	0.325	0.013	4.14%
(0,-75,-50)	0.314	0.042	0.301	0.322	0.010	3.03%
(0,-150,-50)	0.313	0.045	0.300	0.321	0.009	2.94%

Position	Pitching moment coefficient	Rolling moment coefficient	Yaw moment coefficient
(0,0,0)	0.046		
(0,-75,0)	0.049	-0.001	0.001
(0,-150,0)	0.048	0.001	0.002
(0,0,50)	0.048		
(0,-75,50)	0.461	0.000	0.000
(0,-150,50)	0.049	0.001	0.002
(0,0,-50)	0.046		
(0,-75,-50)	0.045	0.001	0.001
(0,-150,-50)	0.047	0.001	0.002

Table 48: Position variation of roof box in Y direction datum position on squareback car

In datum -100mm position

Position	C_D		Total C_D	Corrected C_D	Deviation	% deviation
-	Car	Box	-	-	-	%
(-100,0,0)	0.310	0.039	0.296	0.317	0.005	1.56%
(-100,-75,0)	0.314	0.038	0.301	0.321	0.009	2.99%
(-100,-150,0)	0.311	0.040	0.297	0.318	0.006	1.92%
(-100,0,50)	0.307	0.063	0.298	0.319	0.007	2.20%
(-100,-75,50)	0.306	0.062	0.297	0.317	0.005	1.63%
(-100,-150,50)	0.304	0.064	0.295	0.316	0.004	1.23%
(-100,0,-50)	0.318	0.005	0.298	0.319	0.007	2.22%
(-100,-75,-50)	0.316	0.002	0.296	0.317	0.005	1.44%
(-100,-150,-50)	0.316	0.007	0.297	0.317	0.005	1.71%

Position	Pitching moment coefficient	Rolling moment coefficient	Yaw moment coefficient
(-100,0,0)	0.032		
(-100,-75,0)	0.038	0.000	0.000
(-100,-150,0)	0.035	0.001	0.001
(-100,0,50)	0.034		
(-100,-75,50)	0.035	0.000	0.000
(-100,-150,50)	0.037	0.001	0.000
(-100,0,-50)	0.029		
(-100,-75,-50)	0.028	0.000	0.000
(-100,-150,-50)	0.031	0.001	0.001

Table 49: Position variation of roof box in Y direction datum -100mm position on squareback car

In datum -200mm position

Position	C_D		Total C_D	Corrected C_D	Deviation	% deviation
-	Car	Box	-	-	-	%
(-200,0,0)	0.318	0.009	0.299	0.319	0.007	2.34%
(-200,-75,0)	0.317	0.009	0.298	0.318	0.006	1.99%
(-200,-150,0)	0.314	0.012	0.295	0.316	0.004	1.18%
(-200,0,50)	0.309	0.036	0.295	0.315	0.003	1.08%
(-200,-75,50)	0.314	0.008	0.295	0.316	0.004	1.13%
(-200,-150,50)	0.309	0.038	0.295	0.316	0.004	1.23%
(-200,0,-50)	0.323	-0.032	0.297	0.317	0.005	1.73%
(-200,-75,-50)	0.323	-0.034	0.296	0.317	0.005	1.57%
(-200,-150,-50)	0.322	-0.029	0.296	0.317	0.005	1.45%

Position	Pitching moment coefficient	Rolling moment coefficient	Yaw moment coefficient
(-200,0,0)	0.020		
(-200,-75,0)	0.022	0.001	-0.001
(-200,-150,0)	0.020	0.002	0.000
(-200,0,50)	0.022		
(-200,-75,50)	0.019	0.000	-0.001
(-200,-150,50)	0.027	0.001	0.000
(-200,0,-50)	0.013		
(-200,-75,-50)	0.017	0.001	-0.001
(-200,-150,-50)	0.019	0.003	-0.001

Table 50: Position variation of roof box in Y direction datum -200mm position on squareback car

In datum -400mm position

Position	C_D		Total C_D	Corrected C_D	Deviation	% deviation
-	Car	Box	-	-	-	%
(-400,0,0)	0.329	-0.033	0.302	0.323	0.011	3.54%
(-400,-75,0)	0.326	-0.029	0.300	0.321	0.009	2.75%
(-400,-150,0)	0.320	-0.026	0.295	0.316	0.004	1.14%
(-400,0,50)	0.314	0.002	0.294	0.315	0.003	0.84%
(-400,-75,50)	0.322	-0.033	0.295	0.316	0.004	1.17%
(-400,-150,50)	0.313	0.006	0.294	0.314	0.002	0.72%
(-400,0,-50)	0.334	-0.073	0.299	0.320	0.008	2.58%
(-400,-75,-50)	0.331	-0.075	0.297	0.318	0.006	1.79%
(-400,-150,-50)	0.330	-0.069	0.297	0.318	0.006	1.75%

Position	Pitching moment coefficient	Rolling moment coefficient	Yaw moment coefficient
(-400,0,0)	0.000		
(-400,-75,0)	-0.001	0.001	-0.001
(-400,-150,0)	-0.002	0.002	-0.002
(-400,0,50)	0.002		
(-400,-75,50)	-0.003	0.000	-0.002
(-400,-150,50)	0.005	0.002	-0.002
(-400,0,-50)	-0.014		
(-400,-75,-50)	-0.001	0.001	-0.002
(-400,-150,-50)	-0.008	0.003	-0.004

Table 51: Position variation of roof box in Y direction datum -400mm position on squareback car

In datum -700mm position

Position	C_D		Total C_D	Corrected C_D	Deviation	% deviation
-	Car	Box	-	-	-	%
(-700,0,0)	0.312	0.061	0.302	0.323	0.011	3.52%
(-700,-75,0)	0.310	0.058	0.300	0.321	0.009	2.90%
(-700,-150,0)	0.313	0.059	0.303	0.324	0.012	3.85%
(-700,0,50)	0.308	0.083	0.303	0.324	0.012	3.74%
(-700,-75,50)	0.309	0.056	0.299	0.319	0.007	2.35%
(-700,-150,50)	0.305	0.063	0.296	0.317	0.005	1.49%
(-700,0,-50)	0.314	0.072	0.306	0.328	0.016	4.96%
(-700,-75,-50)	0.313	0.066	0.304	0.325	0.013	4.14%
(-700,-150,-50)	0.314	0.069	0.305	0.327	0.015	4.63%

Position	Pitching moment coefficient	Rolling moment coefficient	Yaw moment coefficient
(-700,0,0)	-0.001		
(-700,-75,0)	-0.021	0.000	-0.003
(-700,-150,0)	-0.019	0.002	-0.006
(-700,0,50)	-0.028		
(-700,-75,50)	-0.024	0.001	-0.004
(-700,-150,50)	-0.014	0.002	-0.005
(-700,0,-50)	-0.039		
(-700,-75,-50)	-0.036	0.001	-0.004
(-700,-150,-50)	-0.031	0.003	-0.006

Table 52: Position variation of roof box in Y direction datum -700mm position on squareback car

Position variation in Z Direction

Position	C_D		Total C_D	Corrected C_D	Deviation	% deviation	C_{PM}
	Car	Box	-	-	-	%	-
Datum							
(0,0,-50)	0.317	0.044	0.274	0.325	0.0129	4.14%	0.046
(0,0,-25)	0.311	0.05	0.272	0.322	0.0096	3.08%	0.046
(0,0,0)	0.309	0.073	0.272	0.323	0.0105	3.35%	0.046
(0,0,25)	0.305	0.084	0.271	0.321	0.0086	2.76%	0.045
(0,0,50)	0.303	0.091	0.270	0.319	0.0073	2.36%	0.048
Datum + 200mm							
(200,0,-50)	0.308	0.124	0.279	0.331	0.0189	6.06%	0.073
(200,0,-25)	0.308	0.137	0.281	0.333	0.0209	6.68%	0.074
(200,0,0)	0.303	0.141	0.278	0.329	0.0171	5.47%	0.070
(200,0,25)	0.305	0.146	0.280	0.332	0.0195	6.26%	0.073
(200,0,50)	0.302	0.149	0.278	0.329	0.0174	5.58%	0.073
Datum - 100mm							
(-100,0,-50)	0.318	0.005	0.269	0.319	0.0069	2.22%	0.029
(-100,0,-25)	0.318	0.023	0.272	0.322	0.0098	3.15%	0.034
(-100,0,0)	0.310	0.039	0.268	0.317	0.0049	1.56%	0.032
(-100,0,25)	0.309	0.053	0.269	0.318	0.0064	2.05%	0.034
(-100,0,50)	0.307	0.063	0.269	0.319	0.0069	2.20%	0.034
Datum - 200mm							
(-200,0,-50)	0.323	-0.032	0.268	0.317	0.0054	1.73%	0.013
(-200,0,-25)	0.323	-0.011	0.271	0.321	0.0092	2.95%	0.019
(-200,0,0)	0.318	0.009	0.270	0.319	0.0073	2.34%	0.020
(-200,0,25)	0.317	0.023	0.271	0.321	0.0087	2.80%	0.026
(-200,0,50)	0.309	0.036	0.266	0.315	0.0034	1.08%	0.022
Datum - 400mm							
(-400,0,-50)	0.334	-0.073	0.270	0.320	0.0080	2.58%	-0.014
(-400,0,-25)	0.327	-0.049	0.268	0.317	0.0053	1.70%	-0.009
(-400,0,0)	0.329	-0.033	0.273	0.323	0.0110	3.54%	0.000
(-400,0,25)	0.320	-0.013	0.268	0.317	0.0051	1.62%	0.000
(-400,0,50)	0.314	0.002	0.266	0.315	0.0026	0.84%	0.002
Datum - 700mm							
(-700,0,-50)	0.314	0.072	0.276	0.328	0.0155	4.96%	-0.039
(-700,0,-25)	0.313	0.064	0.274	0.325	0.0130	4.18%	-0.031
(-700,0,0)	0.312	0.061	0.273	0.323	0.0110	3.52%	-0.001
(-700,0,25)	0.307	0.060	0.269	0.319	0.0064	2.06%	-0.023
(-700,0,50)	0.308	0.083	0.273	0.324	0.0117	3.74%	-0.028

Table 53: Position variation of roof box in Z direction on squareback car

Various Positions of Original Roof Box

Position	C_D		Total C_D	Corrected C_D	Deviation	% deviation	C_{PM}
-	Car	Box	-	-	-	%	-
Fastback							
(-200,0,-50)	0.295	0.035	0.255	0.302	0.086	39.92%	-0.098
(-100,0,-50)	0.283	0.083	0.252	0.298	0.083	38.48%	-0.085
(0,0,-50)	0.271	0.132	0.249	0.295	0.080	37.04%	-0.072
(100,0,-50)	0.260	0.177	0.247	0.293	0.077	35.75%	-0.060
(200,0,-50)	0.249	0.222	0.245	0.290	0.074	34.46%	-0.048
Notchback							
(-200,0,-50)	0.294	0.085	0.261	0.310	0.055	21.75%	-0.082
(-100,0,-50)	0.287	0.126	0.262	0.310	0.056	21.91%	-0.075
(0,0,-50)	0.280	0.168	0.262	0.311	0.056	22.07%	-0.067
(100,0,-50)	0.268	0.190	0.256	0.303	0.049	19.25%	-0.059
(200,0,-50)	0.257	0.213	0.250	0.296	0.042	16.42%	-0.050
Squareback							
(-700,0,-50)	0.314	0.072	0.276	0.327	0.016	4.96%	-0.039
(-400,0,-50)	0.334	-0.073	0.270	0.320	0.008	2.58%	-0.014
(-200,0,-50)	0.323	-0.032	0.268	0.317	0.005	1.73%	0.013
(-100,0,-50)	0.318	0.005	0.269	0.319	0.007	2.22%	0.029
(0,0,-50)	0.317	0.044	0.274	0.325	0.013	4.14%	0.046
(200,0,-50)	0.308	0.124	0.279	0.331	0.019	6.06%	0.073

Table 54: Results of 3 geometries with actual box in various X positions when Y=0 and Z=-50mm

Various positions of Scaled Box

Position	C_D		Total C_D	Corrected C_D	Deviation	% deviation	C_{PM}
-	Car	Box	-	-	-	%	-
Fastback							
(-200,0,-50)	0.280	-0.033	0.245	0.276	0.061	28.07%	-0.047
(-100,0,-50)	0.278	-0.050	0.242	0.272	0.056	26.11%	-0.043
(0,0,-50)	0.268	0.006	0.239	0.269	0.053	24.63%	-0.035
(100,0,-50)	0.235	0.150	0.226	0.254	0.039	17.95%	-0.012
(200,0,-50)	0.227	0.217	0.226	0.255	0.039	18.09%	-0.007
Notchback							
(-200,0,-50)	0.290	-0.042	0.253	0.284	0.030	11.80%	-0.046
(-100,0,-50)	0.289	-0.083	0.248	0.279	0.024	9.50%	-0.040
(0,0,-50)	0.286	-0.036	0.251	0.282	0.028	10.87%	-0.034
(100,0,-50)	0.273	0.033	0.246	0.277	0.023	8.89%	-0.022
(200,0,-50)	0.264	0.143	0.251	0.282	0.028	10.86%	-0.008
Squareback							
(-700,0,-50)	0.292	0.099	0.271	0.305	-0.007	-2.34%	0.002
(-400,0,-50)	0.308	-0.016	0.272	0.306	-0.006	-2.00%	0.017
(-200,0,-50)	0.324	-0.119	0.275	0.309	-0.003	-0.92%	0.024
(-100,0,-50)	0.329	-0.142	0.277	0.312	-0.001	-0.17%	0.028
(0,0,-50)	0.328	-0.108	0.280	0.315	0.003	0.79%	0.030
(200,0,-50)	0.321	0.003	0.286	0.322	0.010	3.10%	0.042

Table 55: Results of 3 geometries with scaled box in various X positions when Y=0 and Z=-50 mm

New Design without Taper on Scaled Box

Position	C_D		Total C_D	Corrected C_D	Deviation	% deviation	C_{PM}
-	Car	Box	-	-	-	%	-
Fastback							
(-200,0,-50)	0.274	-0.063	0.237	0.267	0.051	23.57%	-0.048
(-100,0,-50)	0.272	-0.076	0.233	0.263	0.047	21.81%	-0.041
(0,0,-50)	0.251	0.006	0.224	0.252	0.036	16.78%	-0.022
(100,0,-50)	0.234	0.120	0.221	0.249	0.033	15.34%	-0.013
(200,0,-50)	0.227	0.184	0.222	0.250	0.034	15.82%	-0.007
Notchback							
(-200,0,-50)	0.286	-0.065	0.247	0.278	0.024	9.28%	-0.046
(-100,0,-50)	0.289	-0.108	0.245	0.275	0.021	8.29%	-0.040
(0,0,-50)	0.283	-0.081	0.243	0.273	0.019	7.33%	-0.030
(100,0,-50)	0.275	-0.013	0.243	0.273	0.019	7.41%	-0.016
(200,0,-50)	0.271	0.133	0.255	0.287	0.033	12.92%	0.003
Squareback							
(-700,0,-50)	0.298	0.069	0.273	0.307	-0.005	-1.59%	-0.002
(-400,0,-50)	0.313	-0.038	0.274	0.309	-0.003	-1.10%	0.011
(-200,0,-50)	0.331	-0.138	0.279	0.314	0.001	0.46%	0.019
(-100,0,-50)	0.335	-0.170	0.279	0.314	0.002	0.56%	0.022
(0,0,-50)	0.335	-0.144	0.282	0.317	0.005	1.56%	0.026
(200,0,-50)	0.327	-0.044	0.286	0.322	0.010	3.06%	0.034

Table 56: Results of 3 geometries with variation in design of scaled roof box without taper in various X positions when Y=0 and Z=-50 mm

New Design with Taper on Scaled Box

Position	C_D		Total C_D	Corrected C_D	Deviation	% deviation	C_{PM}
-	Car	Box	-	-	-	%	-
Fastback							
(-200,0,-50)	0.277	-0.067	0.239	0.269	0.053	24.57%	-0.050
(-100,0,-50)	0.274	-0.089	0.234	0.263	0.048	22.12%	-0.045
(0,0,-50)	0.261	-0.038	0.228	0.256	0.041	18.92%	-0.033
(100,0,-50)	0.234	0.077	0.217	0.244	0.028	13.20%	-0.016
(200,0,-50)	0.224	0.150	0.216	0.243	0.028	12.85%	-0.009
Notchback							
(-200,0,-50)	0.284	-0.073	0.244	0.275	0.021	8.11%	-0.048
(-100,0,-50)	0.287	-0.116	0.242	0.273	0.018	7.14%	-0.042
(0,0,-50)	0.282	-0.083	0.241	0.271	0.017	6.65%	-0.034
(100,0,-50)	0.273	-0.015	0.241	0.271	0.016	6.40%	-0.024
(200,0,-50)	0.258	0.065	0.237	0.267	0.012	4.81%	-0.015
Squareback							
(-700,0,-50)	0.294	0.049	0.267	0.300	-0.012	-3.78%	-0.004
(-400,0,-50)	0.312	-0.055	0.271	0.305	-0.007	-2.21%	0.010
(-200,0,-50)	0.328	-0.155	0.274	0.308	-0.004	-1.27%	0.018
(-100,0,-50)	0.334	-0.187	0.276	0.310	-0.002	-0.59%	0.022
(0,0,-50)	0.333	-0.158	0.279	0.314	0.002	0.47%	0.025
(200,0,-50)	0.326	-0.048	0.284	0.320	0.008	2.39%	0.035

Table 57: Results of 3 geometries with variation in design of scaled roof box with taper in various X positions when Y=0 and Z=-50 mm